Superconducting Order Parameter Fluctuation in Doped and Composite Cuprate Superconductors

Annapurna Mohanta

Department of Physics
National Institute of Technology Rourkela

Superconducting Order Parameter Fluctuation in Doped and Composite Cuprate Superconductors

Thesis Submitted to the

Department of Physics
National Institute of Technology, Rourkela
For award of the degree

of

Doctor of Philosophy

by

Annapurna Mohanta

Under the guidance of

Prof. D. Behera and Prof. S. Panigrahi

Department of Physics
National Institute of Technology Rourkela
Odisha (India)-769 008
January 2011

This thesis is dedicated to

my

.....PARENTS.....

Declaration

I hereby declare that this submission is my own work and that, to the best of my knowledge and belief, it contains no material previously published or written by another person nor material which to a substantial extent has been accepted for the award of any other degree or diploma of the university or other institute of higher learning, except where due acknowledgement has been made in the text.

(*Name*)

Date:

NATIONAL INSTITUE OF TECHNOLOGY
ROURKELA -769 008, ODISHA, INDIA.

Certificate

This is to certify that the thesis entitled, ***"Superconducting Order Parameter Fluctuation in Doped and Composite Cuprate Superconductors"*** being submitted by Annapurna Mohanta to the Department of Physics, National Institute of Technology, Rourkela, for the partial fulfillment of award of the degree Doctor of Philosophy, is a record of bonafide research work carried out by her under our supervision and guidance.

This thesis in my opinion, is worthy of consideration for award of the degree of Doctor of Philosophy in accordance with the regulation of the Institute. To the best of my knowledge, the results embodied in this thesis have not been submitted to any other University or Institute for the award of any degree or diploma.

Supervisors

Date:

(Dr. D. Behera)
Associate Professor,
Department of Physics
National Institute of Technology
Rourkela, Odisha, India- 769 008.

(Dr. S. Panigrahi)
Professor,
Department of Physics
National Institute of Technology
Rourkela, Odisha, India- 769 008

Acknowledgement

This report is a result of my efforts as a research scholar towards my Ph. D. at the Low Temperature Physics Lab of Department of Physics, National Institute of Technology Rourkela. During this time, I have been supported by various people to whom I wish to express my gratitude.

I am indebted to Prof. D. Behera my esteemed Guide (Principal Supervisor), he offered me the possibility to work in a liberal environment and given me the freedom to conduct my research in an independent way. The charming personality of Prof. D. Behera has been unified perfectly with knowledge that creates a permanent impression in my mind. His receptiveness to new and different ideas and his willingness to leave his space and time were always important sources of inspiration and motivation.

I wish to express my hearty gratitude to Prof. S. Panigrahi for his kind inspiration, uninterrupted support and utmost help for being as co-supervisor. I am obliged to him for his moral support through all the stages during this doctoral research work. I am indebted to him for the valuable time he has spared for me during this work.

I also express my gratitude to Prof. S. Jena, Professor and Head, Department of Physics for proving me the required facilities to carry out my research in the institute.

I would like to thank to all DSC members and others faculty members of the institute for their co-operation and help.

I would also like to thank to Dr. Rajiv Rawat and Mr. S. Dash, UGC-DAE-CSR, Indore for his support for carrying out some experimental work.

At last but not least, I would like to thank to my colleagues as well as other research scholars, Dr. T. Badapanda, Miss Arpna Kujur, Mr. Alok Pandey and Miss Mousumibala Sahoo, now with the Institute of Low temperature Physics lab, for their co-operation for working in a congenial environment during my stay at NIT Rourkela.

Finally, I am deeply grateful for the support of many kinds I got from my family, friends and flat-mates who were at my side during that time.

Annapurna Mohanta

BIO-DATA OF THE CANDIDATE

Name of the Candidate	:	Annapurna Mohanta
Father's Name	:	Dr. Srikanta Mohanta
Permanent Address	:	AT/PO/PS: Raruan Dist: Mayurbhanj Odisha, Pin: 757 035
Email ID	:	annapurna_physics@yahoo.co.in

ACADEMIC QUALIFICATION

- Continuing **Ph. D.** in Physics, National Institute of Technology, Rourkela, INDIA. Year of degree awarded or expected -2010-11.
- **M. Phil.** in Physics, Utkal University, Vani Vihar, Bubaneswar, INDIA.
- **M. Sc.** in Physics, National Institute of Technology Rourkela, INDIA.
- **B. Sc (Physics Hons.)**, North Orissa University, INDIA.

PUBLICATIONS

(a) In International Journal

1. **A. Mohanta** and D. Behera, Magnetic field dependence of pinning effect in $BaZrO_3$ doped $YBa_2Cu_3O_{7-\delta}$ ceramic superconductor, ***Solid State Communications***. 150 (2010) 1325-1328.
2. **Annapurna Mohanta** and Dhrubananda Behera, Fluctuation Induced Magneto-Conductivity Studies in $YBa_2Cu_3O_{7-\delta}$ + $xBaZrO_3$ Composite high-Tc Superconductors. ***Physica C.*** 470 (2010) 295–303.
3. **Annapurna Mohanta** and Dhrubananda Behera, Temperature Response of $BaZrO_3$-Inclusion to $YBa_2Cu_3O_{7-\delta}$ Probed by Magneto-Transport Measurements. ***Journal of Superconductivity and Novel Magnetism.*** 23 (2010) 275–283.
4. A. Kujur, **A. Mohanta** and D. Behera, Dimensionality Fluctuation of Excess Conductivity in granular YBCO/$BaTiO_3$ Composites, ***International Journal of Material Science***. 5 (2010) 683-690.
5. **A. Mohanta** and D. Behera, Themally Activated Flux Creep and Current Conduction in YBCO + BZO Composites, ***International Journal of Modern Physics B.*** (Accepted for publication).
6. **Annapurna Mohanta** and Dhrubananda Behera, Physica B (2010), doi:10.1016/j.physb.2010.12.017
7. **A. Mohanta** and D. Behera, Intergranular Percolation in Granular YBCO/$BaTiO_3$ Composites, ***Indian Journal of Physics.*** 83:4 (2009) 455-463.
8. **A. Mohanta** and D.Behera, Inhomogeneity Induced Coupling in YBCO/$BaTiO_3$ Composites, ***American Institute of Physics Conference Proceedings.*** 978-0-7354-0593-6/08/ (2008) 422-428.

(b) In National Journal

1. **A. Mohanta** and D. Behera, Effect of Ga and Zn Doping on Coherent Transition of YBCO Superconductor, ***Indian Journal of Pure and Applied Physics.*** 47 (2009) 676-680.

(c) In International Conference/Seminars

1. **A. Mohanta,** S. Dash and D. Behera, Thermally Activated Flux Creep and Current Conduction in YBCO+BZO Composites. ***The international conference on Ceramics (ICE-09)*** organized by Delhi University, Delhi, during 13-17th December, 2009.
2. **A. Mohanta** and D. Behera, Magnetic field induced pinning effect in $YBa_2Cu_3O_{7-\delta}$ + $BaZrO_3$ superconductor, ***International Conference (MSM-09)*** 11th – 14th November, 2009, held at S. N. Bose National Centre for Basic Sciences, Kolkata.

(d) In National Conference/Seminars

1. **A. Mohanta** and D. Behera. Enhancement of Superconducting Properties in the SCOPF Region of YBCO + BZO Composites in National conference on ***Condensed Matter Days,*** 26th –28th August 2009, held at Jadavpur Univesity, Kolkata.
2. **A. Mohanta** and D. Behera. Magnetoresistive effect in YBCO+ BZO composites in National conference on ***Condensed Matter Days,*** 26th –28th August 2009, held at Jadavpur Univesity, Kolkata.
3. **Annapurna Mohanta,** Dhrubananda Behera, Simanchalo Panigrahi and Naresh Chandra Mishra in National conference on ***Condensed Matter Days,*** *29th* – 31st August 2007, held at National Institute of Technology, Rourkela.
4. A. Kujur, **A. Mohanta** and D. Behera, in National Seminar on "***Physics and Technology of Novel Materials"***, 25-27th, 2010 held at School of Physics, Sambalpur University, Jyoti Vihar, Burla, India.

Abstract

This thesis describes work in the area of high temperature superconductors. Attempts have been made for the synthesis of doped and composites of YBCO superconductors to study the electrical and magnetic properties. The general objective of this work is to look at the effect of inhomogeneities and secondary phases on Superconducting order parameter fluctuation (SCOPF) in doped and composite superconductors. The influence of inhomogeneities on the microstructural and electrical properties is investigated for the simultaneous incorporation of Ga^{3+} and Zn^{2+} to the Cu-site of $YBa_2Cu_3O_{7-\delta}$. The evolution of anisotropy has also been analyzed for the effect of both hole doping to the Y- site through Ca, and CuO-chain electronic state anisotropy by Zn doping to the Cu-site through SCOPF analysis. Conductivity fluctuation analysis performed around T_c, provides evidence that dimensionality of fluctuations depends on the doping level in the mean field regimes. The inclusion of sub-μ sized BZO particles and nano-$BaTiO_3$ to the YBCO matrix bring about structural as well as dimensional fluctuation changes in the electrical transport properties. The characteristic scaling of the curves obtained from excess conductivity ($\Delta\sigma$) as a function of reduced temperature, ε for YBCO + x $BaZrO_3$ composites (x = 0, 1, 2.5, 5 and 10 wt.%) in 8 T magnetic field showed a crossover between two to three-dimensional (T_{LD}) behaviors in the mean-field region but the critical region is not witnessed due to smearing out of data points in high magnetic field like 8 T.

Study of magneto-resistance and vortex dynamics in YBCO superconductors has been done to get requisite information for properties such as critical current density, quantized flux trapping and activation energy. The activation energy and critical current density associated with magnetic field gives the vital inferences on inter and intra-granular behaviour. The resistive broadening in the tailing region due to application of magnetic field has been explained on the Ambegaokar–Halperin (AH) phase-slip theory.

When magnetic field is applied to type-II superconductors magnetic flux can penetrate in the form of Abrikosov vortices flux lines, each carrying a quantum of magnetic flux $\Phi_0 = h/2e$. As density of flux lines increases due to application of magnetic field these vortices form flux line lattice (FLL) due to interaction. In order to have a detail understanding of flux pinning mechanism, critical current density studies have also been carried out in YBCO + *x* $BaZrO_3$ (BZO) composites. The flux pinning effect of submicron BZO particles in the composites enhances the current density J_c from 8 x 10^4 A-cm^{-2} for pristine YBCO to 2 x 10^5 A-cm^{-2} for YBCO + 5 wt % BZO composite samples in field varying from 1 – 16 T at a temperature of 40 K.

Contents

Chapter 3

Experimental Techniques

Chapter 4

The effect of inhomogeneities in doped $YBa_2Cu_3O_{7-\delta}$

Chapter 7

Magneto-resistivity and current density in YBCO + BZO composites

Chapter 8

Conclusions

List of Tables

List of Figures

Chapter 1

Background and Motivation

CHAPTER 1

1. BACK GROUND AND MOTIVATION

The intent of this chapter is to provide a brief description of exotic phenomenon of superconductivity, superconductor as perfect diamagnet, types of superconductor with its applications. This chapter further includes the phenomenological models, GL and BCS theories of superconductivity, crystallographic structure of high temperature superconductors (HTSC) like $YBa_2Cu_3O_{7-\delta}$ (YBCO), role of defects, inhomogeneities, superconducting order parameter fluctuation (SCOPF), vortex pinning and fluctuations in understanding the superconductivity. The interplay between the intrinsic thermal fluctuations and extrinsic inhomogeneities are crucial in deciding the observed experimental results in HTSC. This chapter ends with a concise motivation of the present work incorporated in the thesis.

1.1. Superconductivity

For many years, it is known that the electrical resistance of a metal is proportional to its temperature. In 1911, the Dutch physicist Heike Kammerlingh Onnes in Leiden began cooling some mercury with liquid helium. He studied the resistance of metals at low temperatures and found that the resistance of mercury suddenly drops to zero when cooled below -269 ^{0}C (= 4 K) at 4.2 K [1]. The resistance of the metal completely disappeared and Onnes had discovered superconductivity. He was awarded the Nobel Prize in 1913 for liquification of Helium not specially for superconductivity. As the superconducting electrons travel through the conductor they pass unobstructed through the complex lattice. Because they bump into nothing and create no friction they can transmit electricity with no appreciable loss in the current and no loss of energy. Despite the broad range of compounds (both inorganic and organic) that are known to superconduct at very low temperatures, often below the boiling point of liquid helium, the highest superconducting transition temperature recorded before 1986 was 23.2 K for the alloy Nb_3Ge. Below transition temperature T_c, superconducting materials exhibit two characteristic properties:

- Zero electrical resistance (R = 0)
- Perfect diamagnetism (Meissner effect, χ = -ve)

Remarkably, the magnetic behavior of a superconductor is distinct from perfect diamagnetism. It will actively exclude any magnetic field present when it makes the phase change to the superconducting state. There is a critical magnetic field H_c, which, when exceeded, will destroy superconductivity.

In 1957 Bardeen, Cooper, and Schrieffer (BCS) put forth a ground breaking microscopic description of superconductivity that incorporated all previous theories, and explained recent developments [2]. The essence of BCS theory is that electrons in a superconductor pair via a weak attractive interaction due to phonons (lattice vibrations) that exist naturally in the crystal lattice. Since electrons are fermions, when they pair they form bosons, which are not restricted by the Pauli Exclusion Principle, and can thus all condense into a single quantum state (same energy state) forming condensate named Bose-Einstein Condensation.

The distance between individual electrons in each pair is denoted the coherence length, ξ and is a material dependent property of superconductors. BCS puts requirements on pairing, such that pairs of electrons must be of opposite spin and momentum, thus when a pair scatters, momentum is always conserved. This way, these electron pairs, known as Cooper Pairs, can move cooperatively through a crystal without losing forward momentum, and hence superconductivity [2, 3]. BCS theory was the first quantum mechanical description of superconductivity. While it allows a complete description of superconductivity from the point of view of individual particle interactions, it is complicated and difficult to use.

A dramatic change and a great breakthrough occurred in 1986 when Bednorz and Muller [4] discovered superconductivity around 35 K in the Ba-La-Cu-O system. Although this temperature was not very high, the discovery triggered the exploration of a whole class of similar materials, and transition temperatures above 90 K were soon reached in $YBa_2Cu_3O_{7-\delta}$. The discovery of Bednorz and Muller is break through because it crossed the BCS limit of transition temperature, Tc and called high temperature superconductors (HTSC). The transition temperature is above the boiling point of liquid Nitrogen which is abundantly available in nature.

The London theory of superconductivity was the first to describe the Meissner effect [5]. London theory states that a magnetic field impinging on a superconductor is screened exponentially over a characteristic length scale λ, known as the penetration depth [6]. Abrikosov used energy minimization and quantum mechanics arguments to come to the conclusion that magnetic field will penetrate a superconductor in a regular array of magnetic flux tubes [7, 8].

Each flux tube, called a vortex, contains a normal core of electrons where the magnetic field penetrates and superconductivity is destroyed. The area surrounding the vortices is superconducting and no magnetic field passes through. The presence of vortices explains the gradual transition of superconducting materials. As the material is subjected to changing magnetic fields, superconductivity gradually changes a function of the number of vortices induced in the material.

The last two decades brought substantial progress in physics of superconductivity due to the discovery and numerous subsequent investigations of high temperature superconductors. Such new materials have opened up promising possibilities of various applications in advanced technologies. The scientific problem of studying HTSC is one of the most prominent ones in solid state physics, with thousands of laboratories involved. Nevertheless the nature of HTSC impedes the expected technological progress necessary for practical applications. Superconductors have got tremendous applications in various fields. Some of them are listed below:

i) Medical diagnosis -Magnets for MRI machines.

ii) Computing technology-
   a) Cryotrons
   b) Memory devices.

iii) Electronics and measuring technology-
   a) Bolometer-receivers of thermal radiation
   b) Superconducting magnetic lenses.
   c) Masers.

iv) Nuclear power and space-
   a) Magnets for thermonuclear reactions
   b) Elementary particle accelerators.
   c) Bubble chamber
   d) Resonance pumps
   e) Gyroscopes.
   f) Magneto hydrodynamic (MHD) generators.
   g) Protection of astronauts from radiation.
   h) Superconducting Magnets for particle Accelerator

v) Transport and communication
   i. Levitating trains
   ii. Magnetic levitators

1.2. Perfect diamagnetism

The superconductor not only excludes external fields, it expels fields that had been established inside the conductor at higher (than critical) temperatures. The hallmark of superconductivity is exclusion of the internal field B an applied magnetic (H) field, unless the applied field exceeds a critical level (Fig.1.1). The induced magnetic field is strong enough to exclude the magnetic field inside the sample. Hence superconductors behave as perfect diamagnets.

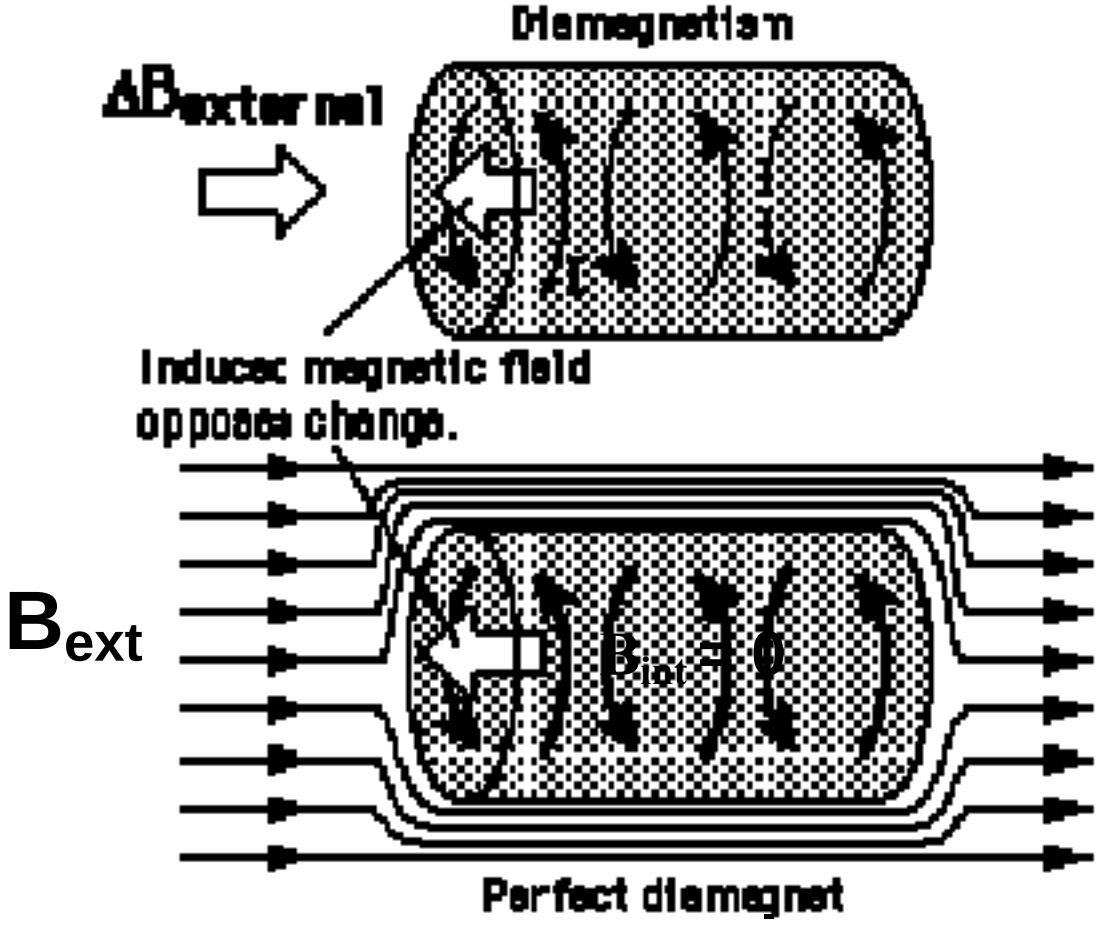

Fig. 1.1. Exclusion of magnetic field from the interior of the sample

Both the electrical and the magnetic properties are combined to specify the quality of the substance to superconduct at low temperature. Basically the superconductors are classified as type-I and type-II depending on their response to magnetic field. According to the behavior of Superconductors in the external magnetic (i.e. Meissner effect) these are categorized in to two groups: type I superconductor and type II superconductor.

1.3. Types of superconductors

There are many metals which exhibit zero resistivity at low temperatures and have the property of excluding magnetic fields from the interior of the superconductor (Meissner effect). They are called Type I superconductors. These superconductors are well described by the BCS theory which relies upon electron pairs coupled by lattice vibration. These are soft superconductors as small amount of magnetic field can destroy the superconducting properties and behave as normal materials. The critical current density is low as compared to the type –II superconductors.

Superconductors made from alloys are called Type II superconductors. Type-II superconductors usually exist in a mixed state of normal and superconducting regions. This is called a vortex state (Fig. 1.2), because vortices of superconducting currents surround filaments or cores of normal material. The superconductors allow complete flux expulsion up to a critical field Hc_1, called the lower critical field. Beyond this field, partial Meissner state is achieved with flux penetration in the sample at vortices up to a higher field Hc_2. In this range of the field, the substance still exhibits superconductivity which is destroyed beyond Hc_2. This type of superconductors is termed as type-II superconductors. The transition from the normal to the superconducting state is the consequence of a phase transition which occurs when temperature is lowered to a critical temperature T_c. In the mixed superconducting state (partial Meissner state) the applied field penetrates in form of quanta of vortex. Different states relating to magnetic field is depicted in Fig.1.3.

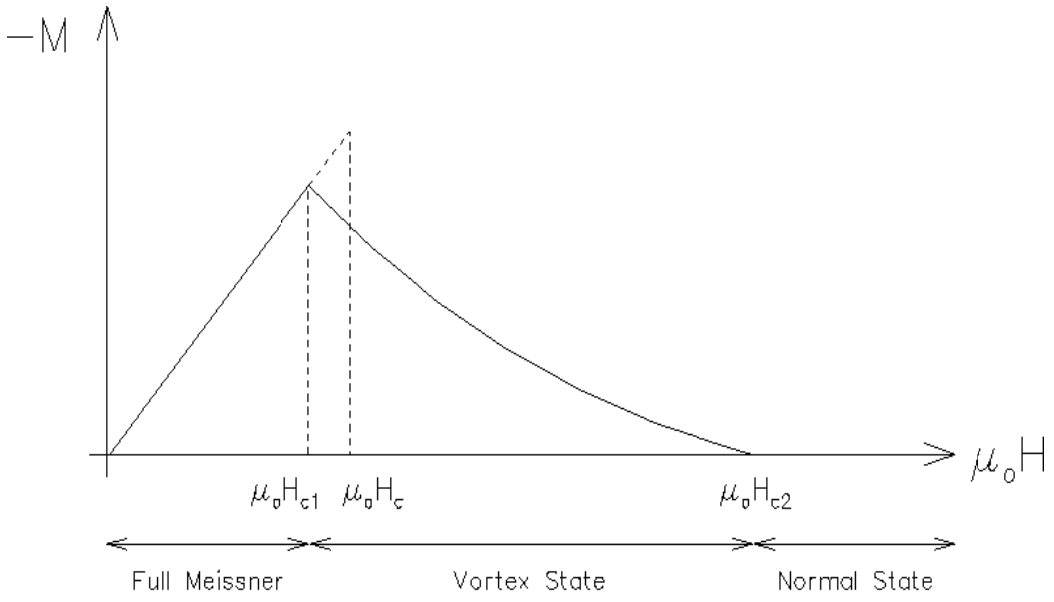

Fig. 1.2. M – H graph showing the different state of a type-II superconductors

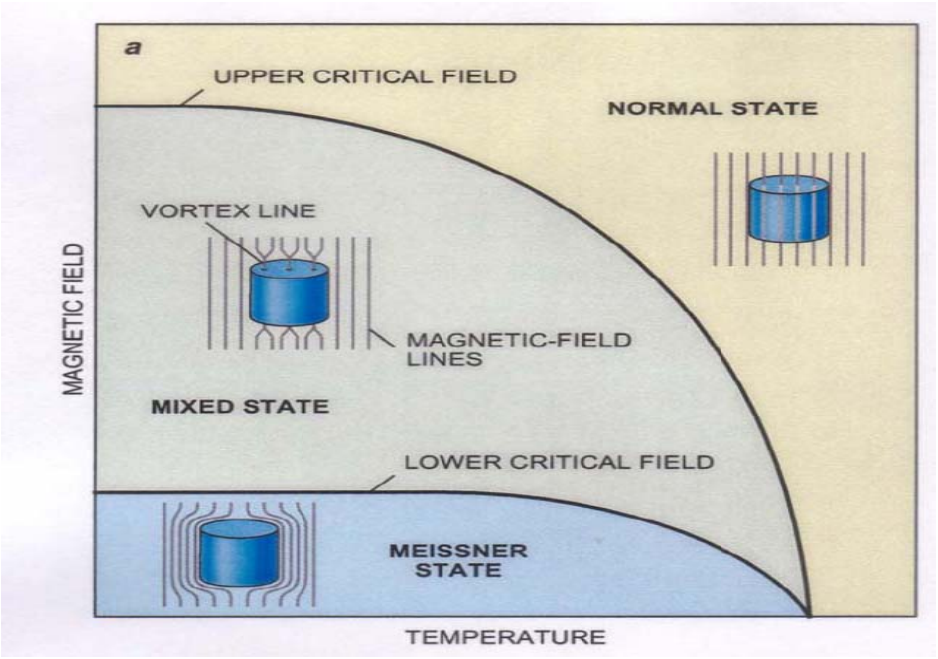

(Courtesy, Scientific American, Feb. 1993)

Fig. 1.3. Magnetic field and temperature phase diagram of type II superconductors

Superconducting state of metal exists only in a particular range of temp and field strength. It is possible to destroy the superconductivity by raising temperature above its critical temperature (T_c) or by applying the magnetic field having strength greater than certain value known as critical field strength.

The variation of critical field with temperature can be represented by

$$H_c = H_o [1-(T/T_c)^2]$$

H_c = critical field strength at Temperature T K

H_o = Maximum critical field strength occurring at 0 K

The field required to destroy superconductor is not necessarily external field. It may arise due to electric current flow in metal. The minimum current that can be passed in sample without destroying its superconductivity is called critical current (I_c).

1.4. Phenomenological models

To understand the superconductivity phenomena, various theories had been put forth. However none of them were suitable to explain the zero resistivity property accompanied by the Meissner state. The only successful theory known as BCS theory could explain the mechanism of superconductivity satisfactorily but did not specify what substance should superconduct at what temperature. The basic ingredient of this theory, the weak electron- phonon interaction even put a limit to the highest T_c achievable around 30 K. So the reach for higher T_c materials during that period met with little optimism.

The fundamental properties of superconductors are the lack of resistivity and the expulsion of any exterior magnetic flux (or perfect diamagnetism). These exceptional characteristics make superconductor materials of tremendous potential. The challenge is to find a superconductor at room temperature which is yet to be achieved. Before a microscopical description of superconductors became available, Ginzburg and Landau [9, 10] used a phenomenological approach to describe the normal-to-superconductor transition in the general frame of thermodynamical second-order phase transitions. The free energy density of a uniform sample is given by GL as [9, 11]:

$$F_s = F_n + \alpha(T) |\Psi|^2 + \beta(T) |\Psi|^4 + \text{ - -----} \quad (1.1)$$

Where β is a const. and $\alpha = \alpha_0 (t-1)$ and $t = T/T_c$. This α changes sign at T_c. Thus above T_c, $\alpha > 0$, F = 0, when the order parameter, Ψ = 0 for normal state ($T = T_c$). Thermal Fluctuation can rise from 0 to kT and Ψ is raised from 0 to δΨ (Fig.1.4 & 1.5).

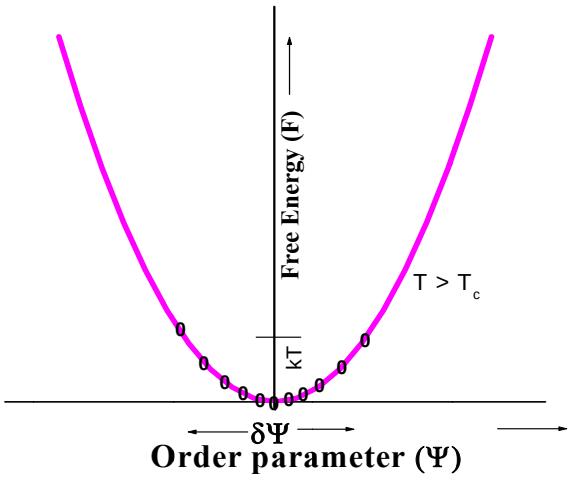

Fig. 1.4 Variation of order parameter with Gibbs free energy

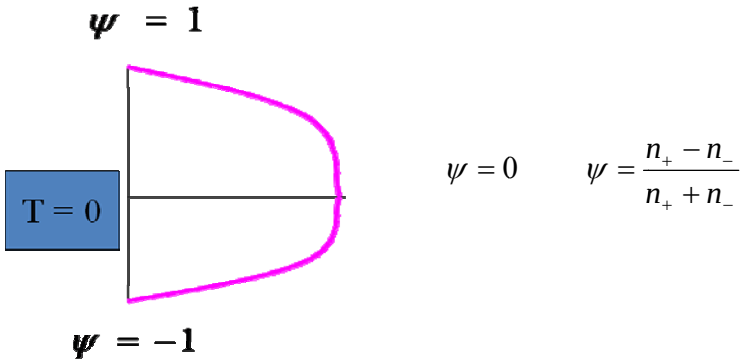

Fig. 1.5. Variation of order parameter ψ at T = 0 and at T = Tc in superconductors and n_+ and n_- are the no. of spins up and down respectively.

We can therefore consider the order parameter and implicitly superfluid density to be a very important physical quantity when describing the strength of the superconducting state and its stiffness to phase fluctuations. The linking of the order parameter to measurable quantities is done by using the London equations [6].

Within Ginzburg-Landau theory, the lower critical field H_{c1} and upper critical fields H_{c2} may be written as:

$$H_{c1}(T) = \frac{\phi_0}{4\pi\lambda(T)^2} \tag{1.2}$$

$$H_{c2}(T) = \frac{\phi_0}{4\pi\xi(T)^2} \tag{1.3}$$

1.5. Basic concepts

Already in 1935 F. London and H. London proposed a phenomenological description [6]. They more or less postulated proportionality between supercurrent and magnetic vector potential. The London equations describe perfect conductivity and flux expulsion. In 1950 the Ginzburg-Landau (GL) [12] theory was proposed as a general way to deal with second-order phase transitions. The idea is that the free energy close to the transition can be expanded as a polynomial in an order parameter. In the case of superconductors the order parameter is the density of electron pairs. This theory allows for treatments of a wide range of phenomena in superconductors, including superconducting fluctuations. The GL theory won general acceptance only after Gorkov [13, 14] showed that it can be derived from the BCS theory. The GL theory is now in many situations considered to be a convenient alternative to the rather complicated BCS theory.

The fact that the maximum transition temperature, T_c, is now higher than 77 K, the boiling point of nitrogen, greatly simplifies cooling the material can simply be immersed in liquid nitrogen. Previously, liquid helium had to be used, which costs more than ten times as much and is more difficult to handle. A theoretical explanation of superconductivity was not found until 1957, when Bardeen, Cooper and Schrieffer (BCS) [2] presented their theory based on electron pairing. The BCS theory and its extensions have been successful in describing the conventional, but there are indications that they fail for the new high-temperature superconductors, where the electron pairing mechanism is still not established.

Theoretical models for superconductivity will now be briefly described, followed by a short introduction to high-temperature superconductors. The concept of superconducting fluctuations will then be introduced. As mentioned above, the mechanism behind superconductivity was not understood until 1957, when Bardeen, Cooper and Schrieffer (BCS) [2] presented their detailed microscopic theory. Much earlier, however, many phenomena of superconductors could be well described using phenomenological models.

The arguments in the BCS theory can be divided into three parts, which together explain superconductivity:

1. Electrons form pairs in the presence of an attractive force. If there is an attractive interaction between electrons at the Fermi surface, no matter how weak, stable pairs will form from electrons with mutually opposite wave vectors and opposite spins. The possibility of pair formation was pointed out already by Cooper [11], and the pairs are called Cooper pairs.
2. The attraction between electrons is caused by crystal-lattice vibrations (phonons). This part of the theory will probably have to be partly modified for the high-temperature superconductors.
3. An energy gap opens up in the electron density of states at the Fermi surface. In a simplified picture, resistive scattering of electrons in a superconducting material requires excitation across the energy gap, and cannot easily occur.

The original BCS theory only applies well to superconductors with weak electron-phonon coupling. Twenty years after the discovery of superconductivity in high-temperature copper oxide superconductors (HTSC), there is still no viable explanation as to what holds the electrons paired together in a Cooper pair. The main characteristics of HTSCs are very similar to the ones observed in classical superconductors, i.e. they show zero electrical resistivity and magnetic shielding (Meissner effect). However, from the very beginning of their physical investigation, it became obvious that such high transition temperatures cannot be explained by electron-phonon coupling and the classical BCS theory of superconductivity, so it was thought that pairing might have an electronic or magnetic nature. It is not only the higher transition temperature that differentiates cuprate superconductors from the classical superconductors but also HTSC show a very complex nature across all their physical properties and exhibit new fundamental physics. Superconductivity is produced by introducing doping in ceramic Mott insulators, so it is not

surprising that these materials are dominated by strong electron correlations (in other words, the on-site Coulomb repulsion between electrons is stronger than the kinetic energy).

Another very important difference between classical superconductors and HTSC is the extent to which their transition temperatures are affected by phase fluctuations of the order parameter. In the case of the classical superconductors, phase fluctuations are not important and the transition temperature is determined by the energy gap Δ.

In addition, the effects of fluctuations are expected to be more pronounced in the under doped region and it is generally believed that phase fluctuations are largely responsible for the suppression of superconductivity when holes are removed from optimally doped CuO_2 planes. In the pseodo-gap state there are preformed superconducting pairs but strong phase fluctuations prevent the occurrence of long-range phase coherence until T_c [15]. The fluctuations hypothesis also accounted for the extremely wide critical region near T_c (around 10 K) in $YBa_2Cu_3O_{6.95}$ crystals [16].

1.6. Basic crystallographic structure of YBCO

All high-T_c superconductors have a layered structure, in which the presence of CuO_2 layers plays a determinant role in their superconducting character. The 2D structure of the cuprate systems is dictated by these CuO_2 layers. The lattice constants in the ab-plane (~3.8 A^0) are governed by the covalently bonded Cu-O bond length (~1.9 A^0). The intercalating metal-oxygen planes are "stretched" to match this dimension of the unit cell in the ab-plane. The atoms in the intercalating planes respond to this stretching by relaxing their positions to form acceptable bond lengths. Superconductivity is believed to be associated with conduction in the Cu(2)-O ab-plane. However, changes in the material features like oxygen content, chemical substitution, pressure etc. which affect superconductivity also affect the bonding along the c-axis drastically.

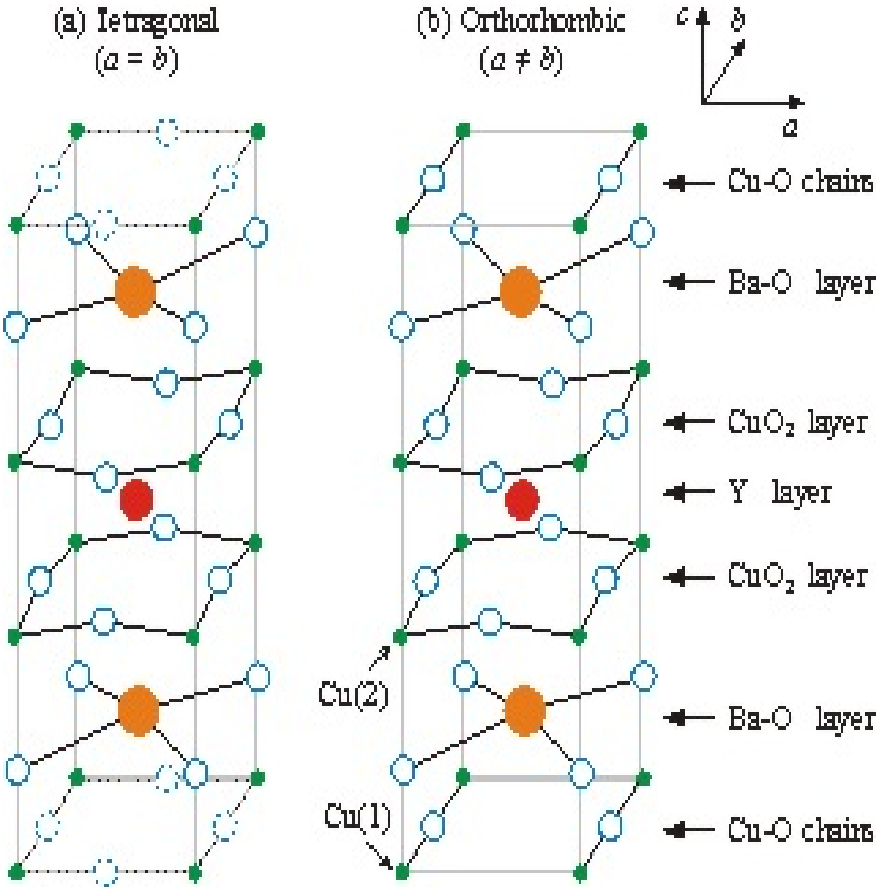

Fig. 1.6. Structure of $YBa_2Cu_3O_{7-\delta}$ showing oxygen vacancies (defects) (a) tetragonal and optimal oxgen content (b) Orthorhombic with different layers of CuO chains and CuO_2 planes.

The carriers only move along these planes, while the other components act as charge reservoirs that regulate the charge density in the CuO_2 planes. In YBCO, each unit cell contains two CuO_2 planes, separated by a plane of Yttrium atoms, and sandwiched by two Barium oxide layers. The compound can present two possible symmetries, tetragonal or orthorhombic, depending on the amount and distribution of oxygen in the final Cu-O layers which close the cell. For low oxygen concentration ($\delta<1$), oxygen atoms are randomly dispersed in their four possible sites between Cu in the top and bottom planes, leading to a tetragonal structure (scheme (a) in Fig.1.6). However, for δ close to zero, oxygen atoms are ordered occupying only inter-Cu sites along the *b*-axis of these planes, and this leads to a orthorhombic structure (In this case, the Cu-O atoms form chains more than planes, and so they are referred. Most of the processes to

obtain YBCO samples result in poorly oxygenated, and then tetragonal structures. In these cases, samples must be oxygenated to obtain the superconducting orthorhombic phase. In order to achieve a material with the optimum oxygen content (optimally doped), samples must be heated in flowing oxygen, at around 400-550 ºC, during a period which depends on the size of the sample. YBCO is a type II superconductor. The flux of carriers along their CuO_2 layers causes a high anisotropy in these materials, whose properties are different in the ab-plane directions and the *c*-axis direction.

YBCO is by structure a defect perovskite. It consists of layers. The boundary of each layer consists of planes with square planar CuO_4 units having four vertices. The planes are sometimes slightly puckered and perpendicular to the planes CuO_4 ribbons share two vertices. The Yttrium atoms are sandwiched between the CuO_2 planes and the barium atoms are found between the CuO_4 ribbons and the CuO_2 planes. Regarding the crystal structure, $YBa_2Cu_3O_{7-\delta}$ is complicated because of its variable oxygen content and two different types of four coordinated Cu. Independent of δ Y123 has two closely spaced (3.2 Å) Cu-O plane separated by a Y plane. These two adjacent Cu-O planes are 8.2 Å from the neighboring sets of Cu-O plane. The phase transition of $YBa_2Cu_3O_{7-\delta}$ superconductor occurs at oxygen of 6.5 that means the structure of the superconductor changes from tetragonal (Y123-O_6) to orthorhombic (Y123-O_7). The transition temperature of Y123-$O_{6.5}$ is 63 K and of Y123-O_7 is 93 K.

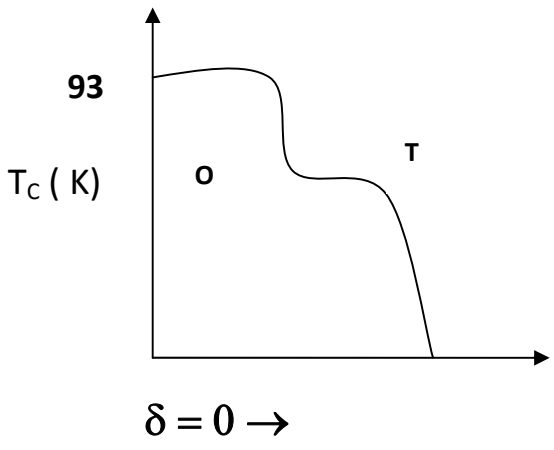

Fig. 1.7. Behaviour of critical temperature (T_c) in $YBa_2Cu_3O_{7-\delta}$, with the δ content.

1.7. Defects in Cuprate superconductors

High T_c superconducting materials present the most complex and elegant structural features amongst the superconductor discovered till date. Particularly in copper oxide superconductors there are many atoms per unit cell with bonds of varying strength and nature. The crystal chemistry in cuprate superconductors is also extremely complicated. Due to broad range of composition high defect concentrations are common in these systems. Ever since the discovery of superconductivity in cuprates it has been realized that defects play a crucial role in controlling the superconducting parameters in these systems. Bednorz and Muller's discovery of superconductivity in La-based system [17] involved incorporation of defects as divalent impurities (Ba/Sr) in place of La. The other high T_c systems having still higher T_c (YBCO, Bi/Tl2223, Hg1223), in addition to accommodating substitution defects, can contain defects of very different kinds like oxygen vacancies, interstitial oxygen, anti-site disorder [18], stacking faults, twin and grain boundaries.

In $YBa_2Cu_3O_{7-\delta}$, the defects are oxygen vacancies located in the basal plane of the structure. The fully oxygenated ($\delta = 0$) structure (b) has the basal plane with Cu-O-Cu-O...chains extending along the b-axis and no oxygen atoms between the Cu ions, along the a-axis. In the defected ($\delta \neq 0$) state, the oxygen atoms can occupy in a random or ordered way, available lattice sites in the chain region of the structure. The range of defect concentrations in this compound is unusually large, allowing the properties to be varied from insulating to superconducting. Though not all the copper oxide superconductors show such a large defect concentration range, most of them can be understood in terms of a doping mechanism that depends on defects in the charge reservoir layer [18]. With so many possibilities, it is not surprising that structural studies have not been entirely definitive in sorting out as to how these defects control the carrier concentration in the CuO_2 conduction planes (Fig. 1.6)

Amongst the many problems as outlined above, the complex crystal structure of the cuprates with many atoms per unit cell has posed yet another problem in identifying and isolating the role of specific ions or group of ions for the occurrence of superconductivity in these systems. Site specific substitutional studies involving both iso-and aliovalent ions have been carried out and their effects on superconductivity and normal state properties have been probed [19]. In $YBa_2Cu_3O_7$ type superconductors for example, no significant change in T_c was found by substitution of rare earth metals (Nd, Sm, Yb, Eu, Ho, Gd, Dy) except Pr, Tb, and Ce at Yttrium

sites [20]. But doping of Sr, Ca, or Pb at Ba sites and Mn^{2+}, Ni^{2+}, Zn^{2+} for Cu in the CuO_2 conduction layer leads to lowering of T_c. The nature of the charge reservoir layer and the mechanism of charge transfer has been studied through preferential chemical substitutions by aliovalent ions like Ga^{3+}, Al^{3+}, Fe^{3+}, Co^{3+} etc. in the CuO basal plane. Due the substitution, the structural phase change from orthorhombic to tetragonal is observed without appreciable change in T_c. So it gives an impression that structural features in the ab-plane may not have much relevance to superconductivity.

However, it has been pointed out that though on a macroscopic scale a transition from orthorhombic to tetragonal structure occurs, oxygen ordering in the local scale still exists [21]. The importance of such local structural details on superconductivity has been demonstrated by [22-24]. The deliberately created substitutional defects therefore have been useful as probes of the properties of copper oxide superconductors.

1.8. Inhomogeneity and secondary phases in Cuprate superconductors

Since the discovery of $La_{2-x}Ba_xCuO_4$ in 1986 [17], despite of much progress in theory, material development, experimental techniques and measurement, many questions still remained unanswered. Much of the difficulty in studying the properties of HTSC's arises from the inhomogeneity of their superconducting behavior, which arises from physical and electronic structure effects. Bulk measurements of the fundamental quantities of superconductors yield limited information about the underlying mechanism because such measurements are averages of locally varying properties. The presence of grain boundaries in various forms of polycrystalline samples (bulk sinters, thick films, tapes and wires) is in many cases, a natural consequence of the preparation conditions from powdered precursors. Sintering at elevated temperatures does not eliminate the intra- and inter-grain boundaries completely. They remain in the samples to a sizable fraction and limit the applicability of these ceramic superconductors. The grain boundaries make the sample brittle deteriorating their mechanical properties. In addition, these high resistive grain boundaries acting like tunnel junctions reduce critical transport current density (J_c) of the grains [25-27]. The cuprate structure being highly anisotropic with resistivity along c-axis, ρ_c orders of magnitude higher than that in the ab-plane, ρ_{ab} further imposes restriction on the flow of current depending on the alignment of the grains. The greater the angle of misorientation at a grain boundary, the worse is the critical current [28]. This is quite different

from that in the case of conventional superconductors where one deliberately introduces grain boundaries to raise the critical current density. Grain boundaries to high T_c superconductors pose interesting and difficult problems in complex oxides whose solutions are essentially vital to practical and related fundamental applications. In cuprate superconductors, the relevance of the grain boundary issue becomes prominent because of their much shorter coherence length, high superconducting anisotropy and reduced dimensionality [29]. This is at variance with classical superconductors whose much higher coherence length is reduced by the presence of grain boundaries.

The layered structure of HTSC with complex crystal chemistry and the inherent granularity lead to strong structural disorder at the microscopic and the mesoscopic levels respectively. A large number of studies have been devoted to investigate the interplay between the superconducting order parameter fluctuation (SCOPF) and the inhomogeneities in HTSC. The inhomogeneities occur at widely varying length scales as in single crystals, grain aligned films, melt-textured and sintered samples. The mesoscopic inhomogeneities like grain boundaries, cracks, voids etc. having much larger length scale than ξ and being temperature independent, do not influence the SCOPF region [30]. These inhomogeneities strongly influence the region, where the zero resistance state is approached from above. The microscopic inhomogeneities such as structural defects (twin boundaries, stacking faults) and chemical imperfections (oxygen deficiencies etc.) occur inside the grains. The length scale of these inhomogeneities is smaller than that of the mesoscopic inhomogeneities, but still larger than ξ. These inhomogeneities therefore are expected to have negligible effect on the SCOPF region [31]. However, many studies have shown that the inhomogeneities crucially influence both the critical and the mean field region of SCOPF [32, 33]. The critical region for example expands with the increase of secondary phases in $YBa_2Cu_3O_{7-\delta}$ (YBCO) and its composites [34]. The inhomogeneities also affect the Lawrence-Doniach crossover temperature, T_{LD} in the mean field region.

1.9. Inhomogeneity and vortex pinning

In type II materials magnetic field penetrates the material up to certain length dictated by the penetration depth λ. Superconductivity is destroyed beyond the limiting field Hc_2. The field inside the material decays exponentially. Abrikosov [35] used energy minimization and quantum

mechanics arguments to come to the conclusion that magnetic field will penetrate a type II superconductor in a regular array of magnetic flux tubes. Each flux tube, called a vortex, contains a normal core of electrons where the magnetic field penetrates and superconductivity is destroyed. The area surrounding the vortices is superconducting and no magnetic field passes through. Quantum mechanics dictates that each vortex must contain exactly the same amount of magnetic flux φ_0 where $\varphi_0 = hc/2e = 20.7$ Gauss μm^2. This differs from the ordinary quanta of magnetic flux by a factor of two, because electrons are in a superconductor are paired. The presence of vortices explains the gradual transition of superconducting materials. As the material is subjected to changing magnetic fields, superconductivity gradually changes a function of the number of vortices induced in the material.

While in an ideal material vortex spacing would be equal, real materials have crystal inhomogeneities that lead to varying amounts of superconductivity and hence varying penalties that must be paid to create a vortex. The vortex motion is a dissipative force and leads to the destruction of superconductivity. The presence of both normal and superconducting domains brings into question whether perfect conductivity still holds in the mixed state. In real materials, inhomogeneities can serve as pinning sites for vortices against the Lorentz force. Under low to moderate currents, vortices will entirely resist motion, and superconductivity will remain. If the Lorentz force, however, exceeds the strength of the pinning site, then the vortices will move and superconductivity will be lost. The questions of what causes pinning and how strong pinning forces are central to the aim and motivation of the experiment. Understanding pinning is crucial to the application of superconductors with high currents and in high fields. It is also a fascinating basic physics question. Since current capacity is directly correlated to vortex pinning strength, vortex pinning is an essential characteristic of superconductivity that requires more study. Much effort has been put towards the study of pinning of vortices through the introduction of inhomogeneities, but primarily from a bulk-flow point of view. Artificial pinning sites are the next step towards more efficient superconductor technology. By finding out what causes the strongest pinning sites, and how to create and arrange them in the crystal, material manufacturers could create higher current capacity superconductors. We have discussed the enhancement of pinning sites and pinning effect in later chapters.

1.10. Superconducting fluctuations and fluctuation conductivity

Due to the specific properties of HTSC, i.e. an extremely short coherence length, a high value of the critical temperature, a low density of charge carriers, and the strong anisotropy determining the effective dimensionality of charge motion. An understanding of the role of fluctuations is also believed to be necessary in advanced technological applications, since the fluctuations may destroy the superconducting state. The effects of fluctuations on static properties and on electrical and thermal transport properties in the a-b plane and along the c axis, the effect of a magnetic field on phenomena, specifically in layered compounds are still undecided. The effect of a magnetic field is still not clear. Specific fluctuations of the vortex lattice in HTSC ceramics as compared to conventional superconductors are still intensely debated. In its clear presentation of the experimental, theoretical and simulation aspects, together with the comprehensive list of references is still unevidenced.

Although a material exhibits superconductivity only below T_c, there are superconducting electron pairs present also above T_c. These pairs are referred to as superconducting fluctuations as they are caused by thermodynamic fluctuations, which continuously create and destroy electron pairs. Due to thermal fluctuation annihilation and creation of cooper pairs occurs. There is always a certain number of pairs present: the closer to T_c, the more pairs. It is, however, only below T_c that a superconducting condensate penetrates the material and the resistivity is zero and global superconductivity sets in. Superconducting fluctuations have a number of measurable effects. They influence, for example, electrical, thermal, and magnetic properties. Fluctuations have particularly large effects in HTSC, partly because of their high anisotropy. The focus of the present thesis is on Superconducting Order Parameter fluctuation (SCOPF) effects on the electrical conduction in doped and composite YBCO superconductors associated with inhomogeneities and secondary phases.

There are several reasons to study fluctuations. Fluctuations may be used to solve various purposes like:

(i) To determine material-dependent microscopic quantities, for example coherence lengths and critical current density of the sample. There are theoretical calculations of the effects of fluctuations. The theoretical formulae contain several microscopic quantities as parameters. By adjusting the values of these parameters until agreement with experiments is obtained, the values of the microscopic quantities can be determined.

(ii) To study fundamental mechanisms, such as pairing symmetry and the role of the chains in $YBa_2Cu_3O_{7-\delta}$.

(ii) To explain anomalies in the electrical conduction and other properties. There are several puzzling observations, for example the c-axis resistivity peak and a negative magnetoresistivity, which have been difficult to understand. It has been shown that some of these effects can be due superconducting fluctuations.

The temperature dependent curve gives an observable effect of fluctuations that can be seen in Fig. 1.8. The resistivity curve is linear, but bends down just above T_c. This decrease in resistivity can be attributed to the superconducting fluctuations.

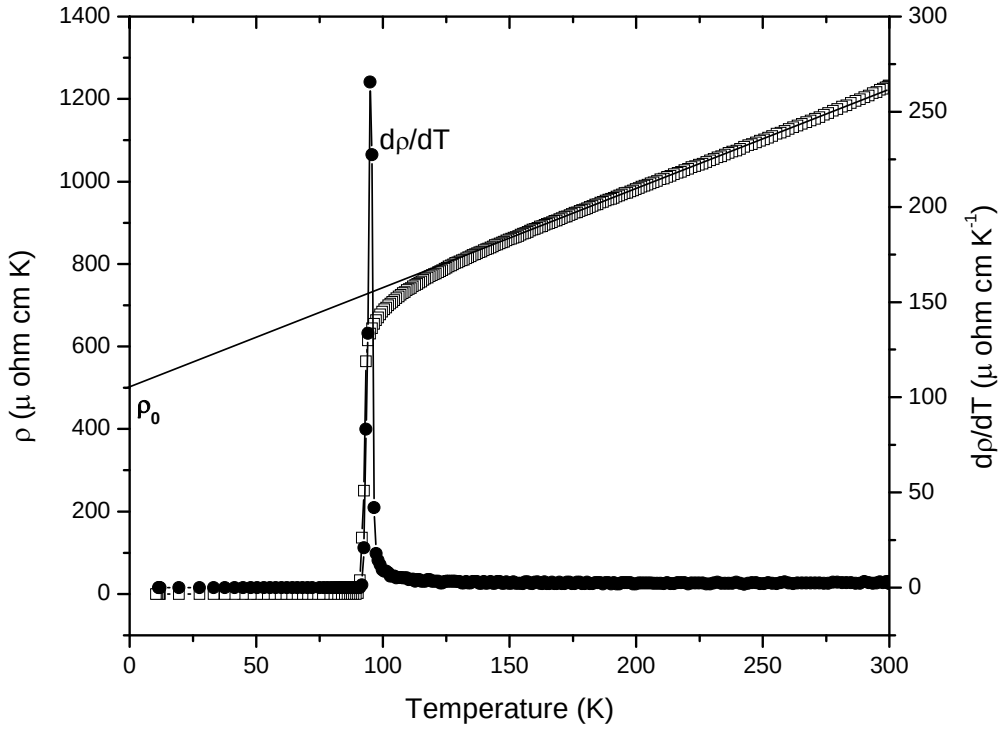

Fig. 1.8. Resistive transition and regular resistivity behavior extrapolated from the normal behavior. Linear fitting of resistivity in the temperature range 150 to 250 K and extrapolated to 0 K gives resistivity slope ($d\rho/dT$) and residual resistivity (ρ_0) for YBCO (pure) sample.

Unfortunately, the fluctuation conductivity is a quantity that is difficult to measure accurately. The reason is that such measurements depend on an extrapolation of the resistivity from higher

temperatures. Although this might seem to pose few problems in the case shown here, where the resistivity is almost perfectly linear outside the fluctuation regime, there are many cases, for example $YBa_2Cu_3O_{7-\delta}$ with reduced oxygen content, where the resistivity may be nonlinear also well above T_c, and a direct extrapolation is infeasible. The determination T_c is done in different ways but the peak observed from $d\rho/dT$ gives the mean field temperature is taken as T_c for accuracy.

Superconducting fluctuations have a number of effects on superconductors. They influence the magnetic susceptibility, the specific heat, the electrical and thermal conductivities and other properties. Although the effects of fluctuations were studied already in conventional superconductors, there was a major revitalization of the field after the discovery of the high-temperature superconductors, in which the effects are large and easy to observe. The emphasis of the present thesis will be on Superconducting Order Parameter fluctuation (SCOPF) effects in the conductivity of $YBa_2Cu_3O_{7-\delta}$, where the famous Lawrence-Doniach model [36] is introduced and the standard expressions for fluctuation conductivity and magnetoconductivity in HTSC are presented, along with several extensions that cover specific cases or problems. First, however, the early history of fluctuations will be briefly accounted for and a short introduction to the theory of fluctuations will be discussed in chapter 2 and also in later chapters.

1.11. Fluctuation conductivity and inhomogeneities

The interplay between the intrinsic thermal fluctuation effects around the superconducting transition and the extrinsic inhomogeneity effects associated with stoichiometric and structural inhomogeneities at different length scales was already an important problem in low temperature superconductors (LTSC). For instance, in summarizing the effects of the thermal fluctuations of Cooper pairs on the electrical resistivity, $\rho(T)$, above the superconducting transition in metallic films, effects that had been actively studied in the last ten years, Kosterlitz and Thouless concluded that the onset of the observed rounding of $\rho(T)$ "may alternatively be a result of film inhomogeneities"[37]. In high temperature superconducting cuprates (HTSC), the dilemma between sample inhomogeneities and thermodynamic fluctuations above T_c was earlier stated by Bednorz and Müller in their seminal work, [17] although they formulated the alternative in an opposite way to that done by Kosterlitz and Thouless for LTSC´s: After having indicated that the observed rounding of $\rho(T)$ around T_c in their LSCO compounds may be due to inhomogeneities,

Bednorz and Müller concluded that "the onset (of the ρ (T) drop) can also be due to fluctuations in the superconducting wave functions".

In fact, mainly due to the smallness of the superconducting coherence length at 0 K, ξ (0) and its anisotropic nature in all directions (both are of the order of the interatomic distances), those are associated with the intrinsic thermal fluctuations and with the extrinsic inhomogeneities, may be very important in the HTSC. This is mainly due, in the case of the thermal fluctuations, to the fact that a small ξ(T) leads to a small coherent volume, which will contain very few strongly correlated Cooper pairs. These fluctuation effects are also enhanced by the layered nature of the HTSC around their superconducting transition. [38]. In the case of the inhomogeneities, the smallness of ξ(T) makes the different superconducting properties of these materials very sensitive to the presence of inhomogeneities, even when they have very small characteristic length, of the order of ξ(T). In addition, their layered nature and the complexity of their chemistry enhance the probability of the presence of extrinsic inhomogeneity effects in real HTSC compounds. When they are present at long length scales (i.e., at length scales much bigger than any characteristic length in the system, as the magnetic field penetration length or, mainly, the superconducting coherence length, ξ(T), even for temperatures relatively close to T_c), these inhomogeneities will not directly affect the thermal fluctuations themselves, but still they may deeply affect, together with the thermal fluctuations, the measured behaviour of any observable around the superconducting transition. [39].

1.12. Motivation

In the present thesis, the challenge is to develop a concise understanding of some our results on the interplay between the inhomogeneities, secondary phases and the thermal fluctuations around the controversial superconducting transition. In particular, we will indicate through some examples how the intrinsic effects (associated with the thermal fluctuations) are affected by the extrinsic ones (associated with inhomogeneities). Aim of the work is to illustrate the fact that in analyzing an anomalous critical behaviour of any HTSC sample it is important to carefully check the possible presence of extrinsic inhomogeneity effects. How the behaviour of paraconductivity is affected by the presence of inhomogeneities. We address the problem around superconducting transitions and the role of inhomogeneities and SCOPF effects in a set of $YBa_2Cu_3O_{7-\delta}/BaZrO_3$ and $YBa_2Cu_3O_{7-\delta}/BaTiO_3$ composite samples. We show that BZO can induce inhomogeneities

both at the mesoscopic and the microscopic level. The mesoscopic inhomogeneities arising due to most of the BZO residing at the grain boundaries strongly influence the tailing region below T_c and the critical regions just above this temperature. A small fraction of Ti in $YBa_2Cu_3O_{7-\delta}/BaTiO_3$ composite diffusing into the grains brings about microscopic inhomogeneities in the form of local T_c variation. Since T_c inhomogeneity has been shown to have insignificant influence on the SCOPF region [30], we explain the strong influence of $BaTiO_3$ and $BaZrO_3$ content in the composites on the mean field region of electronic structure of YBCO. The detail is discussed in the later chapter.

The discussions focus on:

(i) Superconducting fluctuations in the vicinity of the critical transitions;

(ii) Superconductivity fluctuations near the percolation transition; and

(iii) Fluctuations of the vortex lattice at the lattice melting temperature.

The main purpose of this study is to explore the physics of doped and composite cuprate superconductors near the superconducting transitions through the evaluation of SCOPF and the effects of inhomogeneities and secondary phases for YBCO. While the study of superconductivity in doped and composite systems of YBCO, it is crucial for understanding superconductivity, its exploration was previously limited due to the lack of optimal concentrations of dopants in the homogeneous superconducting samples in this region of the phase diagram.

This thesis is organized as follows. In Chapter 2, review of literature for the basic properties of superconductors, the main characteristics of cuprate superconductors with a special focus on phase fluctuations. Chapter 3 describes the experimental techniques used for sample preparation and their characterizations. In Chapter 4, focus has been drawn for understanding the role of inhomogeneities and secondary phases in cuprate superconductors. Chapter 5 explains the method and analysis of superconducting order parameter fluctuation (SCOPF) behaviors in Ca and Zn doped samples of YBCO. This study has been extended in Chapter 6 for $BaTiO_3$ (BTO) and $BaZrO_3$ (BZO) composite samples of YBCO. Finally, Chapter 7 focuses on magnetoresistivity and its response to SCOPF parameters. Chapter 8 deals with conclusions and important findings of the present work. It gives future direction to work on the related aspects.

References

[1] H.K. Onnes, Communications from the Physical Laboratory of the University of Leiden (1911).

[2] J. Bardeen, L.N. Cooper, and J.R. Schrieffer, Physical Review, 108 (1957) 1175.

[3] C. Kittel, Introduction to Solid State Physics, 7th Edition (John Wiley and Sons, New York, (1996) 446.

[4] G. Bednorz and K.A. Muller, Possible High T, Superconductivity in the Ba-La-Cu-O System (Z. Phys B, 64 (1986) 189.

[5] W. Meissner, R. Ochsenfeld, A New Effect Concerning the Onset of Superconductivity (Naturwissenschaften), 21 (1933) 787.

[6] F. London and H. London Proceedings of the Royal Society of London 71 (1935) A149.

[7] A. A. Abrikosov, Zh. Eksperim. i. Teo. Fiz**.,** 32 **(**1957) 1442.

[8] M. Tinkham, Introduction to Superconductivity 2nd Edition (Dover, New York, 1996)

[9] V. L. Ginzburg, Sov. Phys. Solid State 2 (1960) 1824.

[10] F. James Annett, Superconductivty, Superfluidity and Condensate, Oxford University Press

[11] L. N. Cooper, Phys. Rev. 104 (1956) 1189.

[12] V. L. Ginzburg and L. D. Landau, Zh. Experim. i. Teor. Fiz. 20 (1950) 1064.

[13] L. P. Gorkov, Sov. Phys. JETP 9 (1959) 1364.

[14] L. P. Gorkov, Sov. Phys. JETP 10 (1960) 998.

[15] J. Corson, R. Mallozzi, J. Orenstein, J. N. Eckstein, and I. Bozovic. Nature, 398 (1999) 221.

[16] S. Kamal, D.A. Bonn, and N. Goldenfeld et al. Physical Review Letters, 73 (1994) 1845.

[17] J.G. Bednorz and K.A. Muller, Phys. Rev. Lett. 52 (1984) 2289.

[18] J. D. Jorgensen, Physics Today 44 (1991) 34.

[19] A.V. Narlikar, C.V. Narasimha Rao and S.K. Agarwal (Nova Science Publications, New York, 1989), p.341.

[20] R. Beyers, T.M. Shaw, Solid State Phys. 42 (1989) 135.

[21] P. H. Hor, L. Gao, R.L. Meng, Z.J. Huang, Y.Q. Wang, K. Forster, J. Vassilious, C.W. Chu, M. K. Wu, J.R. Ashburn and C.J. Torng, Phys. Rev. Lett. 58 (1987) 911.

[22] B. W. Veal, H. You, A.P. Paulikas, H. Shi and J.W. Downey, Phys. Rev. B 42 (1990) 4770.

[23] B. W. Veal and A.P. Paulikas, Physica C 184 (1991) 321.

[24] H. Shaked, J. D. Jorgensen, B. A. Hunter, R. L. Hitterman, A. P. Paulikas and B.W. Veal, Phys. Rev. B 51 (1995) 547.

[25] Sangmin Lee, Jaehong Park, Gwangseo Park and Kiejin Lee, Supercond. Sci. Technol. 9 (1996) A5

[26] P.H. Hor, L. Gao, R.L. Meng, Z.J. Huang, Y.Q. Wang, K. Forster, J. Vassilious, C.W. Chu, M.K. Wu, J.R. Ashburn and C.J. Torng, Phys. Rev. Lett. 58 (1987) 911.

[27] B.W. Veal, H. You, A.P. Paulikas, H. Shi and J.W. Downey, Phys. Rev. B 42 (1990) 4770.

[28] D. Dimos, P. Chaudhuri, I. Mannhart, F. Legoues, Phys. Rev. Lett. 61 (1988) 219, Phys. Rev. B 41 (1990) 4038.

[29] M. Prester, Supercond. Sci. Technol. 11 (1998) 333.

[30] J. Maza and F. Vidal, Phys. Rev. B 43 (1991) 10560.

[31] E.J. Cukauskas and L.H. Allen, J. Appl. Phys. 84 (1998) 6187.

[32] D.K. Aswal, A. Singh, S. Sen, M. Kaur, C.S. Viswandham, G.L. Goswami and S.K. Gupta J. Phys. and Chem.of Solids 63 (2002) 1797.

[33] T. Sato, H. Hakane, S. Yamazaki and N. Mori, Physica C 372 (2002) 1208.

[34] A. Mohanta and D. Behera, Physica C 470 (2010) 295.

[35] A. A. Abrikosov, (Zh. Eksperim. i. Teo. Fiz., 32 (1957) 1442.

[36] W. E. Lawrence and S. Doniach, in Proc. 12th Int. Conf. on Low Temp.Phys., edited by E. Kanda (Keigaku, Tokyo, 1971), p. 361.

[37] J.M. Kosterlitz and D. Thouless, in Progress in Low Temperature Physics, Edited by D.F. Brewer (North-Holland, Amsterdam) VIIB (1978) 271.

[38] A. Diaz, J. Maza and F. Vidal, Physical Rev. B 55 (1997) 1209.

[39] J.A. Veira and F. Vidal, Physica C 159 (1989) 468.

Chapter 2

Review of Literatures

CHAPTER 2

2. REVIEW OF LITERATURES

2.1. Introduction

This chapter deals with the multidimensional representation of chronological development of superconductivity. This is followed by brief literature review concerning the research work incorporated in this thesis.

Chronological development in the field of superconductivity

- 1911- Superconductivity was discovered by Heike Kamerlingh Onnes in mercury at the boiling point of liquid helium [1].
- 1931- Superconductivity in alloys was discovered by W.J. de Haas and W.H. Keesom [2].
- 1933- The expulsion of a magnetic flux from the interior of a metal cooled below its superconducting transition temperature - Meissner effect was demonstrated by Walther Meissner and his colleague Robert Ochenfeld [3].
- 1934- Cornelius Gorter and H.B.G. Casmir proposed the two fluid models [4].
- 1935- Famous London theory was developed by London brothers: Fritz London and Heinz London [5].
- 1950- Vitaly Ginzburg and Lev Landau developed a theory of superconductivity based on electrodynamics [6]. The role of phonon in superconductivity was discovered by Herbert Frohlich [7]. Maxwell and Renold [8] independently discovered the isotope effect of superconductivity.
- 1953- The concept of coherence length (a characteristic distance within which superconductivity cannot change appreciably) was proposed by Brian Pippard [9].
- 1956- The unstable Fermi Sea in the presence of an attractive interaction between electrons responsible for the formation of Cooper pairs was shown by L.N. Cooper [10].
- 1957- Bardeen, Cooper and Schrieffer proposed the microscopic theory (BCS) of superconductivity [11].

- 1960- Tunneling of Quasiparticles across a metal and superconductor junctions was discovered [12].
- 1961- Deaver and Fairbank [13] showed that the flux can exist in a superconducting ring only in discrete units.
- 1962- The tunneling of Cooper pairs across the junction consisting of two superconductors separated by thin insulating layer by B.D. Josephson predicted [14].
- 1963- The AC and DC Josephson effect was observed by John Rowel [15] and showed that Cooper pairs can carry current across a tunnel junction with no voltage (DC effect) and applying a dc voltage to a tunnel junction, radio frequency waves (AC effect) can be produced.
- 1964- Quantum interference leading to the development of superconductivity quantum interference devices (SQUID) was discovered by Jaklevic et al. [16].
- 1973- Synthesis of Niobium-Germanium A15 compound was done by John Gavaler which showed T_c of 23.2 K [17].
- 1986- High Temperature superconductor (HTSC) in Ba-La-Cu-O system having T_c of 35 K was discovered by J. George Bednorz and K. Alex Mueller [18].
- 1987- Maw-Kuen Wu and C.W. Paul Chu discovered Y-Ba-Cu-O high T_c superconductors having T_c of 90 K [19].
- 1988- Nonrare-earth based cuprate superconductors i.e. Bi2223 (T_c = 110 K) by Meada et al. [20] and Tl2223 (T_c = 125 K) was discovered by Sheng et al. [21].

  Discovery of noncuprate high T_c superconductors $Ba_{1-x}K_xBiO_3$ (T_c = 28 K) was done by Cava et al. [22].
- 1991- Hebard et al. [23] discovered superconductivity in alkaline metal doped C_{60} compound.
- 1993- Schilling et al. [18] observed the T_c enhancement to 133 K in Hg-based ceramic superconductors and it further increased to 164 K under pressure [24].

- 1997- University at buffalo scientists found strongest evidence for the strange and extremely promising phenomenon, called reentrant superconductivity that magnetic field may enhance, not kill superconductivity [25].
- 2000- Superconductor amplifier is devised by Giampiero Pepe of the University of Naples in Italy and colleagues led by Antonio Barone, together with Norman Booth of Oxford University in the UK [26].
- 2001- The possibility of superconductivity iron in its non-magnetic state has been predicted by Katsuya et.al. [27].
- 2001- Zero Resistance without Cooper-pairing has been discovered by Rafael de Picciotto of Bell Labs in US [28].
- 2002- Phonon Influenced HTSC is confirmed by studies at Berkeley Lab's Advanced Light Source (ALS) [29].
- 2003- Nobel Prize in Physics Awarded for pioneering contributions to the theory of superconductors and superfluids jointly to three physicists Alexei A. Abrikosov **(**Argonne National Laboratory, Argonne, Illinois, USA) Vitaly L. Ginzburg **(**P.N. Lebedev Physical Institute, Moscow, Russia) and J. Anthony [30].
- 2004- Physicists got new clues for theory of superconductivity discovered by Stephen Hayden from Bristol University in the UK and colleagues at ISIS, Oak Ridge, Tennessee and Missouri-Rolla studied $YBa_2Cu_3O_{7-\delta}$ (YBCO) and found the collective magnetic excitation "glue" responsible for holding the Cooper pairs together in the material [31].
- 2005- Physicist Julian Brown of the University of Oxford started to claim that protons, and not just electrons, can travel unobstructed through metal [32].
- 2006- Physicists in the US and Japan found that phonons play a key role in high-temperature superconductivity [33-34].
- 2007- Scientists at the U.S. Department of Energy's Brookhaven National Laboratory, in collaboration with colleagues at Cornell University, Tokyo University, the University of California, Berkeley, and the University of Colorado, have discovered why the transition temperature cannot simply be elevated by increasing the electrons' binding energy [35].

- 2008- Scientists reveal effects of quantum 'traffic jam' in high-temperature superconductors which point to new materials to get the current flowing at higher temperatures. [36].
- 2009- Pinning down superconductivity to a single layer was possible by the U.S. Department of Energy's (DOE) Brookhaven National Laboratory which led to precision engineering of superconducting thin films for electronic devices [37].
- 2010- Japanese scientists claimed that they have experimentally determined the mechanism underlying electron pair formation in iron-based, high-temperature superconductors [38].

2.2. Literature review pertaining to doping effect

HTSCs are granular in nature and defect ridden. The defects belonging to atomic size point defects category include the substitution defects, oxygen vacancies, interstitial oxygen and anti-site disorder. In most of atomic size point defects structures, the natural dimensions of the CuO_2 conduction planes and the metal oxygen planes making up the charge reservoir layer are not matched. The CuO_2 planes control the unit cell dimensions in the ab-plane. The defects generally develop at the chain and plane sites of Cu or may be at Y or Ba site of YBCO. The structure of YBCO is given in chapter 1 for reference. The defects can be created due to doping at iso or aliovalent site or can be by composite formation.

YBCO is currently the best suited HTSCs for most bulk applications. Neutron diffraction and XRD studies [39] revealed that the unit cell is orthorhombic with cell parameters a = 3.82 A, b = 3.88 A and c = 11.683 A. Oxygen deficient Y-plane leads to copper ions in five fold coordinated square pyramidal sites which results in 2-dimensional puckered sheets of copper oxygen bonds that extend in a-b plane. Oxygen stoichiometry is found to play important role in determining the superconducting properties of YBCO superconductor [40, 41]. It is established that diffusion of oxygen mainly takes place in the CuO basal plane and migration occurs with ordering of oxygen atom [42]. The diffusion process is highly anisotropic in the YBCO structure. It is about 10 times more rapid in the ab-plane than along the c-direction. In the ab-plane itself, the diffusion along the b-axis is more favorable if oxygen diffuse from end of a chain and the adjacent chain is empty of oxygen and the diffusivity in the b-direction is 100 times more than a-direction. At the maximum oxygen concentration for which compound is stable ($\delta = 0$), only half of the available sites in the charge reservoir layer is occupied by oxygen atoms. It is widely agreed that the quasi

two dimensional motion of charge carriers in the CuO_2 planes play a significant role. The issue of the role of the basal plane (Cu-O chains) contributing to superconductivity is, however, special and exclusive to the YBCO class of compounds. The importance of integrity of chains in these systems is clearly borne out by the systematic reduction of T_c accompanied with orthorhombic to tetragonal transition with removal of oxygen from the Cu-O chains [39, 40].

The relevance of investigating changes in the properties of high T_c superconductors through doping with substitutional elements is evident from the fact that all the high T_c superconductors are resulted from substitution at one or more cationic sites in the parent materials. Since these studies provide a very good probe to understand the mechanism behind superconductivity, they become important from the fundamental point of view as well. In YBCO substitutions have been attempted at sites of all the constituent elements to look for higher Tc's as well as to understand the mechanism of superconductivity. The Y site has been replaced completely or partially with other rare earths and it is found that these substitutions do not affect T_c with the exception of one or two elements like Pr, Tb, Ce, etc. [43]. However, substitution at the Ba site with other alkaline earth elements has been found to decrease T_c [44]. Partial substitution for oxygen by fluorine is also reported [45] which claims a rise in T_c even near to room temperature. Substitution at the Cu site is the most important among all the cations of YBCO, since Cu-O networks have been suspected to play a major role for the occurrence of superconductivity in these materials. For this reason, the Cu site has been doped with almost all the elements. Among them, the 3d transition elements are considered ideal for doping at the Cu site as they have similar electronic configuration and ionic sizes as Cu.

Substitution by metal ions at Cu site in YBCO type superconductors leads to generally unfavorable effect in superconductivity but to different degrees for different dopant metal ions. Incorporation of Zn in CuO_2 planes to form the composition $YBa_2Cu_{3-x}Zn_xO_7$ for example has a dramatic effect on superconducting transition temperature. The dTc/dx in this case is about -13 K/at% [46, 47]. Several models have been proposed in the literature to account for the large suppression of T_c with Zn substitution. Park et al. [48] for example considered the modifications in the magnetic interaction between the copper local moments when magnetic and non-magnetic ions such as Ni and Zn occupy the Cu sites. Zn^{2+} is a non-magnetic and stable 2+ ion. The presence of such ions disturbs the antiferromagnetically coupled spin fluctuations in the CuO_2 planes. As a result, Cu ions at the vicinity of the Zn ions acquire local moments. Existence of

local moments in Zn doped YBCO system has been shown by NQR [49], EPR [50] and magnetic susceptibility measurements [51].

The conventional charge transfer model speculates the transfer of holes from the charge reservoir layer (CuO chains) to charge conduction layer (CuO_2 plane) through the apical oxygen [52]. Therefore, the CuO bonding along the c-axis is important for the effective charge transfer and high T_c. It is experimentally established that T_c increases if Cu(2)-O(1) bond length decreases. But Zn doping in YBCO causes atomic displacement and shortening of Cu(1)-O(1) bond length and elongation of Cu(2)-O(1) bond length by 8 to 12%. This, along with the filled d-shell of the Zn^{2+} ion lead to interruption in the charge transfer and T_c suppression. The hole from the Cu(1) site is interrupted to go to Cu(2) site through the apical oxygen located just below the doped Zn i.e. a hole supplied channel to Cu(2) site is lost by doping a Zn atom. As a consequence, the Tc is reduced.

In YBCO, the nature of the charge reservoir layer and the mechanism of charge transfer has been studied through preferential chemical substitutions by trivalent ions like Ga^{3+}, Fe^{3+}, Al^{3+}, Co^{3+} and monovalent ions like Ag^{1+}, Au^{1+} in the CuO chain. Such substitutional studies have clearly indicated a drastic change in the structure without much change in the superconductivity, thus giving an impression that structural features in the ab-plane may not have much relevance to superconductivity. However, later studies [53] pointed out that though on a macroscopic scale a transition from orthorhombic to tetragonal structure occurs, oxygen ordering in the local scale still exists. As the impurity atoms occupy the lattice sites in the CuO basal plane they change the oxygen coordination around neighbouring Cu(1)s.

Several factors contribute to the observed T_c suppression on doping with trivalent metal ions in the CuO based plane of YBCO. The first and the foremost is the decrease in the hole content due to increased valency of the dopants. Incorporation of Ga^{3+} in the chains for example reduce the formal valence of Cu from 3+ to 2 + and thus reduce the carrier (holes) density in the plane [54]. Another factor that contributes to T_c reduction on substitution is the localization of the charge carriers. Cai et al. [55] have shown that Cu (1) when substituted by trivalent ions like Al and Ga, holes on the oxygen site fond to be localized near impurity ion. The impurity ions also modify the CuO bond length along the c-axis and hence affect the charge transfer process from the charge reservoir to the CuO_2 planes.

It has been established that Cu (2) site substitution in CuO_2 planes lead to formation of magnetic moments which become pair breakers [56]. Doping Zn to the Cu-site of YBCO creates in-plane disorder without affecting the hole-density. Zn substitution changes the charge on O^{2-} site and modulates its position without affecting the oxygen ordering so orthorhombic structure is not disturbed [57]. The presence of spinless divalent ion like Zn in the planes destroys long range order of spin system and leads to strong changes of the superconducting parameters [58]. On the other hand Ga occupies Cu (1) sites along CuO chains and has different magnetic moments. The Cu atoms in the Cu-O chains have a four- fold co-ordination [59]. So there exists a coordination mismatch between the parent and the dopant. Cu(1) site substitution affects the superconductivity mainly through a decrease in P type carriers in CuO_2 planes which affects the transition region [60]. When Ga and Zn ions are substituted simultaneously for Cu, they apparently have a site preference maintaining an orthorhombic structure. The simultaneous substitutions of Cu by Ga and Zn having +3 and +2 charge state respectively have been analyzed [57]. This we attribute to the fact that Zn substitutes at Cu (2) sites on CuO_2 planes in the lattice, whereas Ga^{3+} impurities have a five-fold co-ordination. The reduction of T_c and orthorhombic distortion when Ga and Zn ions are present together, suggest interplay between the local magnetic moments which appear as a consequence of the doping of lattice at both the sites. The purpose of the present investigation is to show the behavior of chain and plane sites on the structural/ microstructural and electrical properties of YBCO. It has been observed [61] that with increase in Zn concentration T_c and T_{c0} values decrease while T_c is not affected by Ga^{3+} as much as it is affected by doping Zn^{2+}.

Superconducting and normal state properties of YBCO system is controlled by charge carriers. Its carrier density can be enhanced either by increase of oxygen content or by on-site cationic substitutions with dopants of lower valence state. Ca doping at Y site has created much interest in the scientific community as this doping turns an oxygen-deficient YBCO system from insulator to superconductor [62, 63]. In addition to affecting T_c, Ca doping decreases normal state resistivity, increases critical current J_c, affects the interlayer coupling strength, J [64] and hence influences the superconducting order parameter fluctuation (SCOPF) region above T_c. Not just the electrical properties even the structure changes from orthorhombic to tetragonal [65] and grain size reduces [66] on Ca doping. On the other hand, Zn substitution suppresses superconductivity most effectively and, like a magnetic field, has little effect on the pseudogap

transition temperature (T*) irrespective of hole concentration [67]. In the present work emphasis has been taken to study the dimensionality of conductivity through analysis of the excess conductivity undergoing a systematic study of the transport properties of the superconducting compound $Y_{1-x}Ca_xBa_2(Cu_{1-y}Zn_y)_3O_{7-\delta}$. The motivation of the study is to examine the suitability and the range of applicability of the Aslamazov and Larkin (AL) relations to various fluctuating regions with different levels of Zn, Ca. Specifically a shrink in the fluctuating region of superconductivity has been witnessed with the increase of Zn content to the Ca substituted YBCO system (Chapter 5).

2.3. Literature review pertaining to composites

In the process of sample preparation during sintering cuprate superconductors have been showing considerable deviations from resistivity measurement in single crystals and polycrystals that represent the intrinsic resistivity of the grains [68, 69], depending on the orientational mismatch of adjacent grains, voids and cracks. Control of granularity in these systems therefore has involved controlling several aspects as grain alignment, grain growth, sample defects and secondary phase formation [70]. One of the approaches to overcome the difficulties arising due to granularity in cuprates has been to make composites of YBCO with such metals as Au, Ag, Al and compounds like $BaZrO_3$ and $BaTiO_3$ which can fill the inter-granular spaces and improve both electrical and mechanical properties [71-74]. $BaZrO_3$ addition to YBCO during the final stage of sintering in particular has been shown to form composites with sizable enhancement in J_c, along with a slight increase in the superconducting transition temperature T_c [75]. In the composite system, most of the $BaZrO_3$ occupies the boundaries of YBCO grains [76] and with the application of magnetic field a secondary peak, in the $d\rho/dT$ curve has been observed for the onset of transition in the intergranular region due to the extra deposition of BZO on the grain boundaries [77]. SEM and XRD analysis of Kang et al. [78] showed that BZO is located at the grain boundaries. It also occurs in clumps filling voids between grains in films and bulk systems [69, 79].

$BaTiO_3$ Being a ferroelectric material, with a perovskite structure similar to that of YBCO possess similar lattice structure (2-3 % lattice match in a-b planes) and crystal chemistry have shown to generate a stress field and act as pinning centers [80, 81]. Thus with an ideal system for experimental study [82, 83] we have tried to analyze fluctuation conductivity in polycrystalline

samples of YBCO + xBaTiO$_3$ with micrometric and nano BaTiO$_3$ inclusions having both inter- and intra-grain modifications. The strong influence of BaTiO$_3$ content in the composites in the mean field region has been explained through nano BaTiO$_3$ induced modifications and an intragranular fluctuation change is observed [84]. Again long-range superconducting order is witnessed for BaTiO$_3$ inclusions of some micrometric size due to thermally assisted percolation process through the weak-links between the grains [85]. This aspect has been discussed in chapter 6.

2.4. Literature review pertaining to fluctuations

It seems that the first experimental observation of effects of superconducting order parameter fluctuations on the conductivity was made in 1967 by Glover [86], who studied of amorphous Bi films. In the history of superconductivity this is of course rather late, but theoretical estimates had indicated that effects of fluctuations should only be detectable in a more or less negligible temperature interval above T_c. When the sample size was reduced, however, as in the thin films of Bi, the fluctuation effects became more pronounced, and could be observed. Soon after Glover's observations there were reports of theoretical calculations of the fluctuation conductivity, using both the microscopic method by Aslamazov and Larkin in 1968 [87, 88] and the Ginzburg-Landau approach [89, 90]. The agreement with experiments was good. Fortunately, this could be explained by including a fluctuation contribution [91, 92] that was neglected in the original microscopic calculations. After Thompson [93] had removed a divergency appearing in the extension to samples of reduced dimensionality (2D), the contribution became known as the Maki-Thompson term. The original term is referred to as the Aslamazov-Larkin term. Superconducting fluctuations can be treated using the GL theory or the microscopic techniques. The GL theory is the more simple and intuitive one, while the microscopic techniques required for calculations of all terms in the more general case. The GL approach will be briefly described below.

The general treatment of fluctuation phenomena (in ferroelectrics, superconductors, etc.) by Ginzburg [94] states, e.g., that anomaly in the specific heat should only be observable at distances of the order of 10^{-3} K from the transition. The smearing of the transition due to deviations from the ideal crystal structure would thus most likely prevent observation. Later work in the 1970s includes measurements in three-dimensional amorphous alloys [95]. In the

usual GL approach, only the AL term close to T_c is obtained. The treatment of fluctuations in the Ginzburg-Landau framework is rather straightforward. The basic idea is that thermodynamic fluctuations can cause the free energy F to fluctuate an amount of roughly $k_\beta T$ above its minimum value. Since the free energy depends directly on the density of superconducting electron pairs, one may calculate the corresponding variation in this quantity.

As already mentioned, the superconducting electron pairs contribute to the conductivity through the Aslamazov-Larkin (AL) and Maki-Thompson (MT) terms. In addition, there is the more recently calculated density-of-states (DOS) term [96-99]. The total fluctuation conductivity can thus be written as:

$$\sigma^{fl} = \sigma^{AL} + \sigma^{DOS} + \sigma^{MT} \tag{2.1}$$

The AL term is the most intuitive one, simply reflecting the fact that the superconducting electron pairs contribute to the conduction. Hence, this term gives a positive contribution to the conductivity (i.e. a decrease of the resistance). The AL term was the first term to be derived and was treated for layered structures already in 1970 by Lawrence and Doniach [100]. The MT term [92, 101] is much more difficult to understand in a simple way. It is usually described as an influence of superconducting fluctuation on the normal quasiparticles. The MT conductivity term is generally positive, like the AL term. As the MT term has a pure quantum nature, it does not appear in the usual thermodynamic Ginzburg Landau (GL) approach.

The importance of the DOS term seems to have been realized only recently [97]. The DOS term is often negligible but may be dominant in HTSC under certain conditions. It originates from the fact that the density of states of the normal-state quasiparticles is affected by the formation of superconducting pairs. This term has opposite sign compared to the AL and MT term, and thus rather surprisingly increases the resistivity. In order to understand this fact, it may help to consider the following very much simplified reasoning: When some electrons form Cooper pairs, the effective number of carriers participating in the normal (one-electron) conduction decreases, and the conductivity goes down. As pointed out by Varlamov et al. [102], the DOS fluctuation conductivity may be estimated from the simple Drude model. If we let Δ_{ne} denote the change in the density of normal-state carriers and n_{pair} the density of superconducting pairs, we have,

$$\sigma^{DOS} = \frac{\Delta n_e e^2 \tau}{m} = -\frac{2 n_{pair} e^2 \tau}{m} \tag{2.2}$$

which in the 2D case results in correct sign and temperature dependence.

The discovery of HTSC led to a renaissance for superconducting fluctuations. This was of course partly due to the fact that all aspects of superconductivity research virtually exploded at the time. Another most important reason for the lasting activity around the world is that fluctuation effects in HTSC are large and easily observable, thanks to the short coherence lengths, the high temperatures involved, and the layered structure. There has also been a substantial theoretical development. For example, the importance of the previously neglected DOS term was realized and it has been found that fluctuations with this term included are capable of explaining several puzzling phenomena in high temperature superconductors, e.g. the peak in the c-axis resistivity [103, 104] and a change of sign in the magnetoconductivity [105]. In this section, the basic model for fluctuation calculations on HTSC, the Lawrence-Doniach (LD) model, will be introduced. The results of calculations based on this model will then be presented Chapter 5 and 6.

A convenient starting-point for theoretical studies of HTSC is the Lawrence- Doniach (LD) model [100]. This model was proposed in 1970 as a means of analyzing results in layered intercalated superconductors, but it is equally well suited for HTSC with its superconducting Cu-O planes. In the LD model, each Cu-O plane is considered to be a two-dimensional (2D) superconductor, separated from the neighboring planes by insulating regions. The layers are coupled by Josephson tunneling. Close to T_c, where the coherence length perpendicular to the plane is much larger than the inter-plane distance, the material effectively acts as a 3D (anisotropic) superconductor, whereas far away from T_c, where the coherence lengths are shorter than the inter-plane distance, it follows a 2D behavior.

Consider as an example the Aslamazov-Larkin conductivity above T_c. In the LD model, it can be written as:

$$\sigma_{LD}^{AL} = \frac{e^2}{16\hbar s}\frac{1}{\left[\varepsilon\left(\varepsilon + r'\right)\right]^{1/2}} \tag{2.3}$$

Where $r' = 4\xi_c^2(0)/s^2$ is an anisotropy parameter, $\xi_c(0)$ is the coherence length perpendicular to the planes at zero temperature, and s is the inter-plane distance. Close to T_c ($\varepsilon << r'$) this expression approaches

$$\sigma_{3D}^{AL} = \frac{e^2}{32\hbar\xi(0)}\frac{1}{\sqrt{\varepsilon}} \tag{2.4}$$

and at higher temperature it approaches

$$\sigma_{2D}^{AL} = \frac{e^2}{16\hbar s}\frac{1}{\varepsilon} \tag{2.5}$$

The cross-over occurs when $\varepsilon \approx r'$, which corresponds to $\xi_c^2(T) \approx s/2$. Expressed in temperature, the cross-over is at

$$T \approx T_c\left(1+4\frac{\xi_c^2(0)}{s^2}\right) \tag{2.6}$$

Although the concept of the Lawrence-Doniach model is mainly used in conjunction with the Ginzburg-Landau model, its principles are also the basis for the microscopic calculations from Feynman diagrams. The material is then treated as a Fermi liquid, and the quasiparticles are allowed to travel within the planes as well as to tunnel between the planes.

In the following subsections, complete expressions for fluctuation conductivity and fluctuation magnetoconductivity will be presented. For easy reference, they will be called the standard expressions. This term is suitable since these are common formulas generally used by us and others for interpretations of experiments, and they provide a good starting point for further discussions.

Parameters:

The fluctuation conductivity is a function of several parameters

$$\sigma^{fl} = \sigma^{fl}\left(s, \upsilon_F, T_c, J, \tau, \tau_\phi, T, B\right) \tag{2.7}$$

The parameters are as follows:

s is the layer spacing, usually taken to be 11.69 Å in $YBa_2Cu_3O_{7-\delta}$.

υ_F is the Fermi velocity in the planes, often taken to be roughly $2\text{x}10^5$ m/s in $YBa_2Cu_3O_{7-\delta}$ [39, 106].

T_c is the critical temperature (mean-field T_c).

J is the hopping integral, corresponding to the probability of hopping between the planes.

τ is the elastic scattering time within the planes.

τ_ϕ is the phase-breaking time. This parameter appears only in the anomalous MT term.

T is the temperature.

B is the magnetic field, which in the standard expressions must be parallel to the crystal c axis.

The main limitation of the theory concerns the temperature interval. There is a lower limit on temperature arising from the fact that the expressions have been derived for the Gaussian regime, i.e. where fluctuations are small enough not to interact significantly. The upper limit comes from the assumption ($\varepsilon << 1$), which has been made in the derivations.

2.5. Outlook of the study

Though BCS theory is thought to be the only successful theory in explaining the superconductivity as evidenced through out the literature survey, it has the following limitations: i) It did not specify what substance should superconduct at what temperature. ii) The basic ingredient of the theory, the weak electron-phonon interaction even put a limit to the highest T_c achievable around 30 K. There are two remaining areas which require further investigation. The first one is a better treatment of the Coulomb repulsion. In particular, the ability to treat large repulsion and antiferromagnetism is essential for HTSC materials. The second one is the analysis of superconducting fluctuations around the achievable critical temperature (T_c) for understanding the electron–phonon coupling. So, the overriding challenge at this stage is to understand the basic physics behind the phenomenon of HTSC along with improving some basic parameters like J_c, T_c and H_c as well as improving the quality of the sample through vortex pinning. Inspired from the whole spectrum of literature survey the present study incorporated in this thesis is planned in the sequential manner

In this study, emphasis has been made to understand the electron-pairing mechanisms through superconducting order parameter fluctuation (SCOPF) studies. Composites are made of YBCO by doping $BaZrO_3$ and $BaTiO_3$. In order to complete the work, some more in-site doping processes were carried out through simultaneous substitution at the Cu site by Ga, Zn and through Ca substitution at Y-site with Zn substitution at Cu site.

References

[1] H. K. Onnes, Communications from the Physical Laboratory of the University of Leiden (1911).

[2] W. J. de Haas and W.H. Keesom 1931.

[3] W. Meissner and R. Ochsenfeld, Naturwissenschaften 21 (1933) 787.

[4] H. G. B. Casimir, Phys. Z. 35 (1934) 963.

[5] Fritz London and Heinz London, Physica, 2 (1935) 241.

[6] V. L. Ginsberg and L. D. Landau, Zh Eksp Teor Fiz 20 (1950) 1064.

[7] H. Frolich, Phys. Rev. 78 (1950) 845.

[8] E. Maxwell, Phys. Rev. 78 (1950) 477.

[9] A.B. Pippard, Proc. Roy Soc A 216 (1953) 547.

[10] L. N. Cooper, Phys. Rev. 104, 1189 (1956).

[11] J. Bardeen, L.N. Cooper, and J.R. Schrieffer, Theory of Superconductivity (Physical Review), 108 (1957) 1175.

[12] I. Giaver, Phys. Rev. Lett. 5 (1960) 147.

[13] B. D. Deaver, Jr, and W. M. Fairbank, Phys. Rev. Lett. 7 (1961) 43.

[14] B. D. Josephson, Phys. Lett. 1 (1962) 251.

[15] J. M. Rowell, Phys. Rev. Lett. 11 (1963) 200.

[16] R.C. Jaklevic, J. Lambe, A.H. Silver and J.E. Mercereau, Phys. Rev. Lett. 12 (1964) 159.

[17] J. R.Gavalar, Appl. Phys. Lett. 23 (1973) 480.

[18] A. Schilling, M. Cantoni, J. D. Guo and H. R. Ott, Nature 363 (1993)56.

[19] M. K. Wu, J. R. Ashburn, C. J. Trong, P. H. Hir, R. L. Meng, L. Gao, Z. L. Huang, Y. Q. Wang and C.W. Chu, Phys. Rev. Lett. 58 (1987) 908.

[20] H. Maeda, Y. Tanaka, M. Fukutomi and T. Asano, Jpn. J. Appl. Phys. 27 (1988) L 209.

[21] Z. Z. Sheng and A. M. Herman, Nature 322 (1988) 138.

[22] R. J. Cava, B. Batlogg, J. J. Krajewski, R. Farrow, L.W. Rupp, A. E. White, K. Short, W.F. Peck, T. Kometani, Nature 332 (1988) 814.

[23] A.F. Hebard, M.J. Rosseinsky, R.C. Haddon, D.W. Murphy, S.H. Glarum, T.T.M. Palstra, A.P. Ramirez and A.R. Kortan, Nature 350 (1991) 600.

[24] C. W. Chu, L. Gao, F. Chen, Z. J. Huang, R. L. Meng and Y. Y. Xue, Nature 365 (1993) 323.

[25] J. Lee, M. J. Naughton, G. M. Danner and P. M. Chaikin: Phys. Rev. Lett. 78 (1997) 3555.

[26] G. P. Pepe, G. Ammendola, G. Peluso, A. Barone, E. Esposito, R. Monaco, and N. E. Booth, Appl. Phys. Lett. 77 (2000) 447.

[27] Katsuya Shimizu, Tomohiro Kimura, Shigeyuki Furomoto, Keiki Takeda, Kazuyoshi Kontani, Yoshichika Onuki & Kiichi Amaya, Nature 412 (2001) 19

[28] Rafeal. De Picciotto, H. L. Stormer, L. N. Pfeiffer, K. W. Baldwin & K. W. West, Nature 411 (2001) 51.

[29] Lynn Yarris, lcyarris@lbl.gov, sciencebeat, Berkeley Lab, January 14, 2002.

[30] V. L. Ginzburg, A. A. Abrikosov, and A. J. Leggett Low Temp. Phys. 29 (2003) 971.

[31] Au. S M Hayden, Au. H A Mook, Au. P Dai, Au. T G Perring, Au. F Dogan T, Nature 429 531-534 (2004) [doi:10.1038/nature02576.

[32] Justin Mullins, News Scientists Physics $ Math Magazine issue 24987 May 2005.

[33] D. Reznik, L. Pintschovius , M. Ito, S. Iikubo , M. Sato , H. Goka , M. Fujita , K. Yamada , G. D. Gu , and J. M. Tranquada Nature 440 (7088) (2006) 1170.

[34] D. C. van der Laan and J. W. Ekin, Applied Physics Letters, 90 (2007) 052506.

[35] D.C. van der Laan and J.W. Ekin, Supercond. Sci. Technol. 21 (2008) 115002.

[36] Karen McNulty Walsh kmcnulty@bnl.gov DOE /Brookhaven National Laboratory,631-344-8350 27-Aug-2008.

[37] Karen McNulty Walsh, (631) 344-8350 or Peter Genzer, Brookhaven National Laboratory News (631) 344-3174 October 29, 2009.

[38] T. Hanaguri, S. Niitaka, K. Kuroki, H. Takagi, Unconventional *s*-wave superconductivity in Fe(Se,Te). Science 328 (2010) 474.

[39] J. D. Jorgensen, W. B. Veal, W. K. Kwok, G. W. Crabtree, A. Umezawa, L. J. Nowicki and A. P. Paulikas, Phys. Rev. B 36 (1987) 5731.

[40] R J. Cava, B. Batlogg, C.H. Shen, E.A. Rietman, S.M. Zahurak, D. Wender, Nature 329 (1987) 423.

[41] C. N. R. Rao, in High Temperature Superconductors, S. V. Subramanyam and E. S. Raja Gopal, eds. (Wiley Eastern, New Delhi, (1989), p 68.

[42] H. Shaked, J.D. Jorgensen, B.A. Hunter, R.L. Hitterman, A.P. Paulikas and B.W. Veal, Phys. Rev. B 51 (1995) 547.

[43] Z. Fisk, J. D. Thompson, E. Zirngiebi, J. L. Smith and S.W. Cheong, Solid State Commn. 62 (1987) 743.

[44] N.S. Raman and B. Viswanathan, Bull. Mate. Sci. 16 (1993) 381.

[45] S. R. Ovshinsky, R. T. Young, D. D. Allred, G. Demaggio and G. A. Van Der Leeden, Phys. Rev. Lett. 58 (1987) 2579.

[46] G. Xiao, M.J. Cieplak, D. Musser, A. Gavrin, L. L. Chien, J. J. Rhyne and J. A. Gottas, Nature 332 (1988) 238.

[47] N. Peng and W. Y. Liang, Physica C 223 (1994) 61.

[48] T. K. Park, B. J. Mean, K. H. Lee, G. S. Go, S. W. Seo, K. S. Hou, M. Lee, H.S. Lee, H.B. Kim and W. C. Lee, Phys. Rev. B 59 (1999) 11217.

[49] A. K. Rajarajan, N. C. Mishra, D. Kuberkar, L. C. Gupta, R. Vijayaraghavan and K. Patnaik International Conference on Superconductivity, Bangalore (1990).

[50] A. M. Ponte Concalves, Chan-Soo Jee, D. Nichols, J. E. Crow, G. H. Myer, R. E. Salomon and P. Schlottmann MRS proceedings Vol 99 (1988) P.583

[51] C. Jee, D. Nichols, J. Ciasullo, J.E. Crow, T. Mihalisin, G.N. Myer, M.V. Kuric, S.H. Blam and R.P. Guertin MRS proceedings Vol 99 (1988) P.769

[52] W. H. Fietz, R. Quenzel, H. A. Ludwig, K. Grube, S. I. Schlachter, F.W. Hornung, T. Wolf, A. Erb, M. Klaser, G. Muller-Vogt, Physica C 270 (1996) 258.

[53] B. W. Veal, A. P. Paulikas, H. You, H. Shi, Y. Fang, J. W. Downey, Phys. Rev. B 42 (1990) 6305.

[54] N. C. Mishra, A. K. Rajarajan, K. Patnaik, R. Vijayaraghavan and L.C. Gupta, Solid State Comm. 75 (1990) 987.

[55] Z. Xiong Cai and S.D. Mohanti, Phys. Rev. B 40 (1989) 6558.

[56] Y. X. Zhou, S. Scruggs, K. Salama, Superconductor Science and Technology 19 (2006) 13-15.

[57] A. K Rajarajan, L.C. Gupta, R Vijayaraghavan, N. C. Mishra, Physica C (1989) 163.

[58] Manzoor Hussain, Shinji Kuroda, Koki Takita, Peak effect observed in Zn doped YBCO single crystals, Physica C. 297 (1998) 176.

[59] G. Baumgärtel, K. H. Bennemann, Phys. Rev. B. 40 (1989) 6711.

[60] M. A. Rodriguez, A. Navrotsky, F. Licci, Thermochemistry of $YBa_2Cu_{3-x}M_xO_y$ (M = Ni, Zn), Physica C. 329 (2000) 88.

[61] A. Mohanta and D. Behera, Indian Journal of Pure and Applied Physics, 47 (2009) 676.

[62] V. B. Geshkenbein, L. B. Ioffe, and A. I. Larkin, Phys. Rev. B 55 (1997) 3173.

[63] V. Emery, S.A. Kivelson, and O. Zachar, Phys.Rev.B 56 (1997) 6120.

[64] F. Vidal, J. A. Veira, J. Maza, F Garcia-Alvarado, E. Moran and M. A. Alario, J. Phys. Condens. Matter 21 (1999) L599.

[65] S. H. Han and O. Rapp, Solid State Commun. 94 (1995) 661. Matter 21 (1999) L599.

[66] Anurag Gupta, Sukalpa Chaudhuri, V Ganesan, I Das, H Narayan, Anil Kumar, A J Zaleki and A V Narlikar, Supercond. Sci. Technol. 14 (2001) 937.

[67] A. Nawazish Khan, H. Ihara , Physica C 403 (2004) 247.

[68] M. Safonchik, K. Traito, S. Tuominen, P. Paturi, H. Huhtinnen, R. Laiho, Supercond. Sci. Technol. 22 (2009) 065006.

[69] J. Gutierrez, A. Llordes, J. Gazques, M. Gilbert, N. Roma, S. Ricart, A. Pomar, F. Sandiumenge, N. Mestres, T. Puig, X. Obradors, Nat. Mater. 6 (2007) 367.

[70] Y. Y. Luo, Y. C. Wu, X. M. Xiong, et al., J. Supercond. 13 (2000) 4

[71] Peurla, M., Huhtinen, H., Shakhov, M.A.: Phys. Rev. B 75 (2007) 184524.

[72] Macmanus-Driscoll, J.L., Foltyn, S.R., Jia, Q.X., et al.: Nat. Mater. 3 (2004) 439

[73] D. Behera, N.C. Mishra, Supercond. Sci. Technol. 15 (2002) 72.

[74] M. Peurla, P. Paturi, Y.P. Stepanov, H. Huhtinen, Y.Y. Tse, A.C. B´ odi, J. Raittila, R. Laiho, Supercond. Sci. Technol. 19 (2006) 767.

[75] A. Mohanta, D. Behera, Solid State Communications 150 (2010) 1325.

[76] A. Mohanta, D. Behera, Physica C 470 (2010) 295.

[77] A. Mohanta and D. Behera J Supercond Nov Magn 23 (2010) 275.

[78] S. Kang, K. J. Leonard, P. M. Martin, J. Li and A. Goyal, Supercond. Sci. Technol. 20 (2007) 11

[79] Nigel M. Kirby, Nigel W. Chen-Tan, C.E. Buckley, Journal of the European Ceramic Society 27 (2007) 2039.

[80] W. Gawalek, T. Habisreuther, K. Fischer, G. Bruchlos, P. Görnert Cryogenics. 33(1993) 65.

[81] Morsy Abou Sekkina, Abdul Raouf Tawfik, Osama Hemeda, Mohamad Ahmad Taher Dawoud, Samy Elattar, Turk J Phys, 29 (2005) 329.

[82] L. T. Romano, O. F. Schilling and C. R. M. Grovenor, Physica C. 178 (1991) 41.

[83] M. Kahiberga, M. Livinsh, M. Kundzinsh, A. Sternberg, I. Shorubalko, L. Shebanovs, K. Bormanis, J. of low temperature Physics. 105 (1996) 1433.

[84] A. Kujur, A. Mohanta and D. Behera, International Journal of Material Science. 5 (2010) 683.

[85] A. Mohanta, D. Behera, S. Panigrahi and N. C. Mishra Indian J. Phys. 83 (2009) 1.

[86] R. E. Glover, Phys. Lett. 25A (1967) 542.

[87] L. G. Aslamazov and A. I. Larkin, Phys. Lett. 26A (1968) 238.

[88] L. G. Aslamazov and A. I. Larkin, Sov. Phys. Solid State 10 (1968) 875.

[89] E. Abrahams and J. W. F. Woo, Phys. Lett. 27A (1968) 117.

[90] A. Schmid, Z. Phys. 215 (1968) 210.

[91] K. Maki, Prog. of Theor. Phys. 39 (1968) 897.

[92] K. Maki, Prog. of Theor. Phys. 40 (1968) 193.

[93] R. S. Thompson, Phys. Rev. B 1(1970) 327.

[94] V. L. Ginzburg, Sov. Phys. Solid State 2 (1960) 1824.

[95] W. J. Skocpol and M. Tinkham, Rep. Prog. Phys. 38 (1975) 1049.

[96] A. Larkin and A. Varlamov, "Theory of Fluctuations in Superconductors" Oxford Science Publication.

[97] I. S. Beloborodov, A. V. Lopatin, V. M. Vinokur, K. B. Efetov , Rev. Mod. Phys 79 (2007) 469.

[98] M. Muller, and L. B. Ioffe, Phys. Rev. Lett. 93 (2004) 256403.

[99] S. Pankov, and V. Dobrosavlijevic, Phys. Rev. Lett. 94 (2005) 046402.

[100] W. E. Lawrence and S. Doniach, in Proc. 12th Int. Conf. on Low Temp.Phys., edited by E. Kanda (Keigaku, Tokyo, 1971), p. 361.

[101] J. E. Crow, R. S. Thompson, M. A. Klenin, and A. K. Bhatnagar, Phys. Rev. Lett. 24 (1970) 371.

[102] A. A. Varlamov, G. Balestrino, E. Milani, and D. V. Livanov, Adv. Phys. 48 (1999) 655.

[103] G. Balestrino, E. Milani, and A. A. Varlamov, Physica C 210 (1993) 386.

[104] G. Balestrino, M. Marinelli, E. Milani, A. A. Varlamov, and L. Yu, Phys. Rev. B 47 (1993) 6037.

[105] J. Axnas, W. Holm, Y. Eltsev, and O. Rapp, Phys. Rev. Lett. 77 (1996) 2280.

[106] J. D. Jorgensen, Phys. Today 34 (1991) 530.

Chapter 3

Experimental Techniques

CHAPTER 3

3. EXPERIMENTAL TECHNIQUES

3.1. Introduction

The present thesis is mainly based on different measurements and characterisations of doped and composites of $YBa_2Cu_3O_{7-\delta}$ superconductors. An overview of methods of synthesising them is reported in Sec. 3.2. Some work in this thesis dealing with Ca and Zn doped samples is discussed in Sec. 3.3. In Sec 3.4 the preparation method for $BaTiO_3$ (BTO) and $BaZrO_3$ (BZO) composite samples has been discussed. Measurements and characterizations of the samples by various experimental techniques are discussed in section 3.5. These techniques include four probe d.c resistivity and magneto-resistivity measurements, M-H measurement for critical current density below the superconducting transition temperature (T_c), x-ray diffraction (XRD), and scanning electron microscopy (SEM) etc.

3.2. Sample preparation

Preparation of $YBa_2Cu_3O_{7-\delta}$ (YBCO) samples can be divided into three steps: intimate mixing of solid reactants in stoichimetric amounts, heat treatment of the crystals to obtain the desired oxygen content and attachment of electrical contacts. These methods have been described in detail before [1] and only an introduction and some complementary information will be given here. A general consideration for the preparation of cuprate superconductors is also included in this section as a prelude to the detailed procedures adopted in the present study. Optimization of the sample properties involves controlling the different parameters of synthesis such as sintering temperature, time, atmosphere and even quenching the samples from different temperatures. Since the preparation of bulk pellets of cuprates has its own importance, a general consideration for the preparation of oxide superconductors is worth mentioning in this chapter.

3.2.1. General consideration for preparation of $YBa_2Cu_3O_{7-\delta}$ (YBCO) superconductors

YBCO can be synthesized by high temperature solid state reaction of constituent oxides and carbonates. The method is a simplest one. The synthesis starts from powders of Y_2O_3, $BaCO_3$,

and CuO, which are carefully mixed and calcined (whereby CO_2 evaporates). For intimate mixing of the reactants, a variation to mixing the solids has been to mix appropriate amounts of cations in their solution. The reaction leading to the formation of the final oxide product still involves heating of the precursor to high temperatures. The calcination does not have the $YBa_2Cu_3O_{7-\delta}$ composition, but when cooled down, crystal structure of $YBa_2Cu_3O_{7-\delta}$ grows out of it. The cooling must be made slowly and preferably in a temperature gradient of 2-3 ^{0}C/min. The as-prepared calcined crystals do not necessarily have the desired oxygen content, and must be further treated.

The reaction of three initial components Y_2O_3, CuO, BaO (or $BaCO_3$) widely used [2] in the preparation of bulk YBCO pellets and YBCO powder employed in the present study for preparation of bulk superconducting pellets is as follows:

$$1/2Y_2O_3 + 2BaCO_3 + 3CuO + 1/2O_2 \rightarrow YBa_2Cu_3O_7 + 2CO_2 \quad (3.1)$$

3.2.2. Preparation method used for bulk $YBa_2Cu_3O_{7-\delta}$ (YBCO) superconductors in the present study

The bulk superconductors used in the present study are YBCO, doped Ca and Zn samples of YBCO and YBCO/$BaTiO_3$ (BTO) and YBCO/$BaZrO_3$ (BZO) composite sintered pellets. For the preparation of YBCO, the chemicals taken were Y_2O_3, $BaCO_3$ and CuO. The chemicals were of high purity (99.9%) except $BaCO_3$ which was 99.8% pure. The samples were prepared by standard solid state reaction of the constituents involving the following steps.

(i) thorough mixing of appropriate amount of chemicals for required composition
(ii) low pressure (20 kg/cm^2) pelletization
(iii) calcination
(iv) grinding of the calcined system
(v) high pressure (100 kg/cm^2) pelletization
(vi) sintering

The steps (iii) and (iv) were repeated four times before the final pelletization (step v) and sintering (step vi) were taken up.

For proper composition of the final product, the constituent oxides were weighed using a single pan electrical balance to an accuracy of 0.1 mg. The weighed chemicals were mixed and

ground well with an agate mortar and pestle for about 2-3 hrs till a gray powder of the compound was obtained. The mixture after pelletization at a low pressure of about 20 kg/cm^2, was transferred to a crucible and was heated inside a temperature regulated box furnace. First heating was done at 900^{0}C for about 20 hrs using the programmable box furnace (Fig.3.1). The furnace was then turned off and the sample was allowed to cool slowly in the furnace. The crucible was removed when it attained room temperature. The black mass was gently dislodged from the crucible to the mortar and reground for 2-3 hrs and then heated inside the furnace. Repeating the calcination process four times assured complete removal of CO_2 by the reaction. The calcined black solids were reground for 2-3 hrs. After thorough grinding, final pellets were made by applying a pressure of the order of 100 kg/cm by a hydraulic press. After pelletization the samples were once again placed in an alumina crucible and sintered at 920 ^{0}C. Then they were slowly (1 ^{0}C/min) cooled to room temperature. All the heatings were done in air except the final sintering stage which was done in oxygen. Slow cooling allows oxygen to be taken up by the sample and provides oxygen stoichiometry close to seven. After cooling the pellets to room temperature, the pellets were preserved in a desiccator to avoid atmospheric moisture and CO_2 degrading the samples.

Fig. 3.1. The programmable furnace (Baisakh make) for varying temperature to 1700^0 C.

3.2.3. Oxygenation

Oxygenation is a most important aspect of crystal production. By changing the oxygen content the properties of the material can be drastically changed, which is useful in studying the mechanisms of superconductivity. The synthesis of cuprate superconductors $YBa_2Cu_3O_7$ is made through a metastable route where oxygen ions are inserted (intercalated) after the thermodynamically stable $YBa_2Cu_3O_{6+x}$ phase forms when x is less than 1. Increasing the oxygen pressure during the first synthesis step does not lead to the formation of $YBa_2Cu_3O_7$ phase. Instead, one fails to synthesize the $YBa_2Cu_3O_{6+x}$ type structure [3]. These phases can exist at any value of x from 0 to 1. Such phases are best prepared by equilibration (relaxation towards equilibrium) at a fixed oxygen pressure and temperature. For a given x, the highest transition temperature Tc is generally found for samples annealed so that interstitial oxygen is well ordered. The oxygen content giving the highest T_c is easily obtained by annealing the crystals in owing O_2 at approximately 500 ^{0}C for 12-20 hours in tubular furnace. Oxygen annealing is done by the method of oxygen displacement during the cooling of the sample after the heat treatment. During cooling down, the sample passes through a nonequilibrium region, while temperatures are still high enough to allow for significant oxygen diffusion and/or redistribution in minutes or even seconds.

3.3. Preparation of $YBa_2(Cu_{0.95}Zn_{0.05-x}Ga_x)_3O_{7-\delta}$ and $Y_{1-x}Ca_xBa_2(Cu_{1-y}Zn_y)_3O_{7-\delta}$ samples

3.3.1. Synthesis of $YBa_2(Cu_{0.95}Zn_{0.05-x}Ga_x)_3O_{7-\delta}$

A series of polycrystalline samples of $YBa_2(Cu_{0.95}Zn_{0.05-x}Ga_x)_3O_{7-y}$(x = 0, 0.012, 0.025) and YBCO has been prepared by the standard solid-state reaction route from appropriate amounts of high-purity powders of constituent oxides and $BaCO_3$. Calcinations of the mixture was done at 850 ^{0}C in air and cooled to room temperature over a period of 10 hours. This process of heating and grinding was carried out four times finally the samples were pressed into pallets and sintered at 900 ^{0}C for 12 hours annealed at 450 ^{0}C for 10 hours in oxygen atmosphere and cooled to room temperature over a period of 10 hours.

3.3.2. Synthesis of $Y_{1-x}Ca_xBa_2(Cu_{1-y}Zn_y)_3O_{7-\delta}$

A series of polycrystalline samples of $Y_{1-x}Ca_xBa_2(Cu_{1-y}Zn_y)_3O_{7-\delta}$ has been prepared by the standard solid-state reaction route from appropriate amounts of high-purity powders of

constituent oxides, $CaCO_3$ and $BaCO_3$. Calcinations of the mixture was done at 900 ^{0}C in air and cooled to room temperature over a period of 10 hours. This process of heating and grinding was repeated four times finally the samples were pressed into pallets and sintered at 920 ^{0}C for 12 hours annealed at 500 ^{0}C for 10 hours in oxygen atmosphere and cooled to room temperature over a period of 10 hours.

3.4. Preparation method used for $YBCO/BaTiO_3$ and $YBCO/BaZrO_3$ composite samples

3.4.1. Synthesis of $BaZrO_3$

Barium nitrate $Ba(NO_3)_2$ and Zirconyl nitrate hydrate $ZrO(NO_3)_2 \cdot x\ H_2O$ were employed for the synthesis of $BaZrO_3$ (BZO) powder, 1: 1 molar ratios of two precursors were taken to a polystyrene bottle and ball-milled for 4 hours in ethanol using zirconia balls as milling medium. The ball-milled mixture was thoroughly mixed at ambient temperature, dried and calcined at 900^0 C for 2 hours at a heating rate of 3^0 C/min in a programmable box furnace.

3.4.2. Synthesis of $BaTiO_3$

$BaTiO_3$ powder has been synthesized through chemical route using solgel method, where it has been calcined at 1250 °C for 2 hrs at a heating rate of 3 °C/min in a programmable box furnace. The precursors used were Barium acetate ($[Ba(CH_3COO)_2]$) and Titanium isopropoxide ($[(CH_3)_2\ CHO]_4$ Ti). Barium acetate is added with acetic acid, the dissolved solution is heated up to 80 ^{0}C where Titanium isopropoxide is added to the solution drop wise. After strong heating the solid powder is ground and sintered at 900 ^{0}C and 1250 ^{0}C separately.

3.4.3. Synthesis of $YBCO/BaTiO_3$ and $YBCO/BaZrO_3$ composites

For the preparation of $YBCO/BaTiO_3$ and $YBCO/BaZrO_3$ composite bulk sintered, $BaTiO_3$ and $BaZrO_3$ were mixed with YBCO powder before the final stage of sintering. The YBCO pellets prepared using the procedure mentioned above were thoroughly ground and mixed with $BaTiO_3$ and $BaZrO_3$ with appropriate proportions to obtain $BaTiO_3$ and $BaZrO_3$ composites with varying wt. fractions. These samples were pressed into pellets, annealed at 920 ^{0}C for 12 hrs and cooled to 400 ^{0}C where they stayed for 12 hrs with oxygen flowing. Then the samples cooled to room temperature at a rate 2 ^{0}C/min. More extensive description can be found in [4].

3.5. Characterization of the samples

The bulk sintered pellets of YBCO and its doped and composites were prepared in our laboratory were studied by the following techniques.

1. DC four probe resistivity measurement at varying temperatures down to 10 K
2. DC four probe magneto-resisstivity measurement at varying temperatures down to 10 K
3. Superconducting critical current density Jc measurement from M-H loop
4. Powder x-ray diffraction (XRD)
5. Scanning electron microscopy

3.5.1. Resistance measurements

The resistance is measured with a standard dc four-probe technique. In order to compensate for thermo power effects (voltages arising because of temperature gradients in the sample and other parts of the measurement circuit), the voltage should be measured both with and without applied current and the difference taken. The sample cooling and temperature control were done by closed cycle *He* refrigerator and the temperature controller.

Electrical contacts

The resistance is measured with a standard dc four-probe technique. Advantage of using four probe technique is that it eliminates the lead resistance as well as the contact resistance which would otherwise influence the measurement of sample resistance. When making electrical connections to the sample there are several problems requiring particular attention:

1. The contact resistance, i.e. the electrical resistance between attached wire and sample, should be low, preferably < 1Ω and at least < 10 Ω. If the current contacts have too high resistance, the crystal may heat up when the measurement current is passed through it. If the voltage contacts have too high resistance, there will be more noise.
2. It should be possible to give the contacts a suitable shape.

3. Contacts should be stable over time in order to allow for several measurements under the same conditions. Contacts made of conducting silver paint fulfill all these requirements, but in order to obtain an acceptable contact resistance, heat treatment is needed, which may disturb the oxygen content and/or oxygen distribution in the crystal. Another contacting method is to sputter silver or gold, but a major problem is then to make the necessary masks for the small samples.

The following units involved in the characterization of samples for resistivity measurements.

❖ *Closed cycle He refrigerator*

Variable temperature from 10 to 300 K was attained using a closed cycle He refrigerator. A two stage, oil sealed mechanical vacuum pump was employed for crating vacuum in the shroud. After the desired vacuum was reached, the valve connecting the vacuum shroud and the pump was closed and the compressor was switched on. The compressor-expander assembly in the closed cycle mode led to the lowering of temperature of the cold head. Once the temperature went below 77 K, condensation of the residual gas in the vacuum shroud caused considerable improvement in the vacuum and cryocooling of the system. Along with the heat isolation achieved through cryocooling, a radiation shield surrounding the second stage of the cold head provided further heat isolation. The radiation shield was attached directly to the first stage of the cold head which could be cooled to 40 K when the temperature of the second stage cold head was 10 K.

❖ *Temperature Controller*

Temperature of the second stage cold head was controlled with a digital temperature controller Lakeshore (model 332). This is a microprocessor based indicator/controller system designed to interface with cryogenic refrigeration systems. The indicator/controller measures and displays process temperature via a silicon diode temperature sensor, and controls power to a heater within the refrigeration system to maintain process temperature at a pre-defined setpoint value. Both the heater and the temperature sensor were located close to the tip of the second stage cold head. The controller is interfaced with the computer for data acquisition. The temperature could be effectively controlled from 10 K to room temperature.

❖ *Current source*

High sourcing accuracy Keithley 6221 AC and DC current source is used for supply of current to the samples. This instrument provides ease of use with low current noise. The Model 6221 sources AC currents from 1pA to 100mA, with 10MHz output update rate. The unit features built-in standard and arbitrary waveform generators with $1MH_z$ to 100 kH_z frequency range.

❖ Digital Nanovoltmeter

The voltage developed in the sample by applying current in the four probe setup, was measured by a Digital Nanovoltmeter (Keithley make, Model 2182A). This is a highly sensitive nanovoltmeter with a large, easy to read 6 1/2 digit displays. It combines microprocessor technology with a new concept in low noise, high-gain front ends, resulting in a programmable instrument with sensitivity down to 10 nV. It provides highly accurate, stable, low noise reading on seven ranges for DC voltage measurements between 10 nV to 1000 V. This is interfaced to computer with GPIB IEEE- 488 bus.

❖ *Data acquisition*

The instruments such as the constant current source, the nanovoltmeter and the temperature controller were interfaced to a computer for automatic resistivity data acquisition as a function of temperature. These three instruments, the nano-voltmeter, current source and the temperature controller had GPIB IEEE-488 interface. Therefore, a straight forward data acquisition is done with all the instruments having GPIB type of interfacing. The software developed in Lab view is made to acquire the resistivity data as a function of temperature. The data are collected during the heating cycles. The programme involves the reversing the current direction to minimize the errors.

3.5.2. Advantage of four probes over two probes

In a linear array of four probes, these are arranged current-voltage-voltage-current, at equal distances across the array. Probes were placed individually. A four point probe is used to avoid contact resistance, which can often be the same magnitude as the sheet resistance. Typically a constant current is applied to two probes and the potential on the other two probes is measured with a high impedance voltmeter. The resistance of contacts can be estimated by comparing the

results of four-probe measurements to a simple two-probe measurement made with an ohmmeter. In a two-probe experiment, the measurement current causes a potential drop across both the test leads and the contacts so that the resistance of these elements is inseparable from the resistance of the actual device, with which they are in series. In a four- probe measurement, one pair of leads is used to inject the measurement current while a second pair of leads, in parallel with the first, is used to measure the potential drop across the device. In the four-probe case, there is no potential drop across the voltage measurement leads so the contact resistance drop is not included. The difference between resistance derived from two-lead and four-lead methods is a reasonably accurate measurement of contact resistance assuming that the leads resistance is much smaller.

3.6. Measurements of resistivity without applied magnetic Field

and temperature dependent resistivity $\rho(T)$ was measured using standard four-probe technique with a Nanovoltmeter (Keithley- 2182 A) and constant current source Keithley 6221) . With the voltage resolution of 10^{-8} V of the Nanovoltmeter, a constant current source of 10 mA flowing through the samples gives a resolution ~1 μW in the measured resistance. A closed cycle Helium refrigerators (JANIS) and a temperature controller (Lakeshore 332) were used for temperature variation (Fig.3.2). The temperature controller used a silicon diode sensor having a temperature resolution of ±0.1 K. A Computer controlled data acquisition system was used to acquire the resistance data from 40 K to room temperature. The resistance data were required during the heating cycle with heating rate confined to 3 K-min^{-1}. The grain morphology of the samples was analyzed by scanning electron microscope (Model No. JSM-6480 LV, Make JEOL) and the compositional analysis was determined by energy dispersive X- ray analysis (EDX) using an INCA Oxford Analyzer attached to a scanning electron microscope.

Fig. 3.2. The block diagram of resistivity measurement at our laboratory

Delta Mode Operation

Keithley originally developed the delta mode method for making low noise measurements of voltages and resistances for use with the Model 2182 Nanovoltmeter and a triggerable external current source. Essentially, the delta mode automatically triggers the current source to alternate the signal polarity, then triggers a nanovoltmeter reading at each polarity. This current reversal technique cancels out any constant thermoelectric offsets, ensuring the results reflect the true value of the voltage. The technique can now cancel thermoelectric offsets that drift over time, produce results in half the time of the previous technique, and allow the source to control and configure the nanovoltmeter. The improved cancellation and higher reading rate reduces measurement noise to as little as 1nV.

3.7. Measurements in Applied Magnetic Field

Magnetoresistance has been done at UGC-DAE-CRS, Indore. The basic features of the system are mentioned as follows;

- Temperature range of 1.4 - 310 K
- DC resistivity precision one part in 10^6
- Magnetic field up to 10 Tesla.
- Automatic data collection and online output on computer monitor
- Sixteen samples at a time

3.8. Critical current density (Jc) measurement

Critical current density is measured from M-H behaviour by vibrating sample magnetometer (VSM) (Fig. 3.3). The basic principle is that magnetic moment is induced when the sample is placed in a uniform magnetic field. If the sample vibrates with sinusoidal motion a sinusoidal electrical signal can be induced in suitable placed pick-up coils. The schematic figure of VSM of 14 T magnet at UGC-DAE-CSR, Indore is depicted below. The block diagram of VSR is shown in fig.3.4.

Fig. 3.3. VSM of 14 T arrangement at UGC-DAE-CSR, Indore.

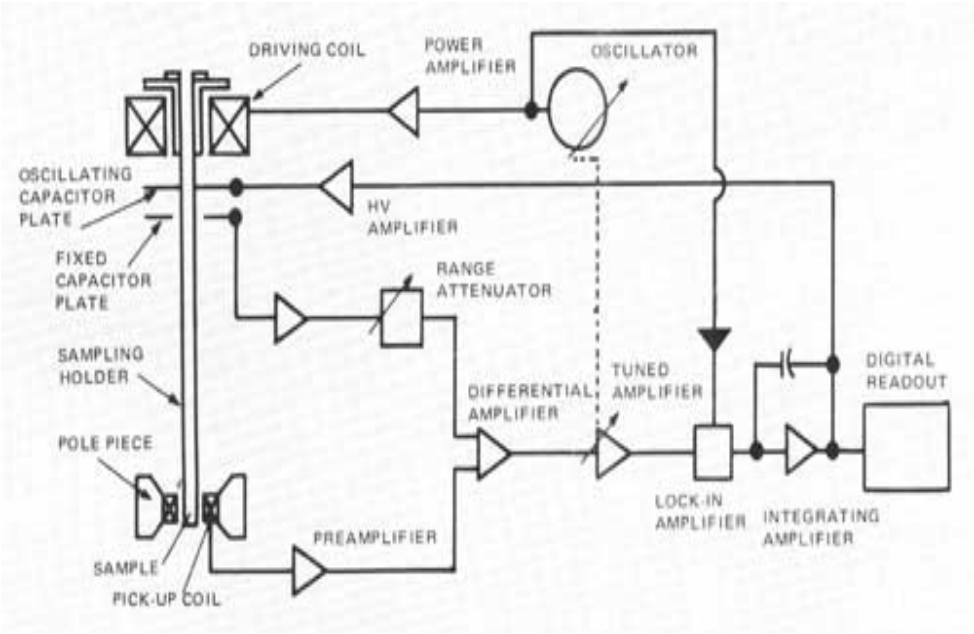

Fig. 3.4. The vibrating sample magnetometer block diagram

Critical current density (J_c) is calculated considering the Bean's critical state model [5]. The formula used for the measurement of critical current density is as follows:

$$J_c = \frac{20\Delta M}{a(1-\frac{a}{3b})} \tag{3.2}$$

Where, a < b and $\Delta M = |M_+| - |M_-|$ which is extracted from M (H) loop and a is the thickness and b is the width of the bar shaped sample.

3.9. X-ray diffraction (XRD)

X-ray powder diffraction has been performed, showing that the samples are free of other superconducting homologues in the system. This generally leads to an understanding of the material and crystal structure of a substance. X-rays are electromagnetic radiation of wavelength about 1 Å, which is about the same size as an atom X-ray diffraction has been in use in two main areas, for the fingerprint characterization of crystalline materials and the determination of their structure. Each crystalline solid has its unique characteristic X-ray powder pattern which may be used as a "fingerprint" for its identification. Once the material has been identified, X-ray crystallography may be used to determine its structure, i.e. how the atoms pack together in the

crystalline state and what the inter-atomic distance and angle are etc. XRD technique has the additional advantage that it requires only very little (<50 mg) sample and is a non-destructive technique (NDT). It is therefore an ideal technique for forensic analysis.

X-rays are electromagnetic radiations with energy in the keV range or wavelength in the Å range. X-ray diffraction occurs by the scattering of x-rays from these set of planes under certain conditions that leads to constructive interference of the scattered x-rays from each atom [6]. The scattered x-rays from the planes will interfere constructively only when the path difference is an integral multiple of the x-ray wavelength (Fig. 3.5). This condition leads to the Bragg's law for x-rays diffraction is given by

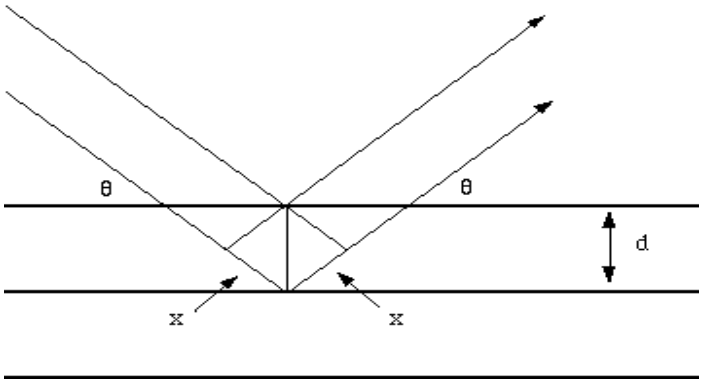

Fig. 3.5. Reflection of x-rays from two planes of atoms in a solid.

$$n\lambda = 2d \sin\theta \tag{3.3}$$

where n is the order of diffraction, λ is the wavelength of the x-ray used, d is the interplanar distance for the set of parallel planes with Miller index (hkl), and θ is the glancing angle, also called as the Bragg angle of diffraction. Thus each (hkl) plane will give a diffraction peak at a particular Bragg angle. It can be seen from the Bragg equation (3.3) that the wavelength of x-ray used should be of the order of the inter-planar distances. The inter-planar distances in inorganic compounds are of the order of few Å and therefore Cu K_α radiation having a wavelength of 1.5418 Å is mostly used for powder diffraction analysis.

The synthesized YBCO sample (pellet) was powdered and loaded in a zero background sample holder, which was a single crystal of Si. This was mounted in a STOE powder X-ray

Diffractometer**.** A schematic diagram of a typical X-ray Difractometer is shown in Fig. 3.6. given bellow.

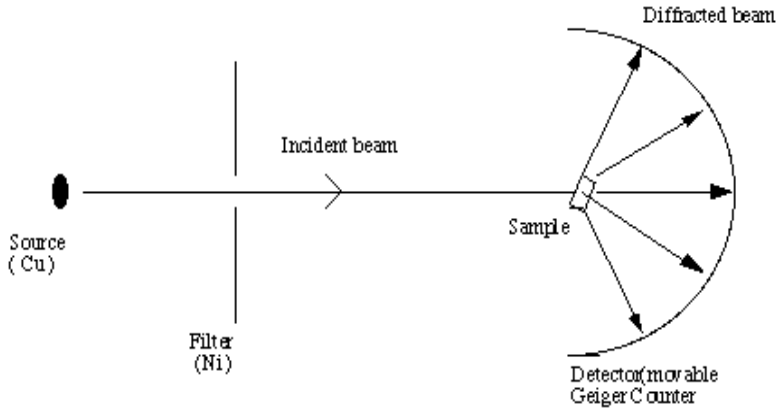

Fig. 3.6. Schematic view of an X-ray powder diffractometer.

All the samples were characterized by X-ray powder diffraction technique (PW 3020 vertical goniometer and 3710 X' Pert MPD control unit, CuK_{α}).

3.10. Scanning Electron Microscope (SEM)

Scanning Electron Microscope images give information about the tomography, morphology, composition and crystallographic information of the specimen. The surface features of an object or "how it looks", The shape, size and arrangement of the particles making up the object that are lying on the surface of the sample or have been exposed by grinding or chemical etching; The elements and compounds the sample is composed of and their relative ratios, The arrangement of atoms in the specimen and their degree of order; only useful on single-crystal particles.

Electron Microscopy is possible through the specimen interaction. The energetic electrons in the microscope strike the sample leading to various reactions as shown in Fig. 3.7. For examining thick or bulk specimens the reactions noted on the top side of the diagram are utilized.

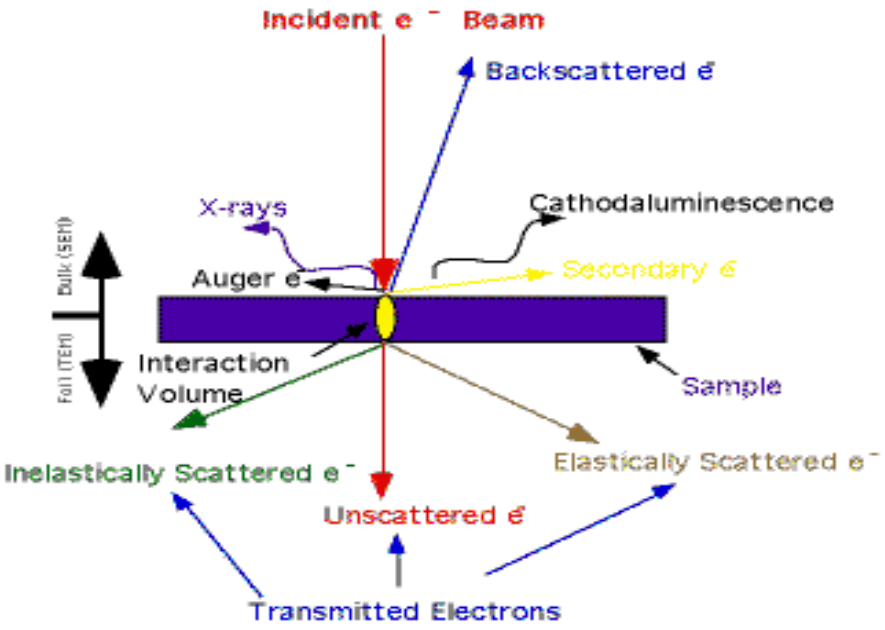

Fig. 3.7. Schematic ray diagram of a scanning electron microscope.

The electron gun at the top is producing a stream of monochromatic electrons. The stream is condensed by the first condenser lens which is used to form the beam as well as to limit the amount of current in the beam. The first condenser lens and the condenser aperture both help to eliminate the high-angle electrons from the beam. The second condenser lens forms the electrons into a thin, tight, coherent beam. The adjustable objective aperture is used to eliminate high-angle electrons from the beam. A set of scan coils then scan the beam determining the scan speed. Finally, the objective lens focuses the scanning beam onto the desired part of the specimen (Fig. 3.8). When the beam strikes and interacts with the sample, the number of interactions are counted and displayed by various instruments in the form of pixels on a CRT. The number of pixels determine rate of reaction. This process is repeated until the grid scan is finished and then repeated, the entire pattern can be scanned 30 times per second.

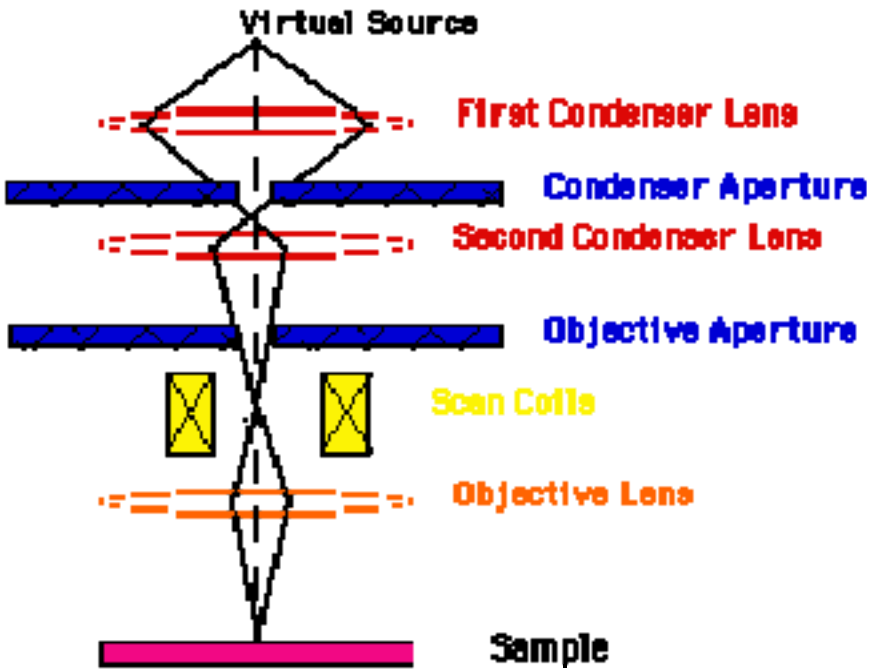

Fig. 3.8. Experimental set up for the scanning electron microscope.

Energy Dispersive X-ray analysis (EDS or EDAX analysis) is a technique used for identifying the elemental composition of the specimen. The EDX analysis system works as an integrated feature of a scanning electron microscope (SEM). During EDX Analysis, the specimen is bombarded with an electron beam inside the scanning electron microscope. The bombarding electrons collide with the specimen atoms' own electrons, knocking some of them off. A position vacated by an ejected inner shell electron is occupied by a higher-energy electron from an outer shell. During this process, transferring of outer electron takes place giving up some of its energy in the form of X-rays. The amount of energy released by the transferring electron depends on which shell it is transferring from, as well as which shell it is transferring to. Furthermore, the atom of every element releases X-rays with unique amounts of energy during the transferring process. Thus, by measuring the amounts of energy present in the X-rays being released by a specimen during electron beam bombardment, the identity of the atom from which the X-ray was emitted is established.

References

[1] A. Knizhnik, Physica C: Superconductivity 400: 25 doi:10.1016/S0921-4534 (03) 01311-X. (2003).

[2] N.V. Vuong, E.V. Raspopina and B.T. Huy, Supercond. Sci. Technol. 6 (1993) 453.

[3] D. E. Morris, N. G. Asmar, J. H. Nickel, R.L. Sid, J.Y.T. Wei, J.E. Post, Physica C 159 (1989) 287.

[4] L. Ciontea, G. Celentano, A. Augieri, et al.: J. Phys., Conf. Ser. 97 (2008) 012289.

[5] W. Gob, W. Lang, and R. Sobolewski, Physica C 1227 (1997) 282.

[6] B.D.Cullity "Elements of x-ray Diffraction", 2nd Edition, Addison- Wesley Publishing Company, Inc. (1978).

Chapter 4

The Effect of Inhomogeneities in doped $YBa_2Cu_3O_{7-\delta}$

CHAPTER 4

4. THE EFFECT OF INHOMOGENEITIES IN DOPED $YBa_2Cu_3O_{7-\delta}$

4.1. Introduction

The interest for the structural and stoichiometric inhomogeneities in $YBa_2Cu_3O_{7-\delta}$ (YBCO) superconductors is enhanced by the fact that they are directly related to the critical current densities in granular and HTSC. Here we discuss some of our recent results on modification of microstructure and superconducting properties due to microscopic and the mesoscopic inhomogeneities in $YBa_2(Cu_{0.95}Zn_{0.05-x}Ga_x)_3O_{7-\delta}$ doped superconductor. These doping to the Cu-site of YBCO has significantly influenced the excess conductive region as well as the tailing region. The strong influence of simultaneous doping of Ga and Zn to the Cu-site of YBCO has been explained based on inhomogeneity induced modifications on the overall electronic structure of YBCO. The presence of structural and stoichiometric inhomogeneities produced in the system due to doping of foreign materials effects the amplitudes of the thermal fluctuation to even bigger than the amplitudes of each observable in absence of fluctuations and, therefore, the mean field like region is got suppressed for this particular system.

4.2. Role of Ga and Zn to $YBa_2Cu_3O_{7-\delta}$ superconductors

For our $YBa_2(Cu_{0.95}Zn_{0.05-x}Ga_x)_3O_{7-\delta}$ system it has been observed that the T_{c0} value decreases with increase in Zn concentration. It has been reported that Zn substitutes Cu(2) sites more preferably i.e., CuO_2 planes are substituted preferentially than chains [1]. Therefore, strong changes in the electronic state as well as superconducting properties are expected with the increasing Zn content in these planes. In Zn doped YBCO samples, it has been observed that the Zn doping creates in-plane disorder without affecting the hole density [1]. Therefore, the T_c values decrease with increase in Zn concentration and the observed resistance is more than that of the pristine YBCO sample. The Ga^{3+} substitutes Cu preferentially at the chain site. The substituted Ga, a trivalent, is known to assimilate extra oxygen [2] into the CuO_2 planes where the actual superconduction occurs is not directly affected [3]. Therefore, T_c is not affected by Ga^{3+} as much as it is affected by doping Zn^{2+} which preferentially substitutes Cu at the plane

site. Incorporation of Zn^{2+} in CuO_2 planes, which is a non magnetic and stable 2+ ion, disturbs the antiferromagnetically coupled spin fluctuations in the plane. The hopping of electrons from chain to plane "proximity coupling", has been suggested by Chen and Hirschfeld [4]. The reduction of T_{c0} and orthorhombic distortion when simultaneous doping of Ga and Zn is done suggests interplay between the local magnetic moments which appears as a consequence of the doping of the lattice at both sites [5].

4.3. Experimental details and interpretations of results

4.3.1. Synthesis and characterization of $YBa_2(Cu_{0.95}Zn_{0.05-x}Ga_x)_3O_{7-\delta}$

A series of polycrystalline samples of $YBa_2(Cu_{0.95}Zn_{0.05-x}Ga_x)_3O_{7-y}$(x = 0, 0.012, 0.025) and YBCO has been prepared by the standard solid-state reaction route from appropriate amounts of high-purity powders of constituent oxides and $BaCO_3$. The details of the sample preparation has been made in Chapter 3. All the samples were characterized trough by the X-ray powder diffraction (XRD) for phase confirmation, microstructure and surface study by SEM, DC four probe electrical resistivity for analysis of transport properties.

4.3.2. Phase formation of $YBa_2(Cu_{0.95}Zn_{0.05-x}Ga_x)_3O_{7-\delta}$

The XRD patterns of all the samples $YBa_2(Cu_{0.95}Zn_{0.05-x}Ga_x)_3O_{7-y}$ (x = 0, 0.012, 0.025) and YBCO are shown in Fig.4.1 are indexed to be in the orthorhombic phase with space group P_{mmm}. The lattice parameters and unit cell volumes of these samples are also determined, it is noticed that the lattice parameter *a* increases while *b* remains almost constant and *c* parameter does not change much with increase in Ga doping. The major YBCO peak at 2θ =32.7 increases with Ga wt.% and other impurity peaks get reduced which is also confirmed by EDX. This analysis shows that, even in the low-concentration doped samples, substituents reside within the grains. The orthorhombic distortion $\delta = 2(b-a) / (b+a)$ and variation of orthorhombicity ((b-a)/a) were found to decrease with increase in Ga^{3+} concentration in agreement with [5]. The Zn doped sample has the orthorhombic distortion (δ) less than undoped YBCO system.

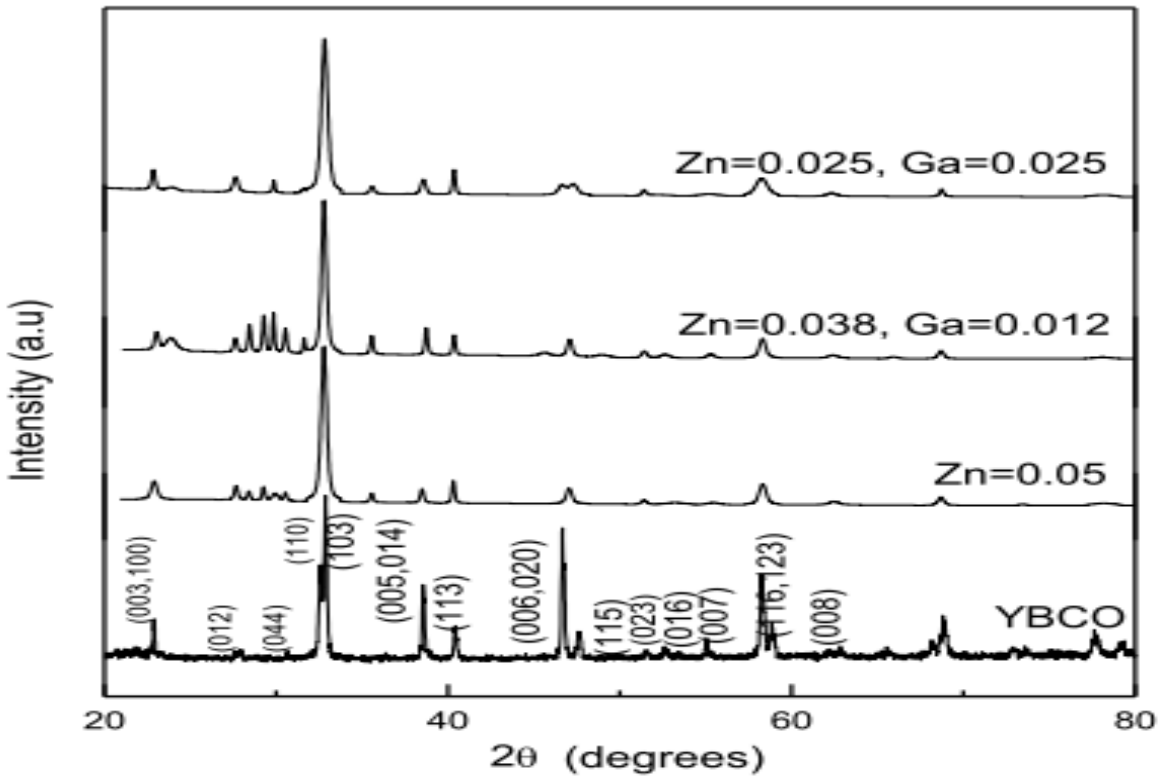

Fig. 4.1. XRD pattern for $YBa_2(Cu_{0.95}Zn_{0.05-x}Ga_x)_3O_{7-\delta}$ with Ga = 0 and Zn = 0 (YBCO), Ga = 0 and Zn = 0.05, Ga = 0.012 and Zn = 0.038, Ga = 0.025 and Zn = 0.025.

4.3.3. Microstructure modifications in $YBa_2(Cu_{0.95}Zn_{0.05-x}Ga_x)_3O_{7-\delta}$

The scanning electron microscopic (SEM) images of the prepared samples are presented in Fig.4.2. This picture depicts that the average grain size decreases with decrease in Zn concentration and from the alignment of the grains it is assumed that the segregation of grains decreases with simultaneous substitution of Ga and Zn. In terms of their contribution to the total volume, the mean grain diameters were around 2 μm. These observations reveal a smooth grain-surface without significant impurities. The metal ionic substitution at the Cu site of YBCO does not affect grain boundaries, as it goes into the grain**.**

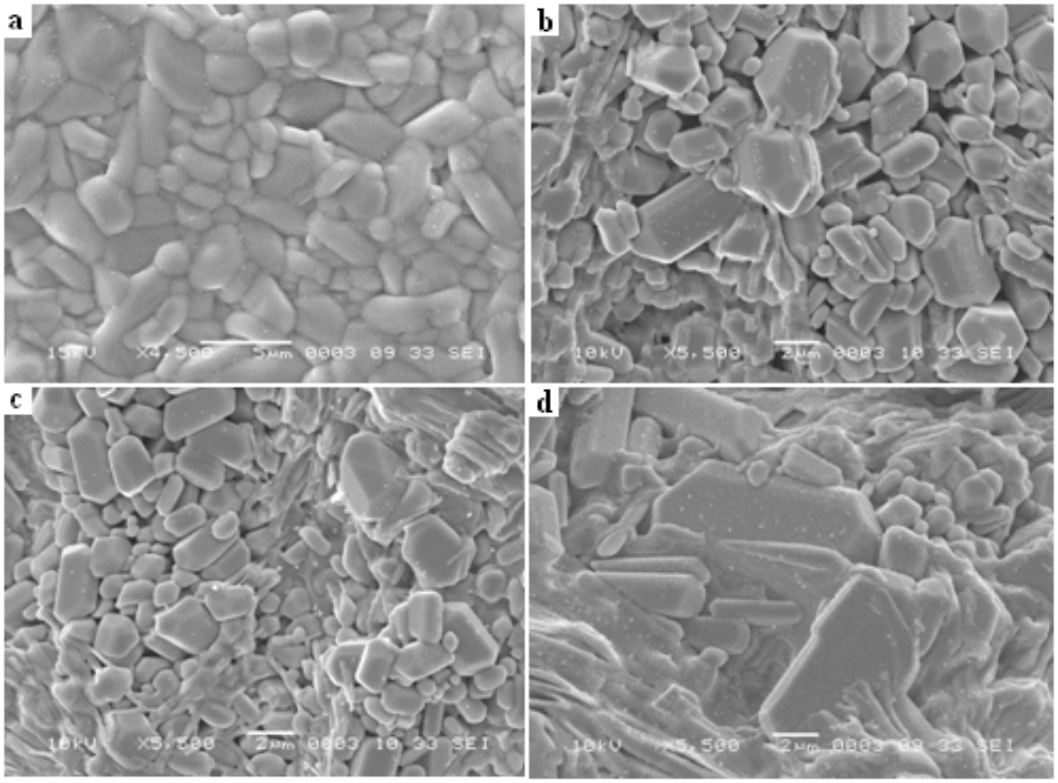

Fig. 4.2. SEM images of Zn and Ga doped samples of $YBa_2(Cu_{0.95}Zn_{0.05-x}Ga_x)_3O_{7-\delta}$ compounds, (a) YBCO (b) Zn 0.05 Ga 0.0 (c) Zn 0.038Ga0.012 (d) Zn 0.025 Ga0.025

4.3.4. Resistivity transitions in $YBa_2(Cu_{0.95}Zn_{0.05-x}Ga_x)_3O_{7-\delta}$

The temperature dependence of resistivity ρ(T) for $YBa_2(Cu_{0.95}Zn_{0.05-x}Ga_x)_3O_{7-y}$ compounds with varying Zn and Ga concentration is shown in Fig. 4.3. Sample for x = 0 i.e. Zn = 0.05 and Ga = 0.0 shows a semiconducting type ($d\rho/dT < 0$) temperature dependence of resistivity from 300 K down to the onset of superconductivity transition which is in agreement with earlier studies [5-8]. Furthermore, the change in electronic state produced by Zn^{2+} is the main reason why superconductivity is depressed by zinc doping so strongly in the resistivity transitions curves. Zinc doping does not change the overall carrier hole density but it gives rise to a redistribution of charges that produces strong electron scattering not only from Zn^{2+} but also from nearby sites which breaks the Cooper pairs and therefore decreases T_c rapidly [7]. T_c of YBCO system containing both Zn^{2+} and Ga^{3+} is lower than the expected value based on interpolation between Zn doped Ga samples [6].

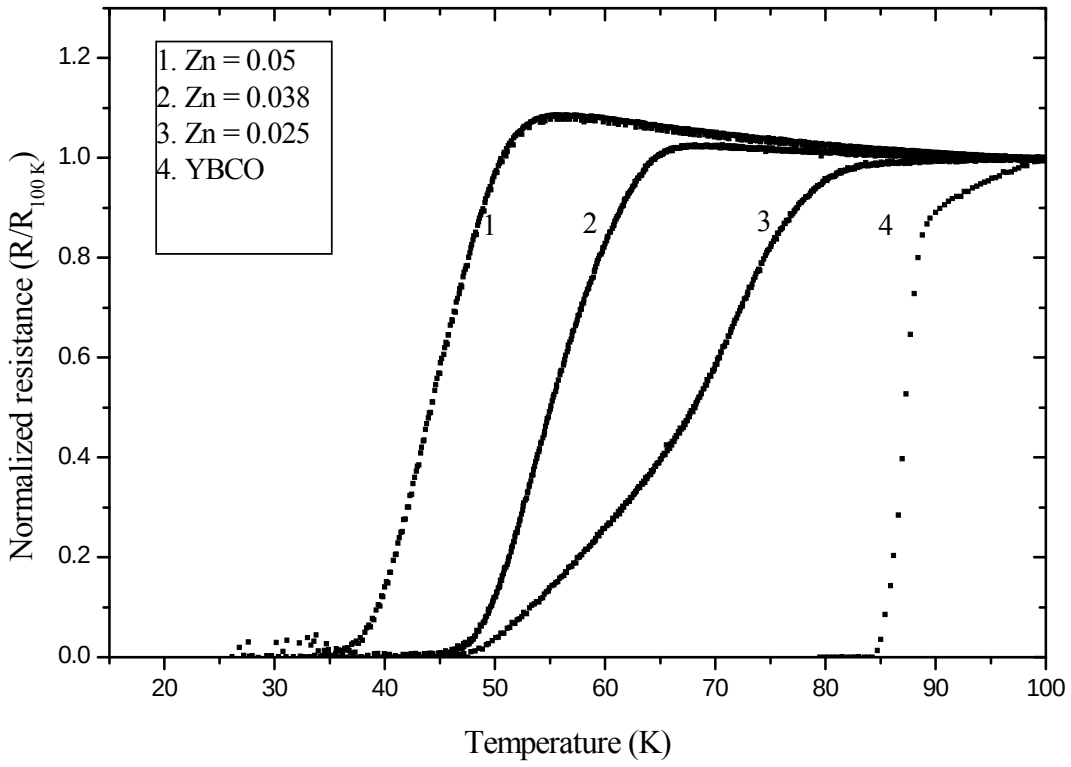

Fig. 4.3. Temperature dependent resistance with varying Zn and Ga concentration in $YBa_2(Cu_{0.95}Zn_{0.05-x}Ga_x)_3O_{7-\delta}$ compounds. (1) Ga = 0.0 and Zn = 0.05, (2) Ga = 0.012 and Zn = 0.038, (3) Ga = 0.025 and Zn = 0.025, (4) YBCO pure.

The system is granular in nature having two components, first the superconducting grains and the second the Josephson weak links. In the tailing region close to T_{c0}, the superconducting grains and the grain boundary weak links through which superconductivity is established through Josephson tunneling. The second component consists of weak links which are not superconducting, either due to the link being too weak or due to the measuring current of the corresponding link or the temperature being higher than the T_c of that link. For $T< T_{c0}$, the first component provides the channel for the transport of supercurrent. For $T_{c0} < T< T_c$, the volume of the first component is not adequate enough to provide a percolative path for super current and the R-T transition shows a tail with $R \neq 0$. Only when $T \leq T_{c0}$, a percolative path through the first component is established and a global superconductivity is achieved in the sample with R going to zero. First superconductivity sets in within the grains and at somewhat lower temperature long-range superconducting order takes place over the whole sample [9]. Just before falling to

zero value the resistive transition abruptly changes drastically the slope and achieves zero resistance, only after a long and flat tail [10]. In the temperature close to Tc_0, attempts have been made to fit the resistance to Eq. (4.1) and the exponent δ values obtained are as shown in Fig. 4.4.

$$R = B\,\varepsilon_0^{\delta} \tag{4.1}$$

Where ε_0 is the reduced temperature (= $(T-T_{c0})/T_{c0}$) and δ is the exponent for fluctuation conductivity and the relevant critical temperature, T_{c0}, which is close to the point where resistivity vanishes, has been observed [11]. For YBCO samples before the resistance attains zero value indicates that the superconducting grains get progressively coupled to each other by Josephson tunneling across the grain boundary weak links and the onset of global superconductivity in these samples is effected only when a percolative superconducting path is established through these links [12, 13].

The region of approach to the zero resistance state reveals the occurrence of a coherence transition at a lower temperature. Focus is on the coherence transition, where the phases of the order parameter in individual grains become long-range ordered and the zero-resistance state sets in. This transition is related to the connective nature of the granular samples and is controlled by fluctuations of the order-parameter phase of individual grains. The electric resistivity falls steeply as a function of temperature. However, just before falling to zero the samples show exponent for fluctuation conductivity. The δ value obtained for pure YBCO is 1.79. This finding gives strong support to the interpretation of the coherence transition as a genuine critical phenomenon.

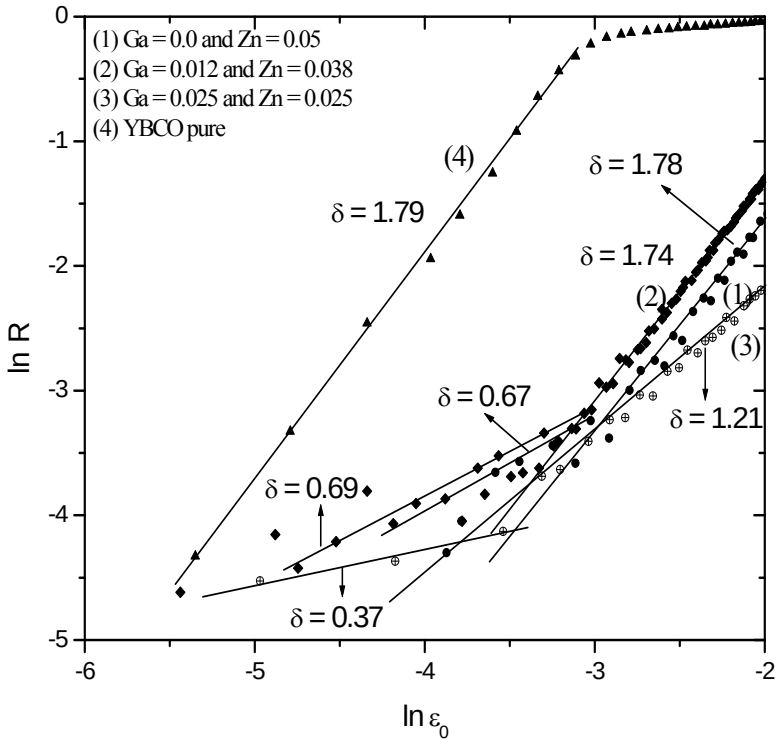

Fig. 4.4. Logarithmic plot of resistance as a function of reduced temperature showing their exponents. (1) Ga = 0.0 and Zn = 0.05, (2) Ga = 0.012 and Zn = 0.038, (3) Ga = 0.025 and Zn = 0.025, (4) YBCO pristine.

The occurrence of two values of δ may be due to weak-link related dissipation organized as a global percolation. Besides the trivial dependence of normalized resistance on sample inhomogeneities the microstructural features of the sample such as average grain size plays an important role towards the existence of two δ values. Exponents in the tailing region are obtained, may be due to the resistance of the weak links which are in a resistive state. Such a resistive state may be produced by penetration of mobile fluxoids in weak superconducting regions [14] or, if the weak links are considered as Josephson junctions, by a transition to a resistive state of these junctions when the thermal energy exceeds the Josephson coupling energy.

4.4. Conclusions

The results drawn here show that the presence of small stoichiometric and structural inhomogeneities may deeply affect the ρ(T) behavior around T_c, even when they have characteristic lengths much bigger than those of the superconductivity. Zinc doping gives rise to a redistribution of charges in the superconducting system which breaks the cooper pairs and decreases the oxygen content, therefore T_c decreases. With increase in Zn concentration both T_c and T_{c0} values decreases. T_c is not affected much by Ga^{3+} as much as it is affected by doping Zn^{2+}. The exponent values the scaling equation for fluctuation conductivity in the T_{c0} region decrease with increase of substitution concentration. The dual exponent character shows that the intergranular weak links develop more resistance with increasing impurities.

References

[1] Li Ang, Ying Xuenong, Xu Xiaoshan, et al., Physica C 337 (2000) 285.

[2] I. H. Song, E. H. Lee, B.M. Kim, I. Song and G. Park, Appl Phys Lett. 74 (1999) 2053.

[3] L. Shkedy, G. Koren and E Polturak ar Xiv: 0502254v1 (cond-mat Supr-con), 10 Feb 2005.

[4] W. Chen and P.J. Hirschfeld ar Xiv: 0811 4240v2 (cond-mat Supr-con 27 Nov (2008).

[5] N. C. Mishra A. K. Rajarajan, K. Patnaik, R. Vijayaraghavan and L. C. Gupta, Solid State Communications 75 (1990) 987.

[6] A. Mohanta and D. Behera, Indain Journal of Pure and Applied Physics 47 (2009) 676.

[7] M. A. Rodriguez and A Navrotsky, F Licci, Physica C 329 (2000) 88.

[8] L. Solderheim, K. Zhang, D. G. Hinks, M. A. Beno, D. Jorgensen and C. U. Serge, Nature, 328 (1987) 604.

[9] V. N. Vieira, P. Pureur and J Schaf, Phys Rev B 66 (2002) 224506.

[10] F.T. Diasa, V.N. Vieira, P. Rodrigues r, et al., Physica C 408 (2004) 688.

[11] A.R. Jurelo, I. Abrego-Castillo, J. Roa-Rojas, et al., Physica C 311 (1999) 133.

[12] D. Behera and N. C. Mishra, Supercon Sci Technol. 15 (2002) 72.

[13] A. Mohanta and D. Behera , J Supercond Nov Magn. 23 (2010) 275.

[14] Y. Song, A. Misra, P. P. Crooker, J. R. Gaines, Phys. Rev. B 45 (1992) 7574.

Chapter 5

Superconducting Order Parameter Fluctuation in Doped Samples of $YBa_2Cu_3O_{7-\delta}$

CHAPTER 5

5. SUPERCONDUCTING ORDER PARAMETER FLUCTUATION IN DOPED SAMPLES OF $YBa_2Cu_3O_{7-\delta}$

5.1. Introduction

In the present chapter we analyze the mechanism of charge transfer in $YBa_2Cu_3O_{7-\delta}$ (YBCO) when its charge reservoir layer is perturbed due to doping. Due to short coherence length, high transition temperature and anisotropy of the system there develops the fluctuation of superconducting order parameter. In this chapter we analyze the effect of doping at different sites (particularly at Y and Cu) of YBCO. To make this chapter selfcontained attempts has been made to explain the role of defects in YBCO (section 5.2) and their consequences in influencing the SCOPF (section 5.3). Our experimental details in synthesizing, measuring and characterizing are illustrated in section 5.4.

5.2. Role of defects in $YBa_2Cu_3O_{7-\delta}$

The superconducting phase in all the cuprates has common features. They are all type II superconductors. The coherence length was found to be very short, of the same order as the unit cell. The superconductivity in these materials is very anisotropic, and the penetration depth of a field applied parallel to the CuO_2 planes can be up to 50 times larger then the penetration depth of a field applied normal to the planes. The critical temperature increases with the doping up to some point known as the optimal doping point, increasing the doping further results in a reduction in T_c. The doping regimes below and above the optimal doping are known as the underdoped and overdoped regimes, respectively. Many works have shown that the boundary between antiferromagnetism and superconductivity is not at all sharp, meaning that antiferromagnetic (AF) correlations still exist in these compounds even at high doping levels and in the superconducting state. Theoretically it is hard to accept that magnetism and superconductivity can coexist, when it is known that the BCS state is completely destroyed by a small amount of magnetic impurities. On the other hand, the small coherence length, and the fact

that there are AF correlations in the CuO_2 planes, led many researchers to suggest that the origin of the superconductivity in the cuprates is magnetic.

By substituting 1 wt.% of the Cu by nonmagnetic impurities like Ni or Zn the extent of T_c suppressions can be measured in an indirect way. Although Zn is not magnetic, it induces magnetic sites in the planes which have Curie like behaviour [1]. By measuring the line shape of the planar Cu, Julien et. al.[2] deduced that the Zn induces a staggered field in its vicinity. This magnetic field decays rather fast, on a length scale of a few lattice constants. They could not tell the exact real space shape of the susceptibility in their experiment. Zn replaces a Cu ion in the planes, it has the same charge but has no spin, so doping with Zn is a way to dilute the lattice. The relevance of investigating changes in the properties of high T_c superconductors by doping with substitutional elements is evident from the fact that all the high T_c superconductors have resulted from substitution at one or more cationic sites in the parent materials. Since these studies provide a very good probe to understand the mechanism behind superconductivity, they become important from the fundamental point of view as well. Substitution at the Cu site is the most important among all the cations of YBCO, since Cu-O networks have been suspected to play a major role for the occurrence of superconductivity in these materials. For this reason, the Cu site has been doped with almost all the elements. Among them, the 3d transition elements are considered as ideal candidates for doping at the Cu site since they posses similar electronic configuration and ionic sizes as Cu.

Amongst the many ions used as substituents at the different cationic sites in the cuprate structure, only a few ions like Ni and Zn have been found to have a preferential occupancy at the Cu site in CuO_2 plane of YBCO. Studies from X-ray and TOF (time-of-flight) Neutron diffractometries [3] show that Ni occupies only Cu(2) site while Zn occupies both Cu(1) and Cu(2) sites with two-third of Zn atoms replacing Cu(1). Many authors [4-6] have shown that Zn preferentially occupies Cu(2) sites. The thermogravimetric studies [7] also suggest that Ni and Zn enter the Cu(2) sites. Substitution by metal ions at Cu site in YBCO type superconductors leads to unfavorable effect in superconductivity to different degrees for different dopant metal ions. Incorporation of Zn in CuO_2 planes to form the composition $YBa_2Cu_{3-x}Zn_xO_7$ has dramatic effects on superconducting transition temperature. The dTc/dx in this case is about -13 K/at% [8, 9]. With same amount of Ni doping, T_c suppression is only about half of that due to Zn doping. The orthorhombic structure of YBCO is retained with substitution by Zn. Several models have

been proposed in the literature to account for the large suppression of T_c with Zn substitution. Zn^{2+} is a non-magnetic and stable 2+ ion. The presence of such ions disturbs the antiferromagnetically coupled spin fluctuations in the CuO_2 planes. As a result, Cu ions at the vicinity of the Zn ions acquire local moments. Existence of local moments in Zn doped YBCO system has been shown by NQR, EPR and magnetic susceptibility measurements [10]. It is also reported that the spin-lattice relaxation rate at 100 K decreases faster than at 300 K for the Zn substitutions. This suggests that the Zn substituents carry no local moment and suppress the antiferromagnetic spin fluctuation between the Cu-3d moments [11]. According to many theories [12, 13] the antiferromagnetically coupled spin fluctuations are essential for superconductivity in cuprate systems. The local moments developed due to slowing down of such fluctuations in Zn doped samples of YBCO reduce the strength of Cooper pairs and hence lead to a large suppression of T_c.

Another explanation for T_c suppression due to Zn substitution which considers the role of apical oxygen O(1) (structure of YBCO in chapter 1) in the charge transfer process has been given by Li et al. [14]. The conventional charge transfer model speculates the transfer of holes from the charge reservoir layer (CuO chains) to charge conduction layer (CuO_2 plane) through the apical oxygen [15]. Therefore, the CuO bonding along the c-axis is important for the effective charge transfer and high Tc. It is experimentally established that Tc increases if Cu(2)-O(1) bond length decreases. But Zn doping in YBCO causes atomic displacement and shortening of Cu(1)-O(1) bond length and elongation of Cu(2)-O(1) bond length by 8 to 12%. This along with the filled d-shell of the Zn^{2+} ion lead to interruption in the charge transfer and T_c suppression. The hole from the Cu(1) site is interrupted to go to Cu(2) site through the apical oxygen located just below the doped Zn i.e. a hole supplied channel to Cu(2) site is lost by doping a Zn atom. As a consequence, the T_c is reduced. In case of Ni substitution, the situation of blocking the channel for transfer of charges through apical oxygen does not occur because Ni atom has unfilled d-shell. This model reasonably explains the fact that in spite of introduction of Ni and Zn into CuO_2 plane, the suppression of superconductivity is much stronger on Zn doping than on Ni doping. In addition to the above effect, some authors suggest that the disturbance in electronic structure in CuO_2 planes can occur even at a low doping of Zn and can suppress the Tc [16]. The XPS studies of the electronic structure of Zn-doped YBCO [6] support this explanation. Park et al. [11] considered the modifications in the magnetic interaction between the

copper local moments when magnetic and non-magnetic ions such as Ni and Zn occupy the Cu sites.

In YBCO, the nature of the charge reservoir layer and the mechanism of charge transfer has been studied through preferential chemical substitutions by trivalent ions like Ga^{3+}, Fe^{3+}, Al^{3+}, Co^{3+} and monovalent ions like Ag^{1+}, Au^{1+} in the CuO chain. Mossbauer spectroscopy by Tamaki et al. [17] has shown that Fe atoms occupy both Cu (1) and Cu (2) sites. X-ray diffraction, thermogravimetric and neutron powder diffraction studies have determined that Co^{3+}, Al^{3+} replace Cu (1) [18]. The preferential substitution of Al, Fe, Co at Cu (1) site is confirmed by Neutron scattering, NMR and XANES [19, 20]. Gold and silver have been shown to substitute exclusively the Cu (1) sites [21].

Small amount of trivalent ions like Al^{3+}, Fe^{3+}, Co^{3+} substituting for Cu(1) at the chain site induces crystallographic phase transformation (orthorhombic to tetragonal) without affecting the T_c significantly [22]. Such substitutional studies have clearly indicated a drastic change in the structure without much change in the superconductivity, thus giving an impression that structural features in the ab-plane may not have much relevance to superconductivity. Other studies [23] have shown that though on a macroscopic scale a transition from orthorhombic to tetragonal structure occurs, oxygen ordering in the local scale still exists. As the impurity atoms occupy the lattice sites in the CuO basal plane they change the oxygen coordination around neighbouring Cu(1)s. Fe, Co and Ni prefer octahedral oxygen coordination site rather than 4-fold co-planar coordination of Cu(1)s. Presence of octahedrally coordinated impurity ions in Cu(1) site disturb the Cu-O chain and cause an averaged tetragonal symmetry.

There are many factors which contribute to the T_c suppression on doping with trivalent metal ions in the CuO plane of YBCO. The first is the decrease in the hole content due to increased valences of the dopants. Ga^{3+} incorporation in the CuO chains reduces the formal valence of Cu from 3+ to 2 + reducing carrier (hole) density in the plane [4]. Secondly, the localization of the charge carriers is shown by Cai et al. [24] that when Cu(1) is substituted by trivalent ions like Al and Ga, holes on the oxygen site fond to be localized near impurity ion. The impurity ions also modify the CuO bond length along the c-axis and thus affect the charge transfer process from the charge reservoir to the CuO_2 planes. The electronic properties of copper oxide superconductors change with doping at chain and plane sites with iso and allovalent ions [4, 25]. To have an understanding of the mechanism of superconductivity a deep insight to the electronic

properties is essential. Ga^{3+} impurities have a five-fold co-ordination. The Cu atoms in the Cu-O chains have a four fold co-ordination. So there exists a coordination mismatch between the parent and the dopant. Rodriguez et al [26] have reported that Cu (1) site substitution affects the superconductivity mainly through a decrease in P type carriers in CuO_2 planes [27] and decreases T_c at a rate 2-5 K/ at. %. When Ga and Zn ions are substituted for Cu, they apparently have a site preference maintaining an orthorhombic structure. The simultaneous substitutions of Cu by Ga and Zn with +3 and +2 charge state respectively have been analyzed [4].

Zn doping of $YBa_2Cu_3O_{7-\delta}$ has been extensively studied, and presents many unresolved questions. The Zn doping rapidly depresses T_c, with about 10 K per atomic percent. This is surprising for a nonmagnetic impurity [28] especially as it is believed to have the same valence (Zn^{2+}) as the Cu in the plane, for which it substitutes [29]. Doping with Zn could affect conduction properties through pair-breaking [30].

Since there should be no pair-breaking from nonmagnetic impurities in superconductors with isotropic s-wave pairing, it is important to note that Zn has been found to cause formation of local magnetic moments [31] by affecting neighboring copper sites. Again, Zn doping creates in-plane disorder without affecting the hole-density. This may be compared with the case of Ca impurities, which are nominally non magnetic magnetic, and yet give smaller T_c depression [32, 33]. Ca doping at Y site has created much interest in the scientific community as this doping turns an oxygen-deficient YBCO system from insulator to superconductor. Again, Ca doping tends to reduce transition temperature T_c in an optimally doped sample [34, 35]. This decrease of oxygen content is countered by extra holes introduced by Ca^{2+} ions [36, 37]. Not just the electrical properties even the structure changes from orthorhombic to tetragonal [38] and grain size reduces [39] on Ca doping. In addition to affecting T_c, Ca occupying Y site in the doped samples of YBCO decreases normal state resistivity, increases critical current J_c, affects the interlayer coupling strength, J [40] and hence influences the SCOPF [41] region above T_c. The SCOPF being basically a precursor to the onset of superconductivity in the grains, attempt has been made to observe the variation of T_{LD} with the addition of Zn to the Ca doped system of YBCO.

Although Zn and Ca are nominally nonmagnetic dopants controlling the electronic properties of YBCO, it has been found to severely depress T_c in $Y_{1-x}Ca_xBa_2(Cu_{1-y}Zn_y)_3O_{7-\delta}$. In this chapter, the evolution of anisotropy has been analyzed for the effect of hole doping, and CuO-chain

electronic state anisotropy by Zn doping to the Cu site and Ca doping to the Y- site through SCOPF below T* (the temperature below which an up turn or down turn of the R-T curve occurs), T* being the temperature related to pseudo-gap regime where onset of fluctuations in the order parameter of superconductors sets in. Fluctuations could well explain experimental data, and values for some microscopic parameters were obtained from fits of theory to experiments.

5.3. Calculation of SCOPF

The thermal fluctuations in HTSC give a finite probability of the formation of Cooper pairs which results excess conductivity during the transport of carriers [42]. The fluctuations due to finite cooper pair formation probability induce excess conductivity or paraconductivity in the normal phase close to T_c [43]. While approaching from higher temperature side, the fluctuations have the characteristics of a quasi-1D and quasi-2D geometries, but close to T_c, a cross over occurs to homogeneous 3D Gaussian fluctuations. The short coherence lengths of the high T_c cuprate superconductors produce a significant rounding of the transition curve, which provides for the possibility to study fluctuating superconducting pairs over an extended temperature region above the transition temperature T_c. Such studies are of interest and may give estimates of microscopic parameters such as the coherence lengths, phase breaking time and dimensionality of the order parameter.

Excess conductivity in high T_c superconductors seems to appear as a consequence of second order phase transition. Explanation for the enhancement in conductivity in the SCOPF region has been given by Aslamazov and Larkin [44], and Lawrence and Doniach [45]. Based on these theories, attempts have been made to ascertain the dimensionality of the fluctuations and probe the dimensionality cross over when the system approaches the 3D superconducting state. Pureur et al. [46] have calculated three Gaussian regimes above T_c in YBCO system. It is however a complicated process to determine the dimensionality in cuprate superconductors, as the adjacent CuO_2 layers are weakly coupled [47]. The analysis of excess conductivity in high T_c superconductors from different fluctuation theories [48-52] has concentrated mostly on investigating cross over from a three-dimensional (3D) fluctuation (exponent, λ, approaching 0.5) at low temperatures to a two-dimensional (2D) one (λ approaching 1.0) on heating across a crossover temperature (T_{LD}) [53-58]. The formation of fluctuating Cooper pairs dominant in

three dimensions whereas the 2D character of the carrier transport originates due to the interaction of the Cooper pairs with the existing normal electrons [42, 59]. As this thesis is concerned with superconducting order parameter fluctuations in composites and doped systems of cuprate superconductors, a brief review of the literature existing in this area [60] is presented in chapter 2.

According to Ginzburg – Landau (GL) [48] theory of second order phase transition, T_c is defined as the temperature at which the coefficient α changes its sign in the leading term of the free energy expansion:

$$F = F_0 + \alpha \left| \Psi \right|^2 + \tfrac{1}{2} \beta \left| \Psi \right|^4 + \quad (5.1)$$

However, just above the transition the free energy is raised by an amount KT_c. The associated thermal fluctuation would thus raise the order parameter Ψ from zero to a finite value proportional to $e^{-F/KTc}$. This leads to the existence of fluctuation induced superconductivity effects above T_c. The corresponding free energy is thus given by;

$$F = \alpha \left| \delta\Psi \right|^2 + \tfrac{1}{2} \beta \left| \delta\Psi \right|^4 \quad (5.2)$$

Neglecting higher order terms in equation (5.2) for the fluctuation amplitude close to minimum of the free energy it modifies to;

$$\left| \delta\Psi \right|^2 \sim KT/\alpha = KT / \alpha_0 (t\text{-}1) \quad (5.3)$$

Since Ψ_0 above T_c is zero, all the superconducting effects including excess conductivity arise from fluctuations $\delta\Psi$. The square of the order parameter amplitude, $(\delta\Psi)^2$ in equation (5.3) diverges as $(T\text{-}T_c)^{-1}$. Below T_c, the expression for minimum free energy is;

$$F_0 = - \alpha^2/2\beta = \alpha_0^2 (t\text{-}1)^2/2\beta \quad (5.4)$$

and this occurs for a non-zero value of the order parameter given by;

$$\left| \Psi \right|^2 = - \alpha/\beta = \alpha_0 (t\text{-}1)/\beta \quad (5.5)$$

The obtained fluctuation-induced excess conductivity or paracoherent phase becomes fully coherent below T_c with zero resistivity or infinite conductivity. A thermodynamic fluctuation in a superconductor is therefore a consequence of the competition of the condensation energy of the Boson pairs and the thermal energy. The excess conductivity ($\Delta\sigma$) in the lower anisotropy

superconductors have been calculated using Aslamazov and Larkin (AL) model involving microscopic approach in the mean field region [44]. According to this approach, the excess conductivity in one, two and three dimensions are given by the formulae;

$$\Delta\sigma\,(1D) = [(\pi e^2 \xi\,(0))/16\hbar s]\varepsilon^{-3/2} \tag{5.6}$$

$$\Delta\sigma\,(2D) = [e^2/16\hbar d]\varepsilon^{-1} \tag{5.7}$$

$$\Delta\sigma\,(3D) = [e^2/32\hbar\xi(0)]\varepsilon^{-1/2} \tag{5.8}$$

where $\xi(0)$ is the coherence length along the *c*-axis at 0 K and *d* is the interlayer separation. ε is the reduced temperature and given by the relation:

$$\varepsilon = (T - T_c)/T_c, \tag{5.9}$$

where T_c is the mean field critical temperature obtained from the point of inflection of ρ versus T curve in our case. The dimensional exponent λ is found from the slope of the ln $\Delta\sigma$ versus ln ε plot. All physical parameters depend on the critical fluctuation dimensionality (D), which is expressed as;

$$D = 2(2 + \lambda) \tag{5.10}$$

It is seen that the 2D to 3D cross over is mainly found above the critical temperature at a particular temperature T_{LD}, which is different for different samples [61-63]. However, it is reported that there is a temperature regime where the superconductor is neither 2D nor 3D and the extent of this regime is controlled by the ratio of the Josephson coupling. Lawrence and Doniach (LD) introduced the concept of interlayer coupling in the vicinity of the critical temperature via Josephson coupling J and in LD model, $\Delta\sigma$ is expressed as;

$$\Delta\sigma = [[e^2/16\hbar d]\varepsilon^{-1}\{1 + [2\xi(0)/d]^2\}^{-1/2} \tag{5.11}$$

This expression predicts a cross over from 2D to 3D behavior of the order parameter fluctuations at temperatures (designated as T_{LD}) on decreasing temperature of the superconductors.

$$T_{LD} = Tc\ \{1 + [2\xi_c\,(0)/d]^2\} \tag{5.12}$$

Equation (5.12) reduces to the AL equation with the approximations $\xi(\varepsilon) \ll d$ and $\xi(\varepsilon) \gg d$ in 2D and 3D regions, respectively. A characteristic temperature T_{LD} is obtained, which is called a crossover temperature. Below and above this temperature the system has 3D and 2D fluctuations

which can be described by the relevant AL equations (5.6- 5.8). The GL theory also breaks down for higher values of ε, because ε no longer remains a small parameter and short-wave fluctuations play a dominant role [48]. In this temperature region typically for $\varepsilon \geq 0.1$, the thermal fluctuations may be deeply affected by the short wavelength fluctuation effects, that appears when their characteristic wavelength become of the order of the superconducting coherence length amplitude (extrapolated to T = 0 K) ξ (0). In this region, known as short-wave fluctuation region, $\Delta\sigma$ is theoretically predicted to be falling sharply as ε^{-3}. Temperature dependence of paraconductivity data in YBCO in a temperature range above the mean field region was quantitatively analyzed by introducing a short-wavelength cutoff into the Gaussian fluctuation spectrum. This implies that the 3D short-wavelength Gaussian fluctuation dominates in YBCO and suggests a rapid attenuation of these fluctuations with decreasing wavelength in short-coherence length systems as compared to the case of the conventional GL theory. In HTSC's, understanding of the thermal fluctuation of the order parameter is still not clear.

Thermal fluctuations create Cooper pairs in superconductors above T_c from a temperature around $2T_c$ and the number of Cooper pairs increases rapidly at the expense of the normal electron density, this gives an excess conductivity, also called paraconductivity. Aslamazov and Larkin [44] gave a phenomenological relation between the excess conductivity and the reduced temperature as a combination of three equations from (5.6- 5.8). We can extract excess conductivity ($\Delta\sigma$) assuming that it diverges as power-law given by;

$$\Delta\sigma = A\ \varepsilon^{-\lambda} \tag{5.13}$$

where, $\varepsilon = T - T_c / T_c$, the reduced temperature defined with respect to the mean field temperature of the normal to superconducting transition. The AL relation is based on the Ginzburg-Landau (GL) mean field theory and is valid only in a mean field temperature 1.01 T_c to 1.1 T_c [64]. The LD theory has been used to extract the coupling strength between superconducting layers (J) which is given by $J = [\xi_c(0)/d]^2$, thus simplifying equation (5.12) we have;

$$T_{LD} = T_c\ [1+ 4J] \tag{5.14}$$

Deviations from AL and LD predictions (based on Gaussian fluctuations theory) very close to T_c could result from entering the critical region where correction terms of higher order in the superconducting order parameter fluctuation $\delta\Psi$, are not negligible in GL free energy. In

Gaussian approximation, individual fluctuations are considered to be independent and only the $|\delta\Psi|^2$ terms are included. Hence it works very well for $T>>T_c$, where fluctuations are small in magnitude. Therefore, it is quite natural to observe a deviation of the experimental $\Delta\sigma$ from Gaussian theory as temperature approaches from room temperature towards T_c.

5.4. Experimental results and interpretation of data

5.4.1. Synthesis and characterization of $Y_{1-x}Ca_xBa_2(Cu_{1-y}Zn_y)_3O_{7-\delta}$

A series of polycrystalline samples of $Y_{1-x}Ca_xBa_2(Cu_{1-y}Zn_y)_3O_{7-\delta}$ has been prepared by the standard solid-state reaction route. The details of the sample preparation are given in Chapter 3. The microstructural features of the sintered pellets were determined with a scanning electron microscope (SEM). All the samples were characterized by X-ray powder diffraction technique for phase confirmation.

5.4.2. Microstructural phase formation

The X-ray analysis of $Y_{1-x}Ca_xBa_2(Cu_{1-y}\ Zn_y)_3O_{7-\delta}$ compounds has been indexed using Chekcell software and presented in Fig.5.1, the phases were confirmed to be orthorhombic at room temperature with a space group P_{mmm}. Appearance of peaks (003), (004), (005) and (006) in the XRD pattern reveals (00*l*)-orientation of YBCO. The (00*l*) peaks of YBCO are observed showing that the basic orthorhombic structure of YBCO is preserved. In $Y_{0.9}Ca_{0.1}$ -123 system, the same peaks of YBCO are observed but with increased intensities without showing any noticeable impurity peaks. With the addition of Zn to the system, the superconducting phases are still retained within the doping range of y = 0.02 to y = 0.04. However, the intensities of all the superconducting peaks of YBCO continued to increase for the entire range leading to the result that no remarkable structural transition occurred for these samples.

The SEM microstructure characterization i.e. grain-size distribution of the composites has been shown in Fig. 5.2. It is clearly visualized that in Y0.9Ca0.1 -123 compound, tiny white spots get imparted to the grains of YBCO in the micrograph thereby modifying the surface morphology of the sample and intra-granular property to some extent. With the addition of Zn to Y0.9Ca0.1 -123 system these small white spots along with some white patches of the order of grain size are observed clearly signifying that some of the superconducting grains are affected

undesirably associated with micro structural modifications. We have also observed that this damage to the superconducting behavior of the grains increases with increase in Zn content leading the system to the semiconducting nature. In the next section of this chapter we have examined the consequence of simultaneous doping of Ca and Zn to YBCO on the superconducting transition temperature, T_c and the crossover temperature, T_{LD} by studying the fluctuation-induced conductivity of these samples.

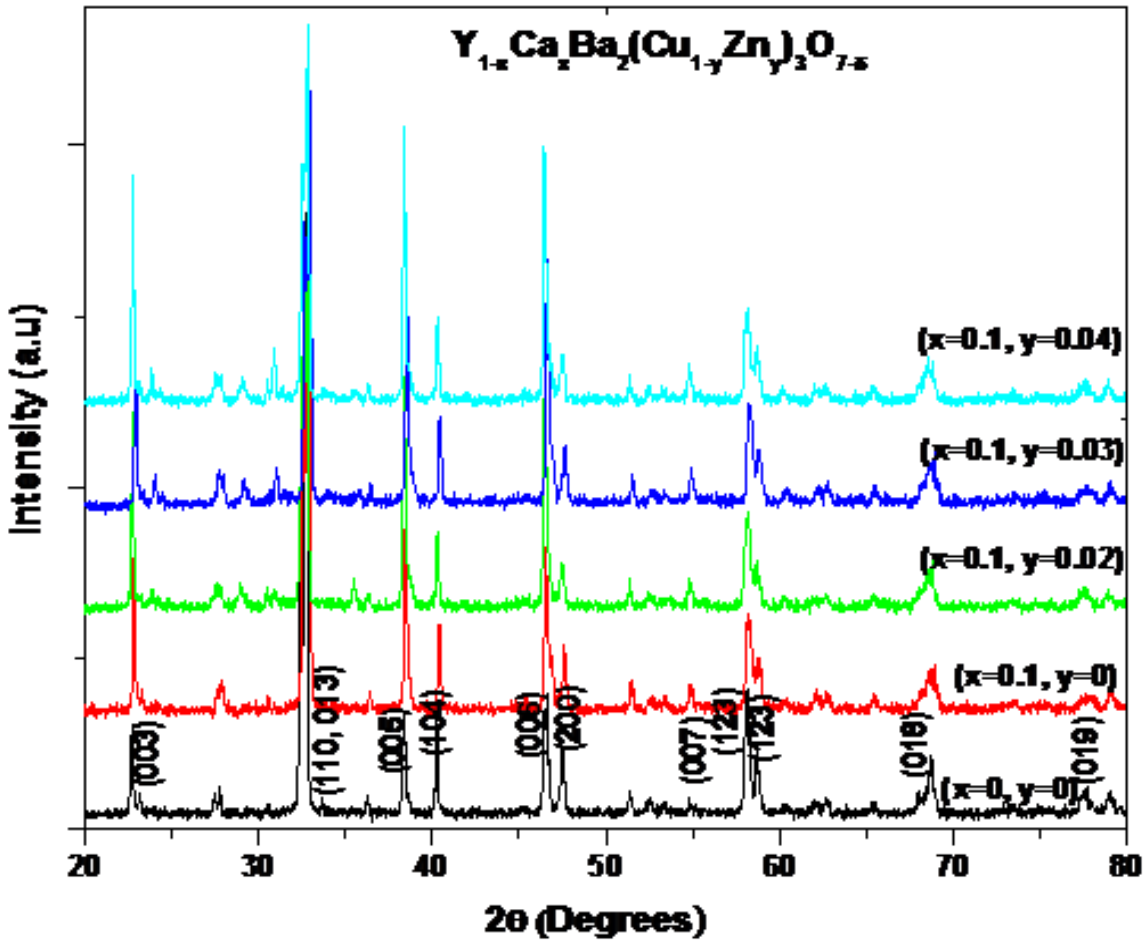

Fig. 5.1. XRD patterns of $Y_{1-x}Ca_xBa_2(Cu_{1-y}\ Zn_y)_3O_{7-\delta}$ compounds.

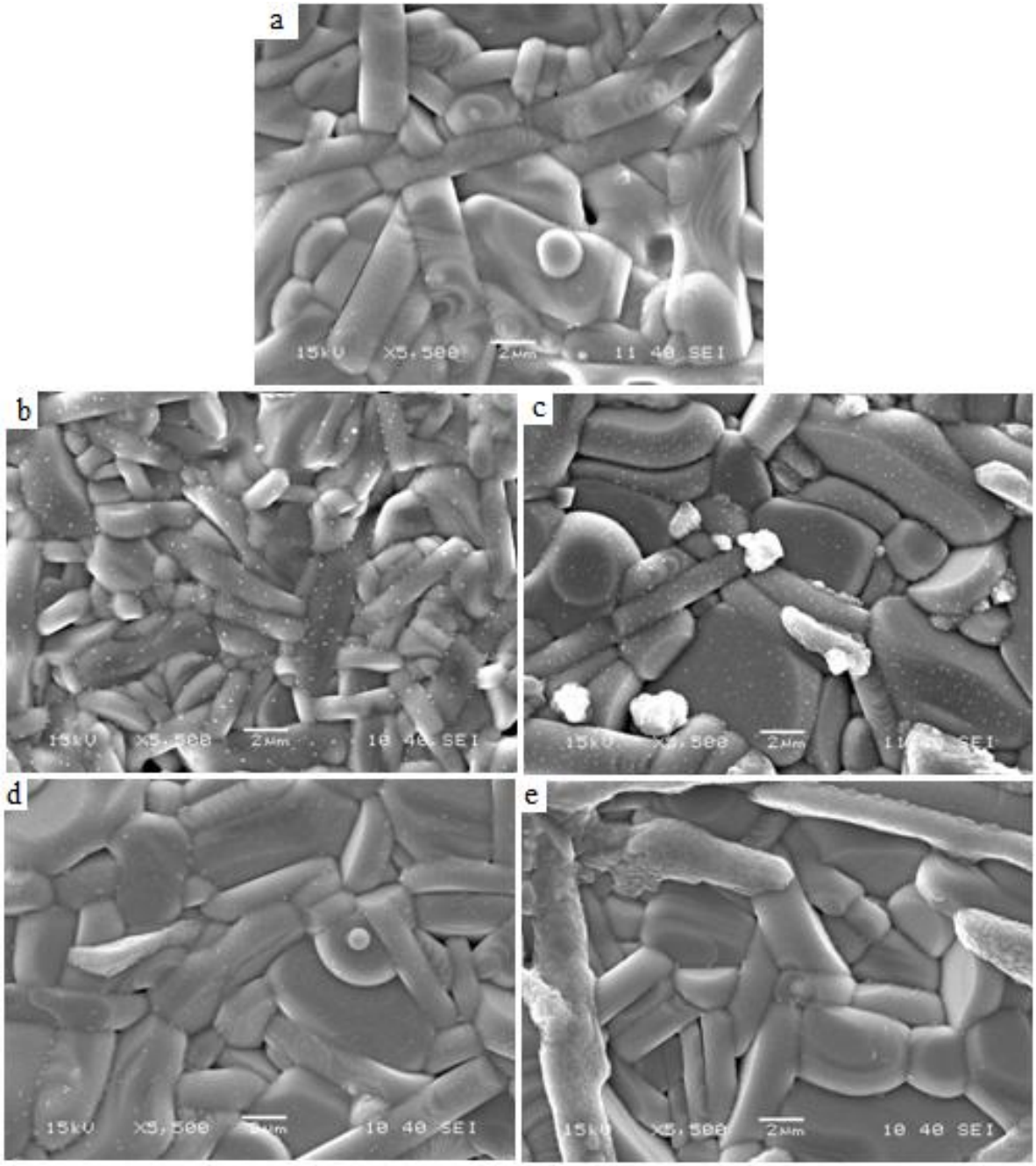

Fig. 5.2. SEM Micrographs for $Y_{1-x}Ca_xBa_2(Cu_{1-y}\ Zn_y)_3O_{7-\delta}$ compounds (YBCO, x = 1.0 and y = 0, x = 1.0 and y = 0.02, x = 1.0 and y = 0.03, x = 1.0 and y = 0.04 marked as a, b c, d and e respectively).

5.4.3. Superconducting fluctuation in $Y_{1-x}Ca_xBa_2(Cu_{1-y}Zn_y)_3O_{7-\delta}$

Figs. 5.3- 5.7 show the temperature dependence of resistivity, ρ(T) measured for $Y_{1-x}Ca_xBa_2(Cu_{1-y}Zn_y)_3O_{7-\delta}$ compounds. As shown in the Fig.5.3 for YBCO and Fig.5.4 for $Y_{0.9}Ca_{0.1}Ba_2Cu_3O_{7-\delta}$ (Y0.9Ca0.1 -123), onset of superconductivity occurs at a temperature, T* where ρ(T) shows a sharp decrease. This is the temperature where onset of fluctuations in the order parameter of superconductors sets inside the grains with grain boundaries still remaining normal. In $Y_{1-x}Ca_xBa_2(Cu_{1-y}Zn_y)_3O_{7-\delta}$ compounds not just the transition temperatures T_c, T_{LD} and T* are affected even the mean field region where thermal fluctuation leads to the excess conductivity is also affected. The ρ vs T plots of Y0.9Ca0.1 -123 and $Y_{0.9}Ca_{0.1}Ba_2(Cu_{1-y}Zn_y)_3O_{7-\delta}$ are shown in the Fig. 5.4 and Figs. 5.5- 5.7 respectively.

It is reported that superconducting transitions degrade significantly with the addition of Zn to the system but the coupling strength is improved along with micro structural modifications [65]. The SCOPF region is least affected in Ca doped sample Y0.9Ca0.1 -123 as compared to $Y_{0.9}Ca_{0.1}Ba_2(Cu_{1-y}Zn_y)_3O_{7-\delta}$ compounds. The shifting of mean field critical temperature (T_c) in Figs. 5.5- 5.7 in response to Ca doping and variation of Zn contents in $Y_{0.9}Ca_{0.1}Ba_2(Cu_{1-y}Zn_y)_3O_{7-\delta}$ compounds point to a single phenomenon in the granular superconductor. That is, both Ca doping to Y-site and Zn doping to Cu site [39] influence the intra-granular characteristics of the sintered granular superconductors as is used in the present study.

5.4.4. Dimensionality of fluctuation in $Y_{1-x}Ca_xBa_2(Cu_{1-y}Zn_y)_3O_{7-\delta}$

The intra-grain modification either due crystallographic or morphologic changes is characterized by various crossover temperatures in the SCOPF region. It has been observed that for Y0.9Ca0.1 -123 the critical region as well as the mean field region is affected in a similar way as is in case of YBCO sample. But in samples $Y_{0.9}Ca_{0.1}Ba_2(Cu_{1-y}Zn_y)_3O_{7-\delta}$ the exponents in the mean field region as well as the Lawrence-Doniach crossover temperature, T_{LD} characterizing the transition from 2 to 3dimensional nature of SCOPF have all been affected by inhomogeneities produced due to doping. This indicates that Zn not only influences the grain boundary characteristics, it also influences the grains themselves. For the analysis of the fluctuation effect, we have used the Aslamazov and Larkin (AL) [44] phenomenological relation between the excess conductivity and the reduced temperature. There are two important parameters for the analysis of excess

conductivity. The first one is based on the calculation of normal state resistivity and the second parameter relies on the correct choice of critical temperature. We have adopted the following method to calculate the excess conductivity.

$$\Delta\sigma = 1/\rho - 1/\rho_n \tag{5.15}$$

where ρ is the measured resistivity and ρ_n is normal state resistivity extrapolated to absolute zero of temperature. The normal state resistivity is calculated by using the following equation:

$$\rho_n = AT + B \tag{5.16}$$

The coefficients A and B are determined by fitting the data to this equation. The normal state resistivity ρ_n was calculated by fitting the data in the temperature range well above T_c, where the variation of resistivity with temperature was linear; in the analysis of results we have followed the same procedure.

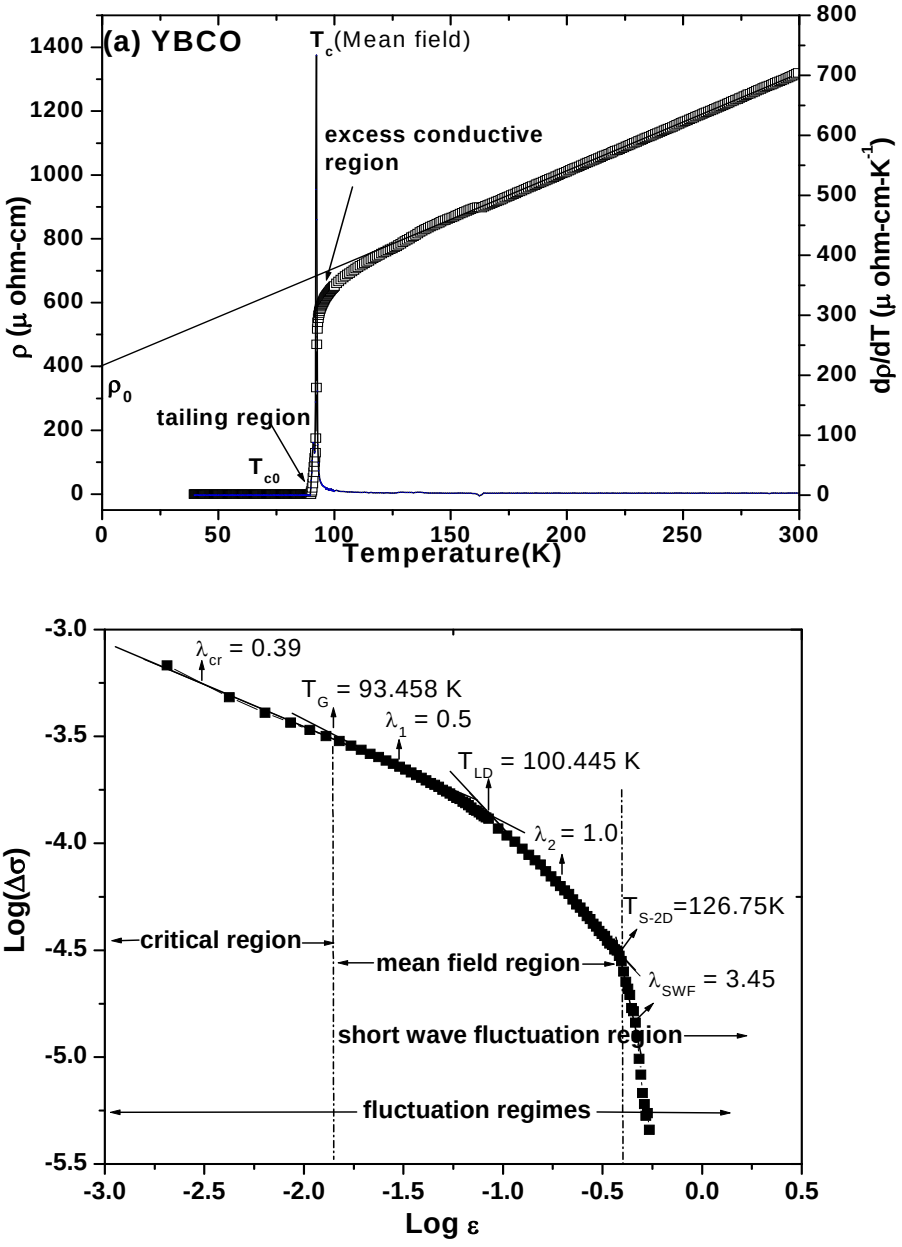

Fig. 5.3. Resistive transition and regular resistivity behavior extrapolated from the normal behavior. Linear fitting of resistivity in the temperature range 150 to 250 K and extrapolated to 0 K gives resistivity slope ($d\rho/dT$), residual resistivity ρ_0 and the log ($\Delta\sigma$) versus log ε plot with the exponent (λ) values gives the excess conductivity behavior of YBCO in different regions.

Excess conductivity ($\Delta\sigma$) has been extracted from the Aslamazov and Larkin [44] phenomenological relation equation (5.13). The most important parameter for the analysis of excess conductivity is the correct choice of critical temperature, T_c, since it arises in the ln $\Delta\sigma$ versus ln ε [$\varepsilon = (T - T_c)/ T_c$] expression. We have used the peak temperature in the $d\rho/dT$ plot as the critical temperature for the analysis to determine the critical temperature. This choice is more appropriate for polycrystalline superconductors because the complete zero resistivity state in these materials is achieved at lower temperatures when the grains are coupled together whereas the grains themselves become superconductors at relatively higher temperatures [66]. Since the compounds $Y_{1-x}Ca_xBa_2(Cu_{1-y}Zn_y)_3O_{7-\delta}$ are anisotropic in nature, we have used the AL theory to analyze our data. The AL relation is based on the Ginzburg-Landau (GL) mean field theory and is valid only in a mean field temperature ~1.01 T_c to 1.1 T_c. The amplitude A is a temperature independent parameter and its value for 2D and 3D cases is $e^2/16\hbar d$ and $e^2/32\hbar\xi_c(0)$ respectively, where d and $\xi_c(0)$ are the effective layer spacing and the GL correlation length respectively. Approaching the superconducting transition temperature from room temperature, the fluctuations exhibit filamentary nature corresponding to one dimension, or planar fluctuation corresponding to 2- dimensions or fluctuation in all 3- dimensions. From log ($\Delta\sigma$)-log ε plot different regions are also identified. In the present studies we have identified λ_1 and λ_{cr} to the exponent in the temperature range below T_{LD}, λ_2 to that of above T_{LD} and λ_{SWF} to that at higher temperatures. The crossover temperature between different regions is assigned such as T_{LD} (2D to 3D) and T_G (3D to critical). Usually, for Zn-free samples, the optimal value of Ca taken by authors lies between 0.05-0.2 [67-69], but this value increase systematically with increasing Zn content [38, 70]. In the present case, we have chosen 0.1 of Ca to Y–site for the Zn-free sample and we have compared various SCOPF parameters with the addition of Zn to the Y0.9Ca0.1 -123 sample.

It can be seen from the resistivity plots that the variation of resistivity versus temperatures deviates from linear behavior at a certain temperature. One possible source of the deviation of ρ from linear behavior is the entering of the material into the pseudo-gap (PG) regime**.** We have tried to locate the PG temperature, T*, with a high degree of accuracy. At this point we would like to emphasize that T* does not represent a phase transition temperature but instead reflect the energy of correlated holes and spins [71, 72]**.** We have investigated the excess conductivity of these samples within the framework of the Gindzburg–Landau mean-field approximation in the region of T* to T_c. In the temperature range T* to T_c the excess conductivity is clearly visible

and is marked by the fluctuations due to onset of pair-formation and breaking. The normal state and superconducting properties, including T*, of high T_c superconductors are highly sensitive to doping and, therefore, it is also important to observe the systematic variation of T* over the entire doping range extending from in-plane disorder like Zn and the crystalline state of the sample in Y site due to Ca in YBCO superconductors. Different regions of the SCOPF and the corresponding temperature values as observed for our samples are given in Table 5.1. It has been observed that for the simultaneous doping of Ca and Zn to YBCO system, instead of a sharp fall at T* the ρ-T plot leap upwards with a convex curve then as the temperature is further decreased the resistance vanishes at T_{c0} where global superconductivity prevails. T_c decreases with Ca doping and it further decreases with Zn doping to the Ca doped system. The PG region is the longest for $Y_{0.9}Ca_{0.1}$ $Ba_2(Cu_{0.96}$ $Zn_{0.04})_3O_{7-\delta}$, from 140.8 to 36.04. This is due to highest inhomogeneities produced in the system due to doping of Zn to an extra amount.

Table 5.1
Different SCOPF regions and the corresponding temperature values for $Y_{1-x}Ca_xBa_2(Cu_{1-y}$ $Zn_y)_3O_{7-\delta}$ samples.

Samples	T_c(K)	T_G(K)	T_{LD}(K)	T_{S-2D}(K)	T*(K)	dρ/dT (μohm-cm.K^{-1})	ρ_0(μohm-cm)
YBCO	92.26	93.45	99.66	126.75	145.46	3.12	400.04
Y0.9Ca0.1 -123	84.65	87.24	96.04	119.99	132.00	3.97	654.28
$Y_{0.9}Ca_{0.1}$ $Ba_2(Cu_{1-0.02}$ $Zn_{0.02})_3O_{7-\delta}$	55.11	--	56.64	57.65	112.27	8.27	3755.87
$Y_{0.9}Ca_{0.1}$ $Ba_2(Cu_{1-0.03}$ $Zn_{0.03})_3O_{7-\delta}$	52.64	--	53.64	54.65	109.6	4.04	1453.30
$Y_{0.9}Ca_{0.1}$ $Ba_2(Cu_{1-0.04}$ $Zn_{0.04})_3O_{7-\delta}$	36.04	--	37.22	37.83	140.8	2.48	1602.53

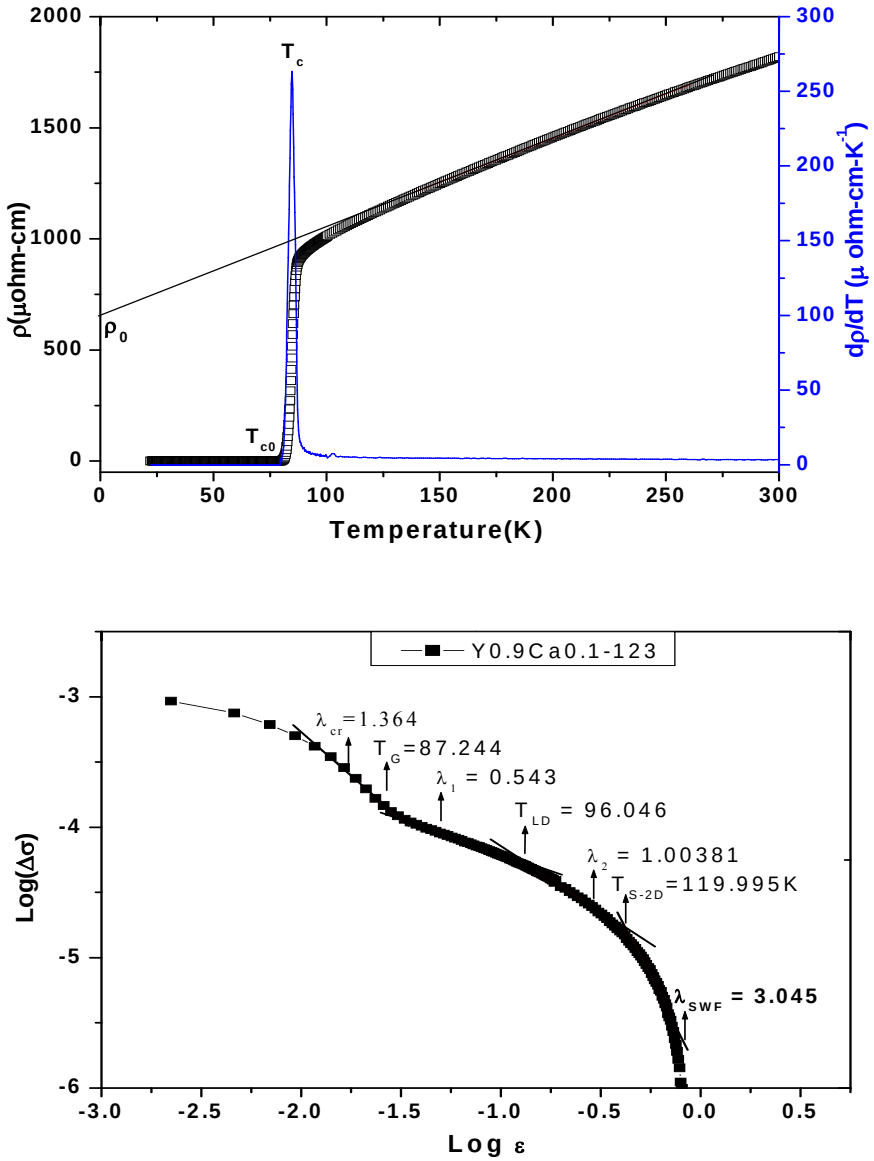

Fig. 5.4. Resistive transition and regular resistivity behavior extrapolated from the normal behavior. Linear fitting of resistivity in the temperature range 150 to 250 K and extrapolated to 0 K gives resistivity slope (dρ /dT), residual resistivity ρ_0 and the log ($\Delta\sigma$) versus log ε plot with the exponent (λ) values giving the excess conductivity behavior of Y0.9Ca0.1 -123 compound.

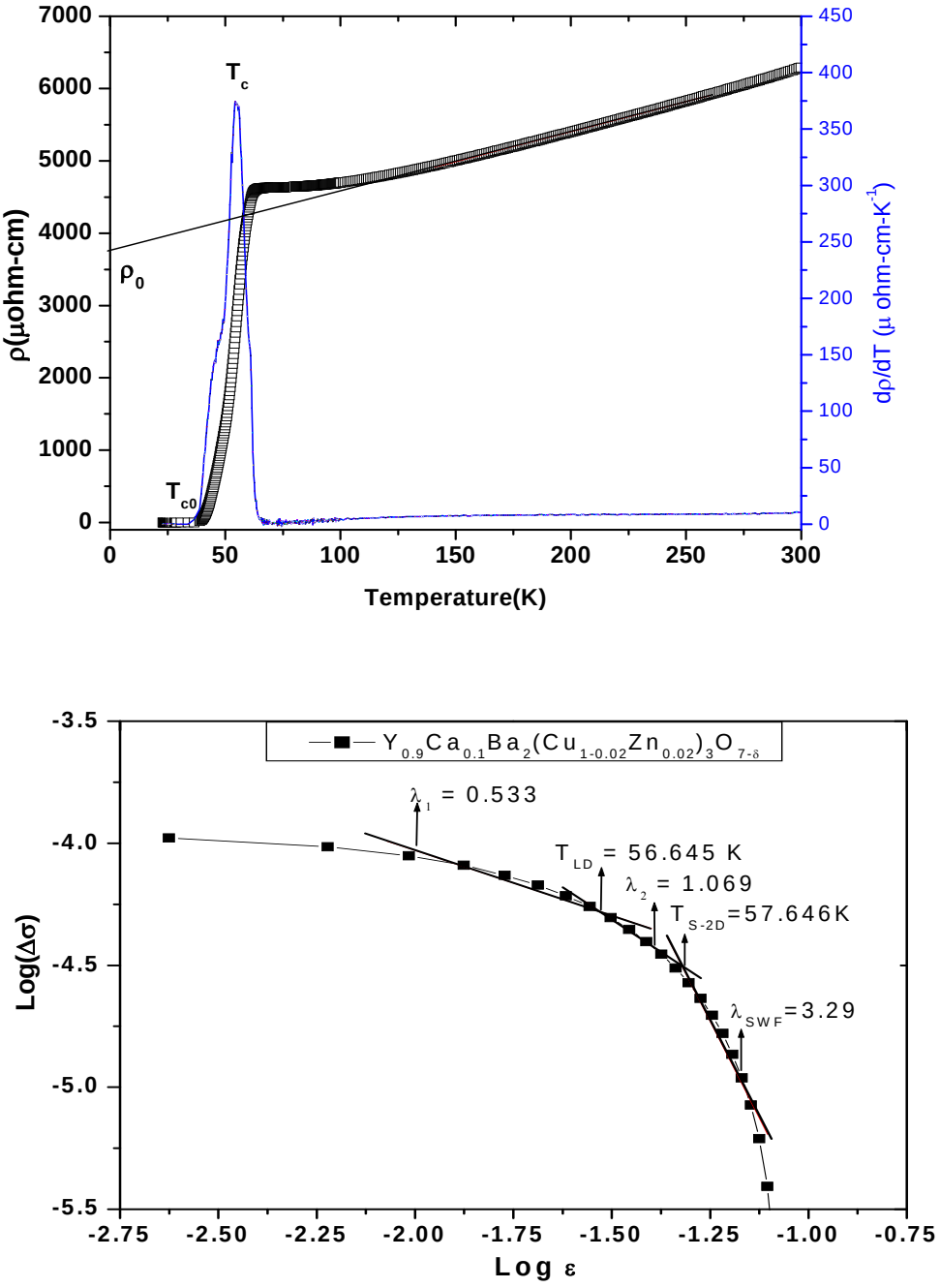

Fig. 5.5. Resistive transition and regular resistivity behavior extrapolated from the normal behavior. Linear fitting of resistivity in the temperature range 150 to 250 K an d extrapolated to 0 K gives resistivity slope (dρ /dT), residual resistivity ρ_0 and the log ($\Delta\sigma$) versus log ε plot with the exponent(λ_1, λ_2 and λ_{SWF}) values gives the excess conductivity behavior of $Y_{0.9}Ca_{0.1}$ $Ba_2(Cu_{1-0.02}$ $Zn_{0.02})_3O_{7-\delta}$ compound.

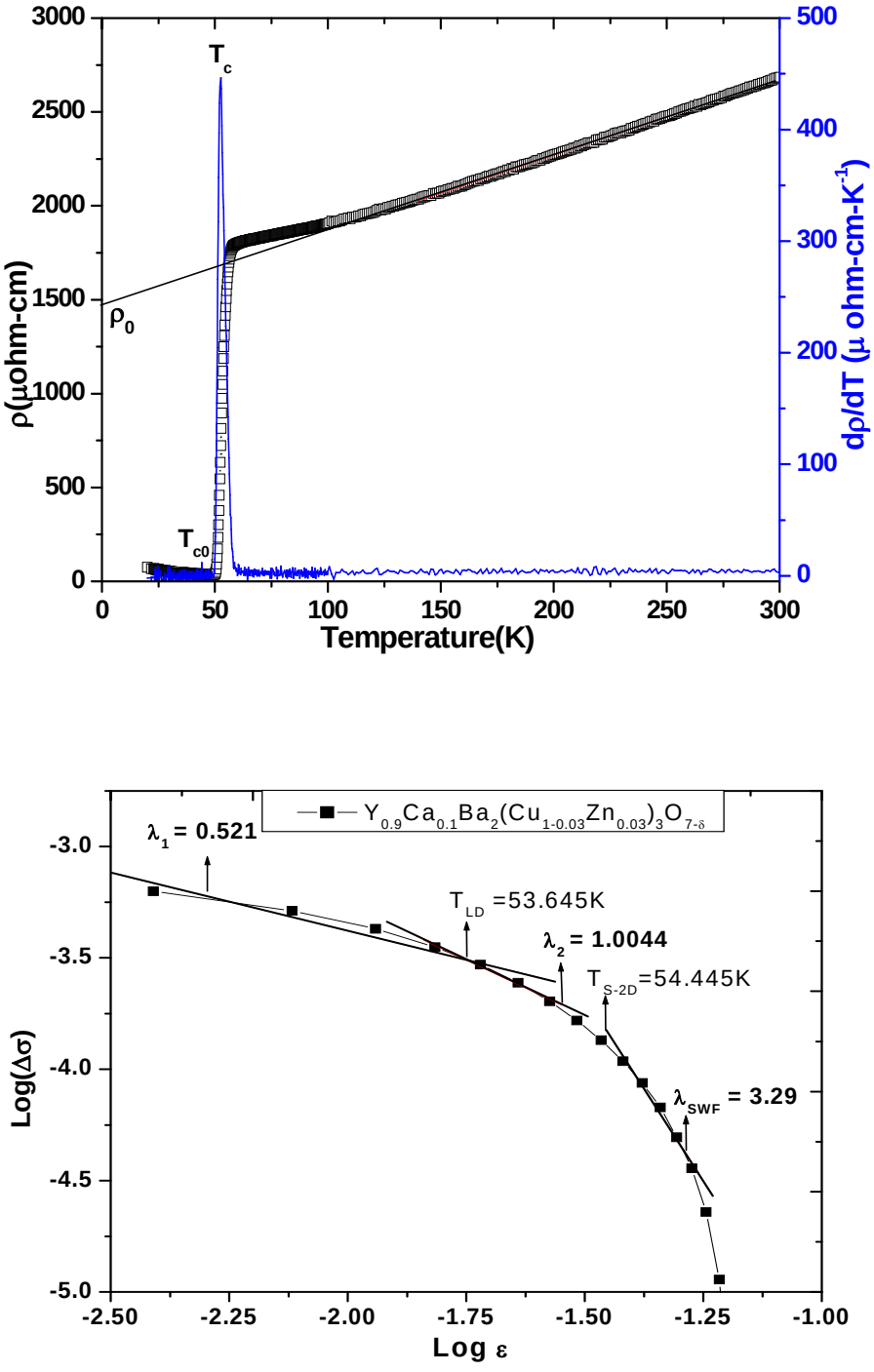

Fig. 5.6. (a) Temperature dependent resistivity, dρ/dT and residual resistivity ρ_0 (b) Log ($\Delta\sigma$) versus log ε plot with the exponent (λ_1, λ_2 and λ_{SWF}) values gives the excess conductivity behavior of $Y_{0.9}Ca_{0.1}Ba_2(Cu_{1-0.03}Zn_{0.03})_3O_{7-\delta}$ sintered.

It is important to note that Zn changes the T* values along with suppressing T_c very effectively for y = 0.02 and 0.03. For example, T*(= 132 K) comes down to 112.27 from Zn-free Y0.9Ca0.1 -123 to Zn doping up to 0.02 and T_c is suppressed from 84. 65 K (Zn-free) to 55.11 K ($Y_{0.9}Ca_{0.1}Ba_2(Cu_{1-0.02}Zn_{0.02})_3O_{7-\delta}$). Similar results have been obtained for Zn-substituted YBCO by other studies [65]. For the Zn doped Y0.9Ca0.1 -123 samples, below T* the temperature dependence changes from T-linear to convex curvature, decreases with increasing carrier concentration but for y = 0.04 due to additional inhomogeneities it raises to higher temperature value. This very different Zn-dependence for T_c and T* can been stated as an indication for the non-superconducting or semiconducting origin of the PG.

Fig. 5.4. shows the effect of Ca in decreasing T_c and T_{LD}. Further when Zn is doped to the system containing Ca Y0.9Ca0.1 -123, T_c, $T_{S\text{-}2D}$ and T_{LD} decrease to large extent (Table 5.1). Ca doping at the Y site is expected to affect the SCOPF parameters as it basically affect the intragrain behavior. Hence it can be inferred that some amount of Ca goes to lattice site. Since microscopic inhomogeneity has been shown to have an insignificant effect on the SCOPF [73], we explain the strong dependence of T_{LD} on Ca and Zn to the Cu site of YBCO by invoking its role in modifying the overall electronic structure of grains. For these reasons RT measurements and the SCOPF analysis even in the presence of strong in-plane electronic scattering by Zn^{2+} ions is a good measure to understand the very mechanism of superconductivity in cuprate superconductors.

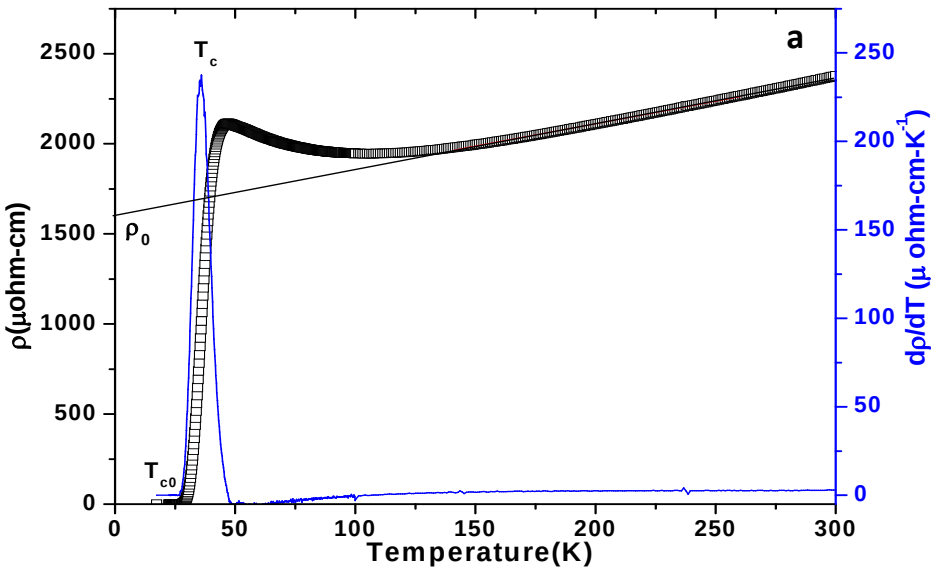

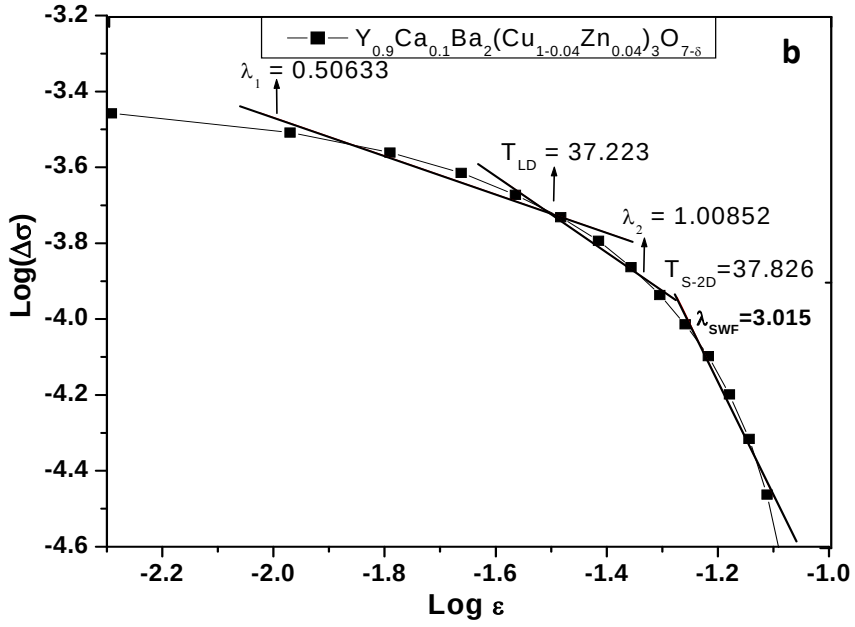

Fig. 5.7. (a) Resistive transition and regular resistivity behavior extrapolated from the normal behavior. Linear fitting of resistivity in the temperature range 150 to 250 K an d extrapolated to 0 K gives resistivity slope (dρ /dT), residual resistivity ρ_0 and (b) the log ($\Delta\sigma$) versus log ε plot with the exponents (λ_1, λ_2 and λ_{SWF}) values gives the excess conductivity behavior of $Y_{0.9}Ca_{0.1}Ba_2(Cu_{1-0.04}Zn_{0.04})_3O_{7-\delta}$ sintered.

Table 5.2
Different exponent values for $Y_{1-x}Ca_xBa_2(Cu_{1-y}Zn_y)_3O_{7-\delta}$ samples.

Samples	λ_{cr} and Temp. range	λ_1 and Temp. range	λ_2 and Temp. range	λ_{SWF} and Temp. range
YBCO	0.39	0.50	1.00	3.45
	92.45 – 93.25	93.85 – 98.05	100.99 – 123.97	129.49 – 135.88
Y0.9Ca0.1 -123	1.364	0.54	1.00	3.04
	85.64 – 87.24	87.24 – 96.64	94.04 – 114.38	123.58 – 144.62
$Y_{0.9}Ca_{0.1}Ba_2(Cu_{1-0.02}Zn_{0.02})_3O_{7-\delta}$	-	0.53	1.06	3.17
		55.84 – 56.84	56.64 – 57.64	57.84 – 59.046
$Y_{0.9}Ca_{0.1}Ba_2(Cu_{1-0.03}Zn_{0.03})_3O_{7-\delta}$	-	0.52	1.00	3.29
		52.84 – 53.84	53.44 – 54.04	54.64 – 55.44
$Y_{0.9}Ca_{0.1}Ba_2(Cu_{1-0.04}Zn_{0.04})_3O_{7-\delta}$	-	0.50	1.00	3.01
		36.42 – 37.42	37.22 – 37.82	38.02 – 38.84

It can be observed in the log–log plot of the excess conductivity vs. the reduced temperature, different λ values or the exponents, for different fluctuation regions above and below the crossover temperature. The regime that is close to T_c in the mean field region has 3D type of fluctuations but at temperature T_{LD} there is a cross over from 3D to 2D region of fluctuations. As we move to higher temperature the superconducting fluctuations follow $1/\varepsilon^3$ behavior, such

fluctuation region where the Ginzberg-Landau theory breaks down is known as the Short Wavelength Fluctuations (SWF). The values of different exponents are listed in Table 5.2. The exponent λ_1, obtained from the slope of the log(Δσ)vs. log(ε) plot, when found closer to 0.5, is reminiscent of a three-dimensional conductivity from AL theory [44] and the exponent λ_2 closer to 1.0 is characteristic of two-dimensional conductivity (2D AL). A good agreement between the observed values and theoretical values is obtained for all the samples. The temperature interval for λ_1 and λ_2 for Zn doped samples is limited to 1K which varies from 93.85 – 98.05 and 100.99 – 123.97 for the YBCO sample. The physical meaning of these changes in the fitting parameters is that as the Zn content is increased, the region of superconductivity shrinks and becomes centered for an optimal value at around 0.03. For Y0.9Ca0.1 -123 sample critical exponent (λ_{cr}) with value 1.364 is also observed which is not found for the Zn doped samples. It reflects the Ca induced mesoscopic modification in the grains, which explains for the widening of the critical region associated with increase in T_G and strong variation of T_{LD} with Ca content in Zn free and Zn doped samples.

5.5. Conclusions

Our study on the temperature dependence of resistivity in polycrystalline sintered samples of $Y_{1-x}Ca_xBa_2(Cu_{1-y}Zn_y)_3O_{7-\delta}$ were significantly modified with various dopants in YBCO superconductor. Analysis of excess conductivity has been done by a power law following Aslamazov–Larkin (AL) type equations for these polycrystalline superconductors. From the analysis of our results, we have also evaluated and extracted a characteristic exponent (λ_{SWF}) for short wavelength fluctuations. The data for all our samples fit well with the 3D AL equation and a cross over from 2D to 3D has been found at a temperature T_{LD}. It is observed that with the increase of Zn substitution to the Y0.9Ca0.1-123 systems the fluctuating region of superconductivity shrinks considerably and becomes centered at lower temperature values. Finally we conclude that temperature range for dimensionality of fluctuations in YBCO superconductors depends on the on-site cationic substitutions. Particularly the simultaneous substitution of Ca as hole dopant and Zn as an in plane disorder contribute significant changes in the characteristic behaviour of pseudogap temperature, T* over the entire doping range. Shrinkage in the fluctuating region of superconductivity has been observed for Zn doped samples

and thus the critical exponent λ_{cr} is suppressed and the cross over region is significantly shifted to lower temperature values.

References

[1] P. Mendels, J. Bobroff, G. Collin, H. Alloul, M. Gabay, J. F. Marucco, N. Blanchard and B. Grenier. Europhysics Lett., 46 (1999) 678.

[2] M.-H. Julien, F. Borsa, P. Carretta, M. Horvatić, C. Berthier, and C. T. Lin, Phys. Rev. Lett. 83 (1999) 604.

[3] J. M. Tarascon, Phys. Rev. B 37 (1988) 7458.

[4] N.C. Mishra, A.K. Rajarajan, K. Patnaik, R. Vijayaraghavan and L.C. Gupta, Solid State Comm. 75 (1990) 987.

[5] J.L. Tallon, C. Bernhand, G.V.M. Willams and J.W. Loram, Phys. Rev. Lett 79 (1997) 5294.

[6] K. Asokan, B.R. Sekhar, K.V.R. Rao and K.B. Garg, Indian J. Phys. 73A (1999) 256.

[7] J. C. Phillips : Physics of High Temperature Superconductors, AT&T : Academic Press 1989.

[8] G. Xiao, M.J. Cieplak, D. Musser, A. Gavrin, L.L. Chien, J.J. Rhyne and J.A. Gottas, Nature 332 (1988) 238.

[9] N. Peng and W.Y. Liang, Physica C 223 (1994) 61.

[10] C. Jee, D. Nichols, J. Ciasullo, J.E. Crow, T. Mihalisin, G.N. Myer, M.V. Kuric, S.H. Blam and R.P. Guertin MRS proceedings, 9 (1988) 769.

[11] T. K. Park, B. J. Mean, K. H. Lee, G. S. Go, S. W. Seo, K. S. Hou, M. Lee, H. S. Lee, H. B. Kim and W. C. Lee, Phys. Rev. B 59 (1999) 11217.

[12] S. Sugai, Phys. Rev. B 38 (1988) 6436.

[13] J.E. Hirsch, E. Loh Jr., and D.J. Scalapino, Phys. Rev. Lett. 60 (1988) 1668.

[14] A. Li, Y.N. Wang, X.N. Ying, Q.M. Zhang and W.M. Chen, Supercond. Sci.Technol. 12 (1999) 45.

[15] W.H. Fietz, R. Quenzel, H.A. Ludwig, K. Grube, S.I. Schlachter, F.W. Hornung, T. Wolf, A. Erb, M. Klaser, G. Muller-Vogt, Physica C 270 (1996) 258.

[16] A.V. Inyushkin, A.N. Taldenkov, S. Yu. Shabanov, L.N. Dem'yanets and T.G. Uvarova, J. Superconductivity, 7 (1994) 331.

[17] T. Tamaki, T. Komai, A. Ito, Y. maeno and T. Fujita, Solid State Commun. 65 (1988) 43.

[18] T. Siegrist, S.M. Zahurak, D.W. Murphy, R.S. Roth, Nature 334 (1988) 231.

[19] J. V. Andersen, N. H. Andersen, O. G. Mauritsen and H. F. Poulsen, Physica C 214 (1998) 143.

[20] R. Suryanarayan, L. Ouhammou, O. Gorochov and H. Pankowska, Physica C 199 (1992) 37.

[21] H. Renevier, J. L. Hodeau, T. Fournier, P. Bordet and M. Marezio, Physica C 172 (1990) 183.

[22] F. Licii and L. Raffo, Supercond. Sci. Technol. 8 (1995) 245.

[23] B. W. Veal, A. P. Paulikas, H. You, H. Shi, Y. Fang, J. W. Downey, Phys. Rev. B 42 (1990) 6305.

[24] Z. Xiong Cai and S.D. Mohanti, Phys. Rev. B 40 (1989) 6558.

[25] M. K. Rajneesh, K. Singh, S. Bhattacharya, M. Dixit and N. K. Gaur, Solid State Commun., 141 (2007) 605.

[26] Rodriguez M A, Navrotsky A & F Licci, Physica C 329 (2000) 88.

[27] Zhou Y X, Scruggs S & Salama K, Supercond Sci Technol. 19 (2006) 13.

[28] A. Schilling, M. Cantoni, J. D. Gou, and H. R. Ott, Nature 363 (1993) 56.

[29] R. Villeneuve, I. Mirebeau, G. Collin, and F. Bour_ee, Physica C 1597 (1994) 235.

[30] J. Axnas, W. Holm, Y. Eltsev, and O. Rapp, Phys. Rev. B 53 (1996) R3003.

[31] S. Zagoulaev, P. Monod, and J. J_egoudez, Phys. Rev. B 52 (1995) 10474.

[32] J. Maza and F. Vidal, Phys. Rev. B 43 (1991) 10560.

[33] Z.H. Wang, Mod. Phys. Lett. B 10 (1996) 1027.

[34] V.B. Geshkenbein, L.B. Ioffe, and A.I. Larkin, Phys. Rev. B 55 (1997) 3173.

[35] V. Emery, S.A. Kivelson, and O. Zachar, Phys.Rev.B 56 (1997) 6120.

[36] J. Maly, B. Janko, and K. Levin, Phys. Rev. B 59 (1999) 1354.

[37] S. H. Han, Yu. Eltsev, O. Rapp, Phys. Rev. B. 61 (2000) 11776.

[38] Anurag Gupta, Sukalpa Chaudhuri, V Ganesan, I Das, H Narayan, Anil Kumar, A J Zaleki and A V Narlikar, Supercond. Sci. Technol. 14 (2001) 937.

[39] Nawazish A. Khan, H. Ihara , Physica C 403 (2004) 247.

[40] F. Vidal, J. A. Veira, J. Maza, F Garcia-Alvarado, E. Moran and M. A. Alario, J. Phys. Condens. Matter 21 (1999) L599.

[41] S. H. Han and O. Rapp, Solid State Commun. 94 (1995) 661. Matter 21 (1999) L599.

[42] D.S. Fisher, M.P.A. Fisher, D.A. Huse, Phys. Rev. B 43 (1991) 130.

[43] P.C. Hohenberg, B.I. Halperin, Rev. of Mod. Phys. 49 (1977) 435

[44] L.G. Aslamazov and A.I. Larkin, Fiz. Tverd.Tela 10 (1968) 1104 (Sov. Phys. Sol. St. 10 (1968) 875.

[45] J. Lawrence and S. Doniach in Proc. 12th Conf. Low-temp. Phys. Kyoto 1970 ed. E. Kanda (Tokyo, Keigaku) P.361.

[46] P. Pureur, R. Menegotto Costa, P. Rodrigues jr, J. Schaf , J.V. Kunzler, Phys. Rev. B 47 (1993) 11420.

[47] Z.X. Gao, Phy. Rev. Lett 71 (1993) 3210.

[48] V.L. Ginzberg and L.D. Landau, Zh. Eksperimi, Teor Fiz.20 (1950) 1064.

[49] Z. H. Wang, Physica C 306 (1998) 253.

[50] P. Rodrigues Jr., L. Ghivelder, P. Pireur and S. Reich, Physica C 211 (1993) 13.

[51] P. Pureur, J. Schaf, M.A. Gusmao and J.V. Kunzler, Physica C 176 (1991) 357.

[52] L.B. Loffe and A.I. Larkin, Zh. Eksp.Fiz.81 (1981) 707 (Sov. Phys. JETP 54 (1981) 378.

[53] G. Deutscher, O. Entin Wohlman, M. Rappaport and Y. Shapira. in: Inhomogeneous superconductors-1979, AIP Conf. Proc. 58, ed. D.U. Gubser, T.L. Francavilla, J.R. Leibowitz and S.A. Wolf (Am. Inst. Phys., New York, 1980) P.23.

[54] J.P. Straleur, Phys. Rev. B 15 (1977) 5733.

[55] C.J. Lobb, M. Tinkham and W.J. Skoepot Solid state Commun. 27 (1978) 1273.

[56] G. Deutscher and M.I. Rappaport, J. Phys. Coll. 39 (1978) 6581.

[57] H.J. Herrman, B. Derrida and J. Vannimenus, Phys. Rev B 30 (1984) 4080.

[58] S. Marcelja, W.E. Masker and R.D. Parks, Phys. Rev. Lett. 22 (1969) 124.

[59] S. H. Han and O. Rapp, Solid State Commun. 94 (1995) 661.

[60] A. Mohanta, D. Behera, Physica B (2010), doi:10.1016/j.physb.2010.12.017

[61] A. K. Ghosh, S. K. Bandyopadhyay, and A. N. Basu, J. Appl. Phys. 86 (1999) 3247.

[62] M. Ausloos, Ch. Laurent, S. K. Patapis, C. Politis, H. L. Luo, P. A. Godelaine, F. Gillet, A. Dang, and R. Cloots, Z. Phys. B: Condens. Matter 83 (1991) 355.

[63] P. Konsin, B. Sorkin, and M. Ausloos, Supercond. Sci. Technol. 11 (1998) 1.

[64] A. Carrington, D. J. C. Walker, A. P. Mackenzie and J. R. Cooper Phys. Rev. B 48 (1993) 13051

[65] Yu X Zhou, W. Lo, Tong B. Tang and Kamel Salama, Supercond. Sci. Technol. 15 (2002) 722.

[66] J. Roa-Rojas, D. A. Landínez Téllez, Revista Colombiana De Física. 34 (2002) 1.

[67] A. Augieri, T. Petrisor, G. Celentano, L. Ciontea, V. Galluzzi, U. Gambardella, A. Mancini, A. Rufoloni, Physica C 401 (2004) 320.

[68] A. Augieri, G. Celentano, L. Ciontea, V. Galluzzi, U. Gambardella, J. Halbritter, A. Mancini, T. Petrisor, A. Rufoloni, A. Vannozzi Physica C 17 (2006) 437.

[69] S. H Naqib, J. R. Cooper and J. W. Loram, Phys. Rev. B 79 (2009) 104519.

[70] Takahiko Masui, Yuta Uraike, Kouta Nagasao and Setsuko Tajima, Journal of Physics: Conference Series 150 (2009) 052152.

[71] M. Mumtaz, N.A. Khan, Supercond. Sci. Technol. 20 (2007) 1228.

[72] M. Prester, E. Babic, P. Stubicar Mand Nozar , Phys. Rev. B 49 (1994) 6967.

[73] P. K. Nayak, S. Ravi, Supercond. Sci. Technol. 19 (2006) 1209.

Chapter 6

Superconducting Order Parameter Fluctuation in Composite Systems of $YBa_2Cu_3O_{7-\delta}$

CHAPTER 6

6. SUPERCONDUCTING ORDER PARAMETER FLUCTUATION IN COMPOSITE SYSTEMS OF $YBa_2Cu_3O_{7-\delta}$

6.1. Introduction

This chapter deals with the superconducting order parameter fluctuation (SCOPF) behavior in granular YBCO+xBaTiO$_3$ and YBCO+xBaZrO$_3$ composites. One important phenomenological investigation of thermodynamic fluctuations in the transport properties of high T_c superconductors (HTSC) has appeared to explain the cause of excess electrical conductivity ($\Delta\sigma$) related to the structural properties. YBCO structure can be viewed as constituted of superconducting layers composed of CuO_2 planes separated by isolating CuO chains with complex crystal chemistry and granularity. The principal aim of this chapter is closely related to the inclusion of paraelectric ($BaZrO_3$) and ferroelectric ($BaTiO_3$) materials to change the superconducting properties of the material. Since the discovery of HTSC, on-site substitution studies have proved to be very useful in understanding the mechanism of high-temperature superconductivity [1, 2]. Analysis of the temperature dependence of normal state resistivity in a series of these samples with varying $BaZrO_3$ and $BaTiO_3$ contents enable us to quantify the effect of fluctuation induced conductivity in these systems in terms of weak-link resistivity across grain boundaries arising due to the misaligned grains and sample dependent defects such as voids and cracks.

The inherent granular nature of YBCO has drawn attention for the intrinsic properties due to the grains and the extrinsic properties due to grain boundaries leading to strong structural disorder [3, 4] at the microscopic and mesoscopic levels respectively. The transition of the electrical resistance offered by these polycrystalline samples is a two-stage process [5-7]. As the temperature decreases, it is first observed a pairing transition and then a coherence transition. At the pairing transition, the superconductivity stabilizes in homogeneous regions within the grains at a temperature which virtually coincides with the critical temperature,T_c of the bulk sintered. A large number of studies have been devoted to investigate the interplay between SCOPF and the inhomogeneities [8-12]. The mesoscopic inhomogeneities such as grain boundaries, cracks,

voids etc. having much larger length-scale than the superconducting coherence length ξ and being temperature independent are expected to influence the room temperature characteristics. The microscopic inhomogeneities such as structural (twin boundaries, stacking faults) and chemical imperfections (oxygen deficiencies etc.) inside the grains occur in a length-scale smaller than the mesoscopic inhomogeneities, but still larger than ξ.

The temperature dependent resistivity of the composite system depends on the connectivity of the grains. It has been claimed that for non-superconducting inclusions to be effective as pinning centers, their size should be of the order of the coherence length [13]. These defects with size in the range of few times of coherence length have been found to act as a means to inhibit vortex motion, which results in the significant enhancement of critical current density (J_c) at high temperatures and applied magnetic fields. This aspect of J_c enhancement has been currently analyzed and discussed in chapter 7. In recent years great strides have been made in order to increase the pinning of vortex lines, which is an essential achievement for useful applications of YBCO superconductors in general, and of cuprate superconductors in particular. The mixed-state flux dynamics in HTSCs is an interesting and thrust area for contemporary research and is discussed in chapter 7. Several models [14-16] have been proposed to describe the complete shape of resistive transition in presence of magnetic fields. However, Aslamazov-Larkin (AL) approximations are valid in the effect of fluctuations in superconducting order parameter. It gives rise to the effective existence of order parameter and the renormalization of relaxation time of electronic excitations.

To make this chapter selfcontained attempts has been made to explain the role of composit systems in YBCO insection 6.2 and SCOPF behavior in $YBa_2Cu_3O_{7-\delta}$ + $BaZrO_3$ and $YBa_2Cu_3O_{7-\delta}$ + $BaTiO_3$ composites in section 6.3.

Our experimental details and interpretation of results for phase formation and microstructure modification are given in section 6.4. Experimental details and interpretation of results for SCOPF behaviour $YBa_2Cu_3O_{7-\delta}$ + x$BaZrO_3$ & $YBa_2Cu_3O_{7-\delta}$ +x $BaTiO_3$ composites are listed in sections 6.5 & 6.6 respectively**.** This chapter ends with an elaborate conclusion in section 6.7

6.2. Role of composite systems in YBCO

In HTSCs, the grain boundaries depress the superconducting state and the phase coherence between neighbouring grains is established by Josephson tunneling across the weak links. As the temperature is lowered, the number of weak links becoming superconducting in the granular YBCO system increases until a connecting path through the grains is established which gives rise to macroscopic superconductivity. The current conduction process in granular cuprate superconductors is very complex due to the frustration arising across the misaligned grain surfaces of randomly oriented grains and sample defects such as cracks and voids. Grain boundaries and intragranular defects (e.g. twins) act as weak link Josephson junctions and tunneling barriers, and the transport current flows by percolation through the weak link network. The resistive grain boundaries reduce critical current density, J_c to a value much lower than the intrinsic J_c of the grains [17, 18]. One of the approaches to overcome the difficulties arising due to granularity in cuprates has been to make composites of YBCO with metals such as Au, Ag, Al [19-22] and compounds like $BaZrO_3$, $BaTiO_3$, SiO_2 etc.[23-32] which can fill the intergranular spaces and improve both electrical and mechanical properties. $BaTiO_3$ and $BaZrO_3$ addition to YBCO to form composites affects for sizable enhancement in J_c, reduction in normal state resistivity without much reduction in the superconducting transition temperature T_c [28, 33]. In our study for the composite systems, most of the $BaZrO_3$ and $BaTiO_3$ occupied the boundaries of YBCO grains [24, 34] and only a small fraction of $BaTiO_3$ diffused into the grains [35]. To analyze the normal state and superconducting fluctuating properties of the cuprates, SCOPF approach has been widely used in the literature [36-41]. The implication of these intragranular and inter granular modifications on the SCOPF behavior due to the composite formation has been analyzed and discussed in the present Chapter.

6.3. SCOPF behavior in $YBa_2Cu_3O_{7-\delta}$ + $BaZrO_3$ and $YBa_2Cu_3O_{7-\delta}$ + $BaTiO_3$ composites

Composites of YBCO + x $BaZrO_3$ with sub-μ-sized $BaZrO_3$ and YBCO + x $BaTiO_3$ with nano-sized $BaTiO_3$ provide ideal system for experimental study. The widely undertaken analysis of excess conductivity in the composite system from different fluctuation theories [42-48] has concentrated mostly on investigating crossover [49-51] from a three-dimensional (3D) fluctuation (exponent λ, approaching 0.5) at low temperatures to a two-dimensional (2D) one (λ

approaching 1.0) on heating across a crossover temperature (T_{LD}). A relatively small number of investigations have been done on fluctuation conductivity along the c-axis of the HTSC. The pioneering work of Baraduc et al. [52] sets the basis for explaining results in the mean-field region. The excess conductivity of the Aslamazov–Larkin (AL) type in the normal state, close to T_c [53] follows a quasi-universal behavior, which is strongly related with Gaussian and genuinely critical fluctuations. Such studies are of interest and may give estimates of microscopic parameters such as the coherence lengths, phase breaking time and dimensionality of the order parameter, thus it can be possible to separate what are the fundamental disorders at microscopic and mesoscopic levels. In addition, theoretical concepts of the critical regime close to T_c or of the pair-formation may help to reveal the mechanism of superconductivity in YBCO.

6.4. Experimental details and interpretations of results (I)

6.4.1. Synthesis and characterization of $BaZrO_3$

Barium nitrate $Ba(NO_3)_2$ and Zirconyl nitrate hydrate $ZrO(NO_3)_2 \cdot x\ H_2O$ were employed for the synthesis of BZO. The details of the preparation method are discussed in Chapter 3. The X-ray analysis revealed that, BZO is of single phase having a cubic structure with $P_{m\text{-}3m}$ symmetry. At a sintering temperature of 900^0 C the peaks corresponding to barium carbonate and zirconia disappeared while corresponding BZO crystalline phases are observed similar to the results obtained by Ciontea et al. [28]. Zeta particle analyzer was used to estimate the particle size and their distribution in the calcined powders. The microstructural features of the sintered powders were determined with a scanning electron microscope (SEM). The results from SEM shows that the average particle size distribution in the calcined mixture ranges between 500-800 nm and can also be better confirmed by the results from Zeta particle analyzer (Fig. 6.1). The above microstructure has been further discussed in connection with the analysis of electronic transport measurements in absence and presence of an externally applied magnetic field.

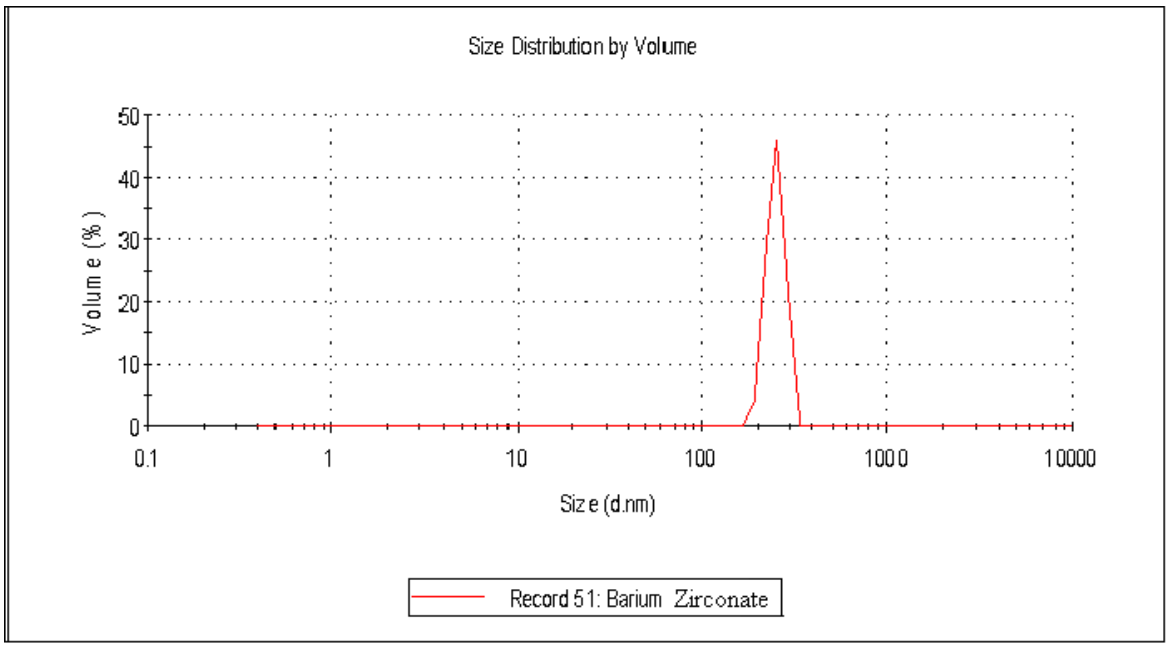

Fig. 6.1. Particle size analysis of $BaZrO_3$.

6.4.2. Synthesis and characterization of $BaTiO_3$

$BaTiO_3$ powder has been synthesized through chemical route, where it has been calcined at 1250 °C for 2 h at a heating rate of 3 °C/min in a box furnace. The details of the preparation method are discussed in Chapter 3. The X-ray analysis revealed that, $BaTiO_3$ is of single phase having a tetragonal structure with P_{4mm} symmetry. Zeta particle analyzer was used to estimate the particle size and their distribution in the calcined powders. The results from particle size analysis shows that the average particle size of calcined powders of $BaTiO_3$ ranges between 100 - 400 nm (Fig. 6.2). The idea of making composites of YBCO with $BaTiO_3$ is to strengthen the intergrain coupling to enhance the transport properties as fine $BaTiO_3$ act as weak links in granular YBCO superconductors. Though composition variation at the grain boundaries is not expected to influence the onset of superconductivity inside the grains, these sources of fine particles through composite formation would increase the coupling between the grains and hence the transport properties of oxide superconductors.

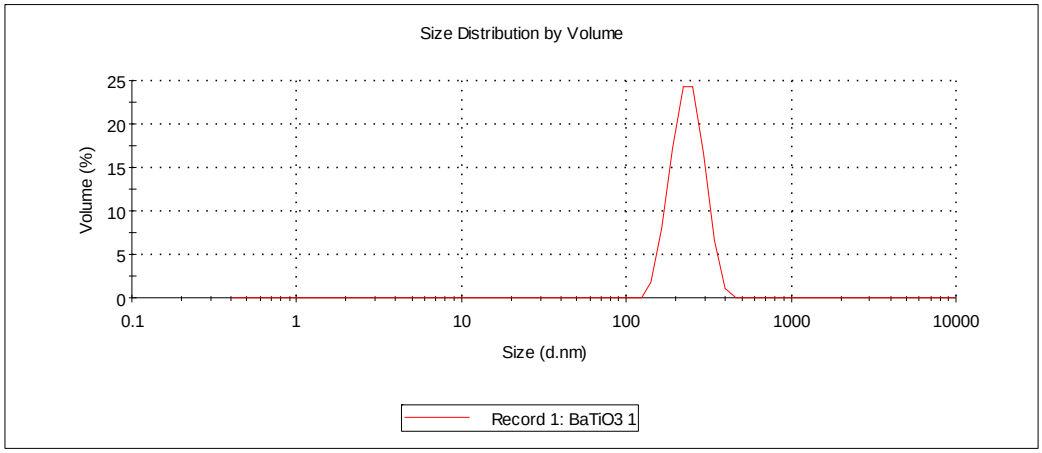

Fig. 6.2. Particle size analysis of $BaTiO_3$.

6.4.3. Synthesis of $BaZrO_3$ and $BaTiO_3$ composites of $YBa_2Cu_3O_{7-\delta}$

The preparation procedure for YBCO phase has been detailed in chapter 3 that was used as the precursor along with various wt.% (0, 1.0, 2.5, 5.0, 5.0) of $BaZrO_3$ and $BaTiO_3$ for the composite preparation. The superconducting composite samples of YBCO + x $BaTiO_3$ and YBCO + x $BaZrO_3$ with varying wt.% were ground for homogenous mixing. The pellets were cut into rectangular shapes for DC four probe resistivity measurements. All the samples were characterized by X-ray powder diffraction technique.

6.4.4. Phase formation in $BaZrO_3$ and $BaTiO_3$ composite systems of $YBa_2Cu_3O_{7-\delta}$

X- Ray Diffraction Analysis for YBCO + x $BaZrO_3$ composites

The diffraction pattern analysis of the composite samples of YBCO + x BZO were indexed using Chekcell software and the phases were confirmed to be orthorhombic at room temperature with a space group Pmmm (Fig. 6.3). Appearance of peaks (003), (004), (005) and (006) in the XRD pattern reveal (00*l*)-orientation of YBCO. Tiny peaks of BZO having (200) and (211) orientation increase with respect to corresponding intensity at an angle $2\theta = 43^0, 53^0$ in the XRD spectrum confirms that BZO resides at the grain boundary. However, XRD peaks at 32^0, were shifting towards lower angles indicating an increase in lattice parameter due to the formation of composite. An extra hump was observed which sharpens down in the peak at 32^0 higher

intensities with increase in wt.% of BZO. This shows the dependence of average size of BZO to the pristine YBCO system. This is a clear indication of a systematic adhesion of sub-micron BZO particles on YBCO grains. In YBCO + BZO 1 wt.% composite, BZO primarily resides at the grain boundaries. Luo et al. [54] have added that at higher BZO contents, BZO is pushed out of the sample and forms a layer on the surface during sintering and shows separate identity phases in diffraction patterns. A natural suspicion that arises whether the data obtained for YBCO + x BZO composites from the sintering temperatures at 900 ^{0}C leading to macroscopic chemical phase combination or not. It is worth noting that the annealing procedures for YBCO + x BZO crystals were exactly same as for all the composite samples. Instead, our data points to a physical mechanism like interlayer coupling of the Josephson junctions.

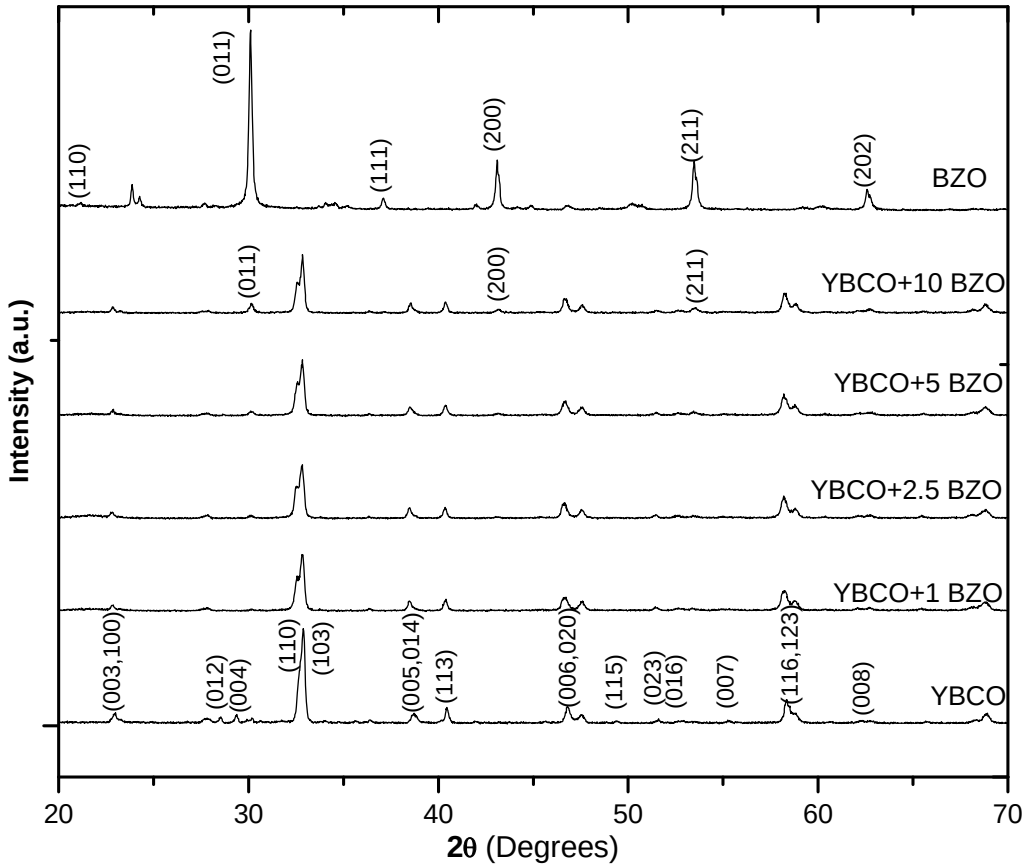

Fig. 6.3. XRD Patterns of YBCO, BZO and YBCO + x BZO composites with different BZO wt. %.

In addition to its own complex dynamics at the sintering temperature, a major interest arises from easy incorporation of such sub-μ-particles of BZO directly into the grain boundaries of YBCO. Since the nano-microscopic nature of the additional pinning centers related to the BZO incorporation is attributed by the YBCO + x BZO interface, it was found that some sort of bridging is taking place which transforms YBCO to a better superconductor. Sintering at elevated temperatures does not eliminate the intra and inter-grain boundaries completely, but they remain in the samples to a sizeable fraction and limit the applicability of these ceramic superconductors [11]. BZO being a dielectric material particularly fills the inter-granular spaces and improves both mechanical and electrical properties of superconductor. In bulk sintered material superconducting grains are separated by three-dimensional grain boundaries. This granular nature of YBCO and its consequence on the charge transfer process related to magnetic fields were studied as function of BZO content.

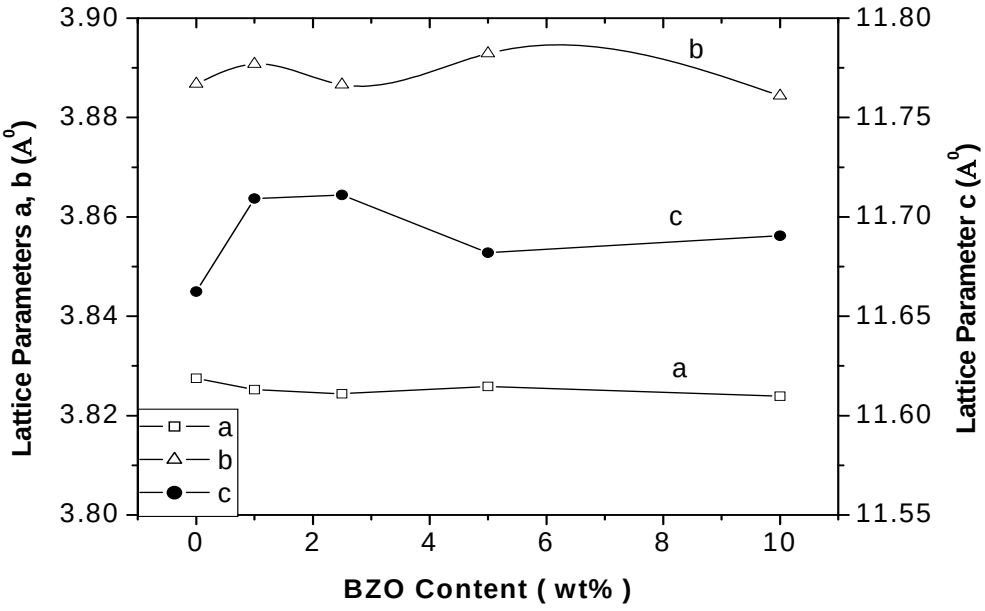

Fig. 6.4. Variation of lattice parameters in the YBCO + x BZO composite systems.

The values of lattice parameters for each sample obtained from ChekCell software are given in Fig. 6.4. It is evident that 'c' parameter and unit cell volumes have a comparatively higher value

than the pristine YBCO, while the 'a' parameter gets reduced for all. The c-axis elongated character is estimated due to incorporation of submicron size BZO particles.

X- Ray Diffraction analysis for YBCO + x $BaTiO_3$ composites

The diffraction pattern analysis of the composite samples of YBCO + x $BaTiO_3$ were indexed using Chekcell software and the phases were confirmed to be orthorhombic at room temperature with a space group P_{mmm}. Fig. 6.5 shows the XRD patterns of YBCO + x $BaTiO_3$ composites (x = 0.0, 1.0, 2.5, 5.0 wt.%). Appearance of peaks (003), (004), (005) and (006) in the XRD pattern reveal (00*l*)-orientation of YBCO. The (00*l*) peaks of YBCO are observed showing that the basic orthorhombic structure of YBCO was preserved. With increasing $BaTiO_3$ content, broadening in the XRD peaks of composites increases at $2\theta = 22°$. This broadening of the peak can be described by the theory of kinematical scattering as: (i) lattice defects are present in a large enough amount (ii) Crystallites become smaller than about a micrometer [55]. The XRD patterns of composite system showed no noticeable impurity peaks. The crystalline phase peaks of $BaTiO_3$ are not observed in the XRD pattern up to a doping level of 5 wt.% however, the peak intensities decreased subsequently in the composites. It reveals that, though the composites tend towards amorphous structure the orthorhombic phase is still maintained. It gives some clue that lattice site is affected in the composites (Fig. 6.6).

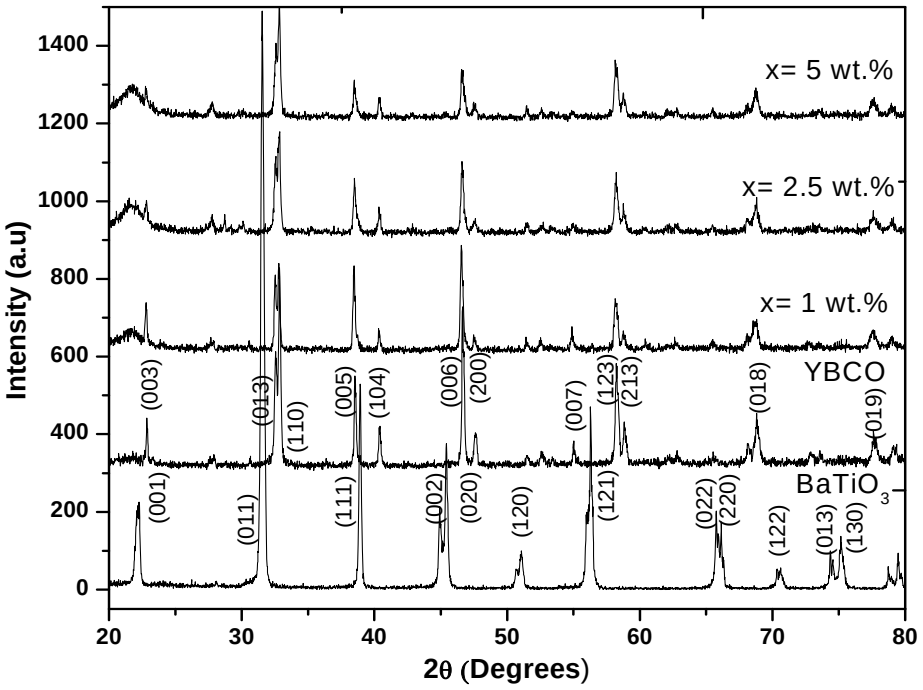

Fig. 6.5. XRD Patterns of YBCO, $BaTiO_3$ and YBCO + x $BaTiO_3$ composites (x = 0.0, 1.0, 2.5 and 5.0 wt.%).

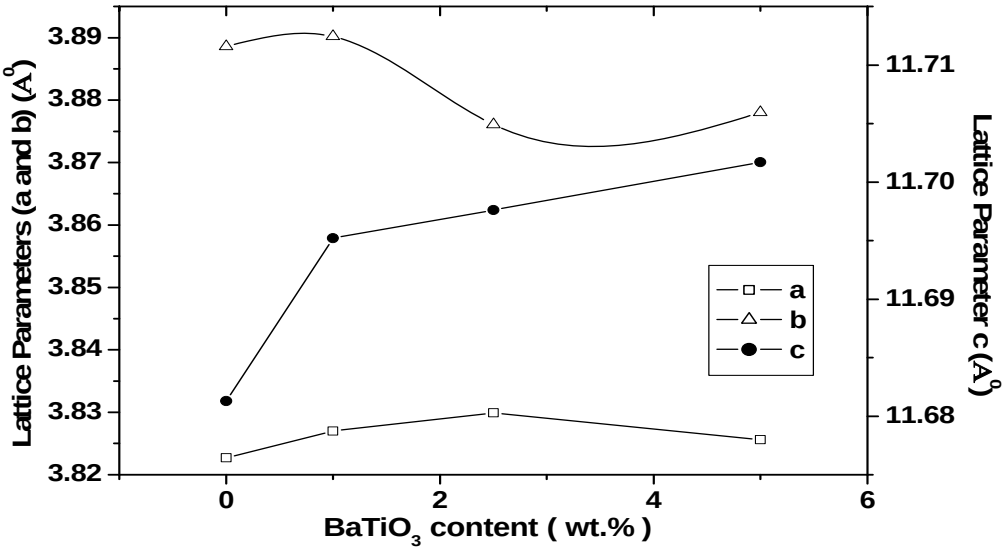

Fig. 6.6. Variation of lattice parameters for YBCO + x $BaTiO_3$ composites (x = 0.0, 1.0, 2.5 and 5.0 wt.%).

6.4.5 Microstructure modifications in $BaZrO_3$ and $BaTiO_3$ composite systems of $YBa_2Cu_3O_{7-\delta}$

Microstructure characterization for YBCO + x $BaZrO_3$ composites

The typical morphologic features of $BaZrO_3$ particles and YBCO pristine have been shown in figure 6.7. Figure 6.8 shows the morphologic feature of YBCO + x BZO samples. It shows that pristine YBCO sample exhibits elongated grains randomly oriented in all directions with size varying from 1 to 5 μm in length. With BZO addition two changes in microstructure are observed, firstly the grains become rounder and white patches of BZO increases with the BZO content and secondly small particles of BZO are seen sticking on the surface of all the grains leading to increase in grain connectivity and filling up of cracks and voids. It can be seen from Fig. 6.8b that the connectivity/interlink between the grains is observed more prominent in BZO 1wt.% sample. In the compositions of 2.5, 5 and 10 wt.% extra deposition of BZO layers are observed, gives a clue support to XRD results in which BZO stays as an adhering material on the grain boundaries.

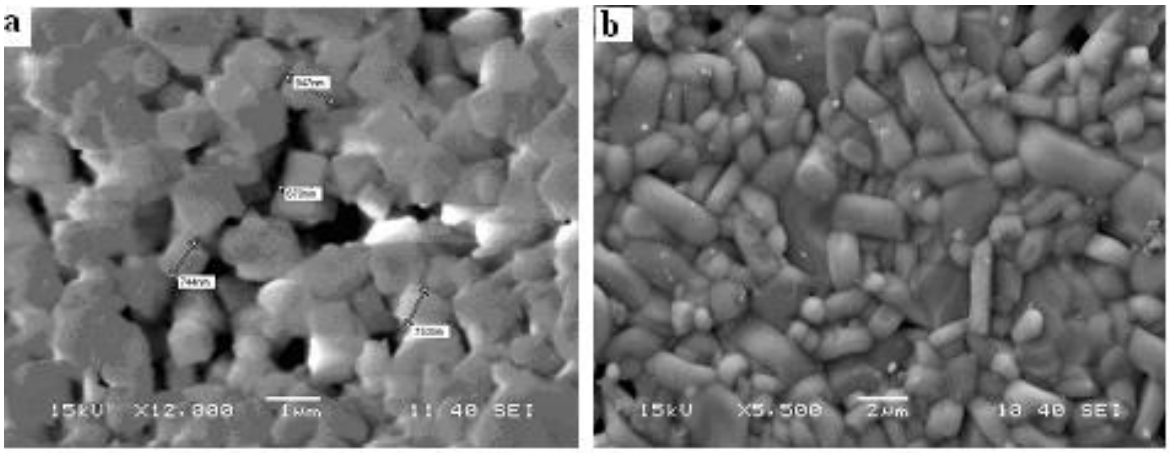

Fig. 6.7. SEM images of (a) $BaZrO_3$ particles and (b) of YBCO pristine

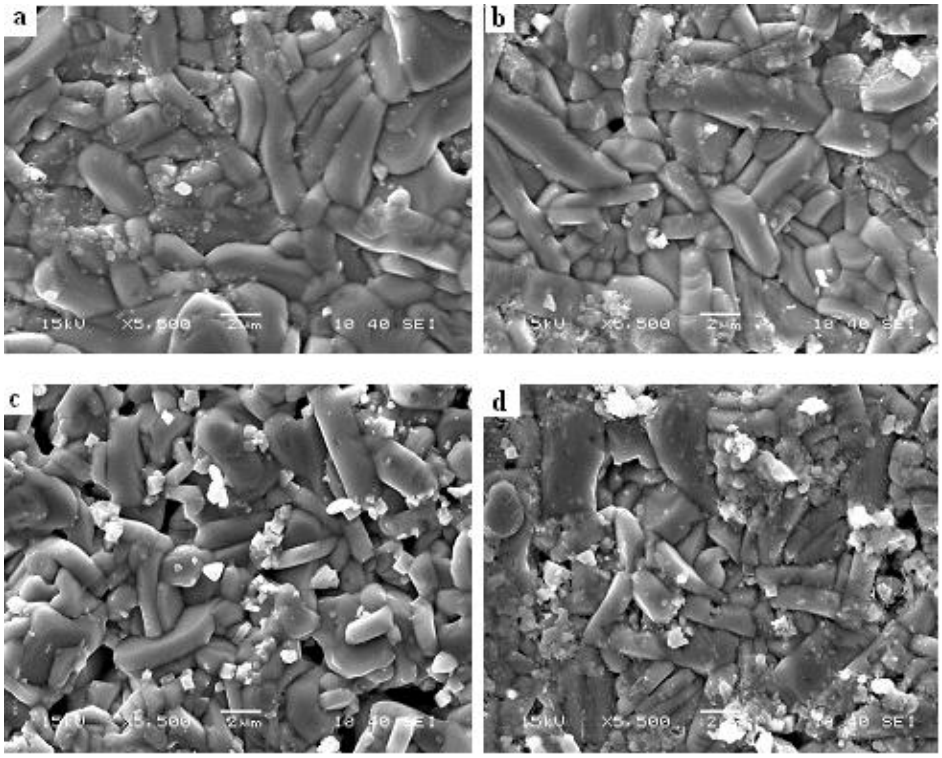

Fig. 6.8. SEM images of (a) 1 wt % BZO, (b) 2.5 wt % BZO, (c) 5 wt % BZO and (d) 10 wt % BZO composites of YBCO.

In the compositions of 2.5, 5and 10 wt % existence of BZO fraction prevents the formation of continuous metallic region throughout the sample (Fig. 6.8(b, c, d)). The following images support to XRD results that BZO does not dissolve in Y123 structure and stays as an adhering material on the grain boundaries.

Microstructure characterization for YBCO + $xBaTiO_3$ composites

The microstructure characterization i.e., grain-size distribution of the composites has been shown in Fig. 6.9. These images support to XRD results that $BaTiO_3$ diffuses into the YBCO grains resulting in a rounding up of the grains. It is clearly visualized that 1 wt.% $BaTiO_3$ representing white patches in the micrograph developing connectivity among the grains thereby diminishing the granular property to some extent. In 2.5 wt.% composites diffusion of particles (marked with arrows in Fig. 6.9) taking place into the grains along with some segregation in the grain

boundaries and in 5 wt.% $BaTiO_3$ composites of YBCO, grains are diffused to the optimal level and hence the shape of the grains get rounded up with maximum segregation outside the grain boundaries. We have also observed a decrease in the grain size of these samples with increase in wt.% and tried to develop a correlation between the granular structure and the superconducting properties. The intragranular properties are mostly affected due to these micro-structural modifications for the samples with $BaTiO_3$ content less than 5 wt.%. This observation clearly indicates that, in addition to $BaTiO_3$ occupying the inter-granular region, a fraction of Ti ion also goes into the grains. The extent of diffusion of $BaTiO_3$ into the grains has been shown to depend on the particle size and wt.% content of $BaTiO_3$. In the next section we examine the consequence of $BaTiO_3$ going into the grains on the superconducting transition temperature, T_c and the cross over temperature, T_{LD} by studying the fluctuation-induced conductivity of these samples.

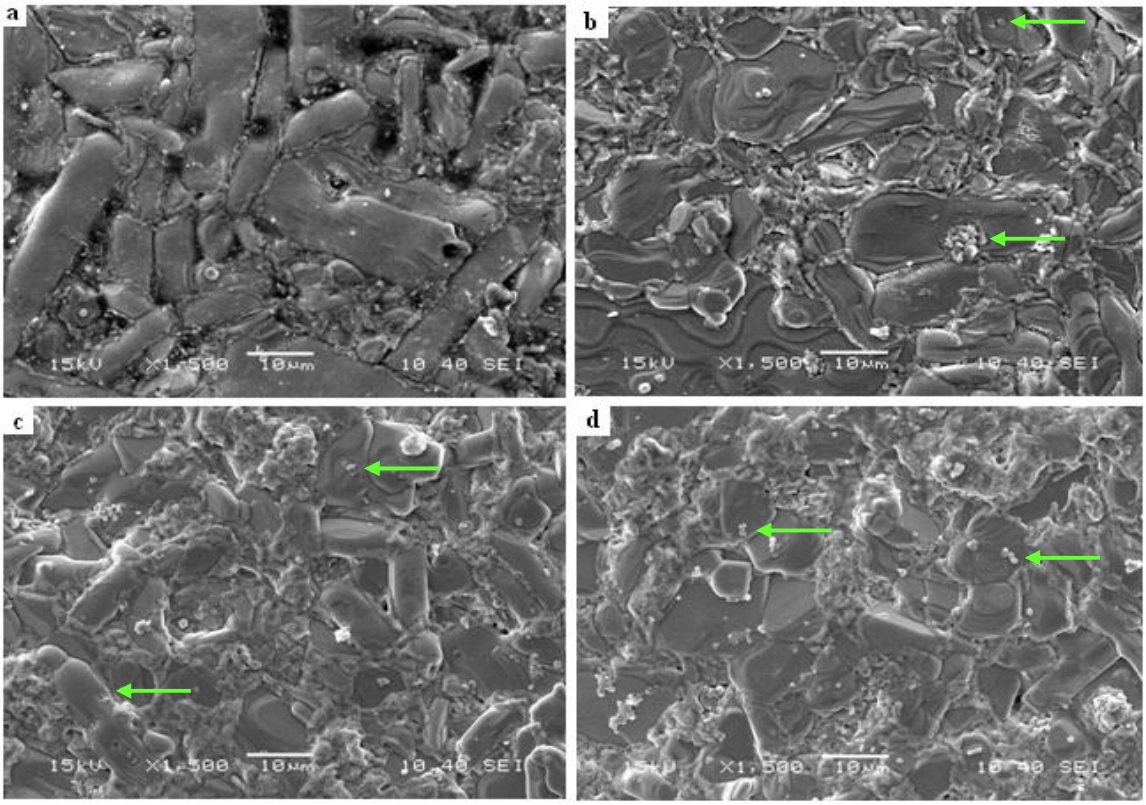

Fig. 6.9. SEM Micrographs for YBCO + x $BaTiO_3$ composites (x = 0.0, 1.0, 2.5 and 5.0 wt.% marked as a, b, c and d respectively).

6.5. Experimental Details and Interpretations of Results (II)

6.5.1. Resistivity Transitions in $BaZrO_3$ Composite systems of $YBa_2Cu_3O_{7-\delta}$

(i) In zero fields

Fig. 6.10 depicts the ρ(T) curves for all the samples of magnetic field at 0 T with the corresponding T_c values. The Y-axis (Fig. 6.10a) has been normalized by the ρ_{100} value. From the plot it is observed that, the metallic behaviour in normal state of ρ vs. T decreases with increasing BZO wt.% in the composite. The dρ/dT was calculated from the ρ vs. T curve in a temperature interval closer to T_c. The two stage transition is marked in dρ/dT behaviour at lower temperature side of resistivity measurement. There are two apparent observations has been noted. Firstly, with increase of BZO content the slope dρ/dT at the first transition decreases monotonically except for 1 wt. % which has higher value than the others composites. Secondly, for all the samples the superconducting transition falls apparently except for 1 wt% BZO, which has a remarkable T_c increase from that of YBCO pristine in zero magnetic fields.

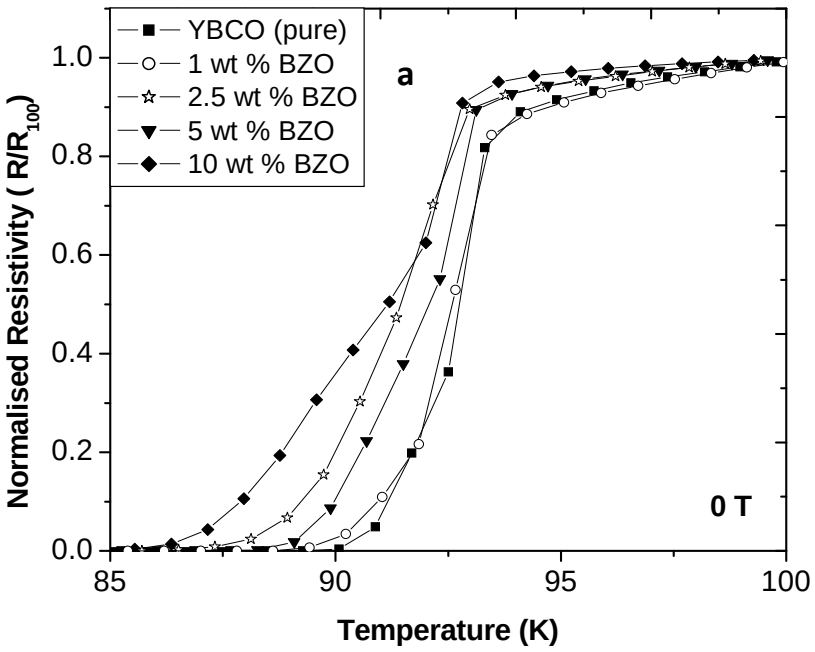

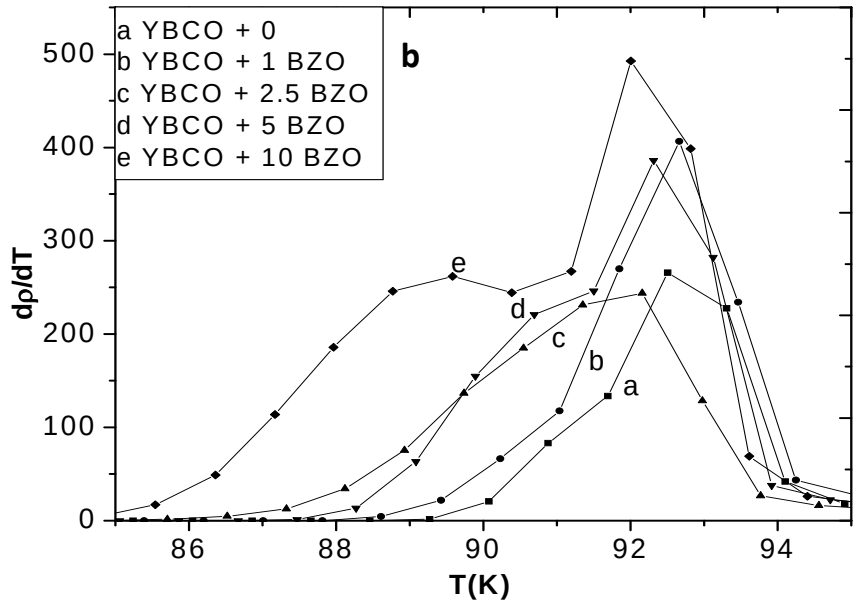

Fig. 6.10. (a) Normalised Resistivity with temperature in zero applied field (b) Temperature derivative of resistivity in zero applied fields.

(ii) In high fields

The normalized resistivity and temperature derivative of resistivity for different BZO composite samples of YBCO in an external field of 8T are presented in Fig. 6.11. Two distinct peaks are clearly observed for the onset of critical temperature. It is ascertained that the impurities appear to decrease Tc_{on2} greatly to the lower-temperature values as a function of BZO content and affects Tc_{on1} to some extent. As a result, Tc_{on1} for 10 wt % BZO comes down to 88.88K from 92.15K, due to the appearance of secondary peak in presence of field 8T.

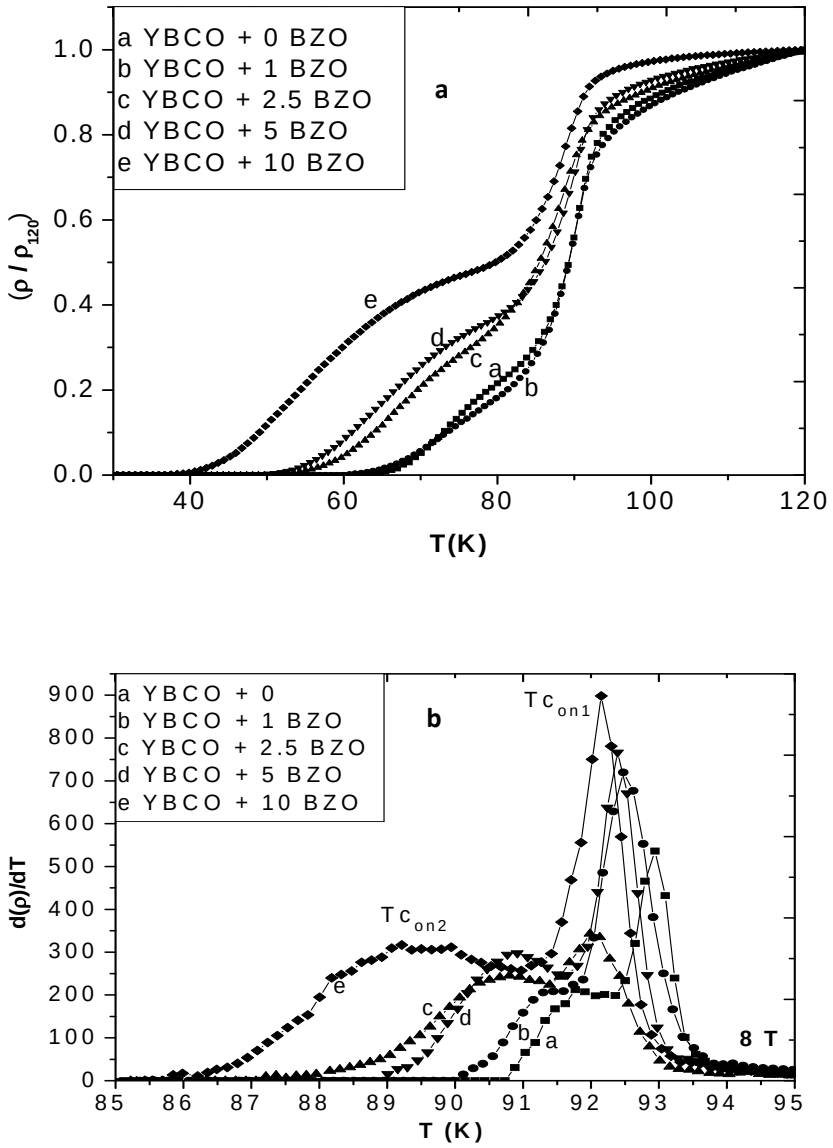

Fig. 6.11 (a) Normalised resistivity (b) Temperature derivative of resistivity in 8T.

6.5.2. Excess conductivity studies in $YBa_2Cu_3O_{7-\delta}$ + $xBaZrO_3$ Composites

Superconducting Order Parameter Fluctuation (SCOPF) analysis is related to the compilation of problems in the mean-field critical temperature (T_c). These fluctuations due to finite cooper pair formation probability induces excess conductivity or Para-conductivity in the normal phase near T_c. Explanation for the enhancement of conductivity in the SCOPF region has been given by Aslamazov and Larkin [44] and Lawrence and Doniach [45]. These theories ascertain the

dimensionality of the fluctuations and probe the dimensionality crossover when the system approaches the 3-D superconducting state. Current analysis establishes the role of power-law in predicting microstructure- property relationships in binary composites over bulk behavior.

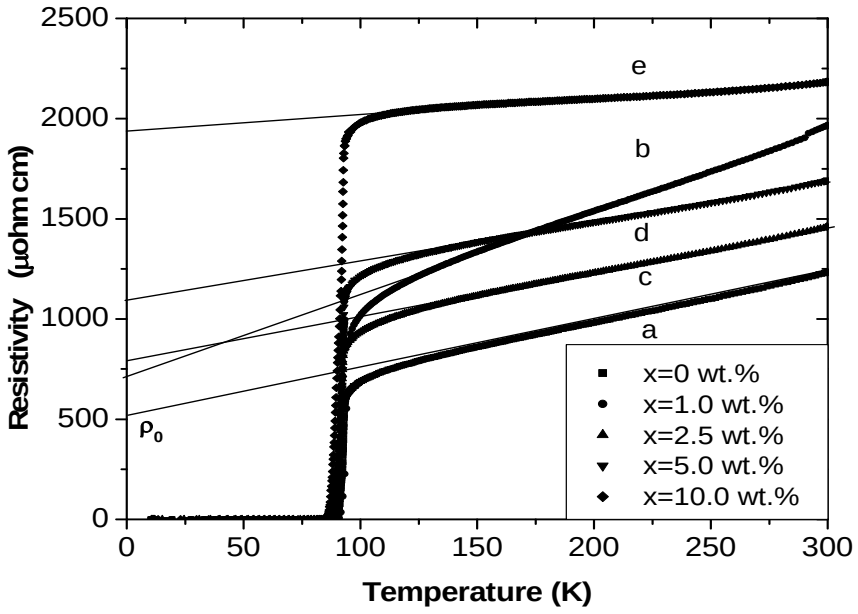

Fig. 6.12. Temperature dependence of the resistivity for YBCO + *x*BZO composites (x = 0, 1, 2.5, 5 and 10 wt.%). The linear fitting of the resistivity in the temperature range 150–250 K, extrapolated to 0 K gives resistivity slope (dρ/dT) and residual resistivity (ρ_0).

Attempts to determine T_c directly, many authors [5, 56] have calculated three Gaussian regimes above T_c in YBCO system. Direct determination of T_c has been attempted by extrapolating the excess conductivity raised to the inverse critical point, λ (equation 6.3) where T_c is determined from the intercept on temperature axis in the mean field region. The magnitude of ρ_0 which is a measure of the grain boundary resistivity decreases at a much faster rate from $\rho_{300\,K}$ in 1 wt.% as compared to other composites within the percolation threshold for conduction through BZO channels. This can be seen from Fig. 6.12 by comparing their resistivity values. It provides an essential evidence that 1 wt.% of BZO was found to be a better composite than the others. From Table 6.1 it was found that the dρ /dT value 4.0141 is the highest for the sintered series of samples. The residual resistivity for 1 wt.% comes down to 728.02 which cross over the general trend from rest of the samples.

Table 6.1
Variation of normal state and superconducting parameters in the composites with different BZO wt.%

BZO wt. %	ρ_{300}(μ ohm-cm)	dρ /dT(μ ohm-cm K^{-1})	ρ_0(μ ohm-cm)
0.0	1232.00	2.40	501.56
1.0	1966.08	4.01	728.02
2.5	1459.92	2.21	786.73
5.0	1693.67	1.94	1067.56
10.0	2183.87	0.61	1954.20

6.5.3. Fluctuation conductivity in zero magnetic fields for $YBa_2Cu_3O_{7-\delta}$ + $xBaZrO_3$ composites

In order to describe the conductivity in zero magnetic field, for YBCO + *x*BZO crystals within the framework of Ginzburg-Landau mean field theory [46], the temperature dependence of excess conductivity is defined as Landau mean field approximation:

$$\Delta\sigma\,(T) = 1/\rho(T) - 1/\,\rho_R(T) \tag{6.1}$$

where $\rho(T)$ is the measured electrical resistivity and $\rho_R(T)$ is the regular resistivity obtained by linear extrapolation of resistivity data from room temperature to T_c. Assuming that the resistivity $\rho(T)$ follows a linear temperature dependence at higher temperature and is obtained by linear fitting of resistivity curve and extrapolating the same to below T_c. The determination of $\Delta\sigma$ involved the determination of ρ_R for temperatures near T_c by extrapolating the high temperature behavior of $\rho(T)$ as follows:

$$\rho\,(T) = \rho_0 + (d\rho\,/dT)T \tag{6.2}$$

where ρ_0 and dρ /dT are constants.

The linearity of $\rho_R(T)$ is observed in all composites above 150 K. The dρ/dT is calculated from ρ vs. T curve in a temperature interval between 150 K and 250 K. GL mean field theory is valid only in a mean field temperature range ~$1.01T_c$ to 1. $1T_c$.

6.5.4. Gaussian fluctuations in $YBa_2Cu_3O_{7-\delta}$ + $xBaZrO_3$ composites

The analysis of fluctuation conductivity shows the occurrence of homogeneous 2D and 3D Gaussian regimes closely above the T_c. The data obtained at zero magnetic fields were studied as per the classical AL (Aslamazov and Larkin) phenomenological theory [44]. The excess conductivity ($\Delta\sigma$) shows a temperature dependence of the form:

$$\Delta\sigma = A\,\varepsilon^{-\lambda} \tag{6.3}$$

where 'ε' is the reduced temperature which is defined as $(T - T_c)/T_c$. Amplitude, A is a temperature dependent parameter and its values for 3-D and 2-D are: $A = e^2/32\hbar\xi(0)$ and $e^2/16\hbar d$ respectively. 'ξ(0)' is the zero-temperature coherence length or GL correlation length and'd' is the effective separation of CuO_2 layers. 'λ' is the Gaussian critical exponent which depends on the dimension (D) of the system and defines the dimension as λ = 2 - D/2. From equation (6.3) for 3D fluctuation conductivity, the effective λ value was found to be limited in the interval from -0.5 to -1.0 [56]. Therefore equation (6.3) for 3D fluctuation conductivity allows us to describe both 3D (λ=0.5) and 2D (λ=1) AL cases as well. Lawrence and Doniach (LD) [45] extended the AL model for layer superconductors, where conduction occurs mainly in 2D CuO_2 planes and these planes are coupled by Josephson tunneling. Assuming coherence length, ξ(0) equal for all the layers, the excess conductivity parallel to layers in the LD model is:

$$\Delta\sigma = (e^2/16hd\varepsilon)[1+B_{LD}\varepsilon^{-1}]^{-1/2} \tag{6.4}$$

where LD parameter, $B_{LD} = [2\,\xi_c(0)/d]^2$

This expression predicts a cross over from 2D to 3D behavior of the order parameter fluctuations in the mean field region at temperature;

$$T_{LD} = T_c\{[1+[2\xi_c(0)/d]^2\} \tag{6.5}$$

which performs conductivity fluctuation measurements in composites. Close to and above T_c, the conductivity fluctuation analysis revealed the occurrence of two fluctuation regimes characterized by the critical exponents λ_1 (3D) = ~ 0.50 and λ_2 (2D) = ~ 0.1, respectively.

According to Drude's formula the various contributions of fluctuations to the electrical conductivity has been determined through the exponent, λ as;

$$\Delta\sigma = (2e^2n_s\tau)/m \tag{6.6}$$

Where 'n_s' is the density of Cooper pairs, τ is the lifetime of the evanescent superconducting droplets, 'e' is the charge and 'm' is the mass of electron. Thus, the exponent for the fluctuation conductivity is written as [34];

$$\lambda = \nu(2+z-D-\mu) \tag{6.7}$$

Where 'ν' is the critical exponent for the coherence length, 'z' is the dynamical exponent, 'D' is the dimensionality, and 'μ' is exponent for the order-parameter correlation function. In the mean field region, GL theory predicts ν = 1/2, z = 2 and μ = 0. Thus the mean field exponents obtained from equation (6.7) depends on the dimensionality as;

$$\lambda=2-D/2 \tag{6.8}$$

Hence, the regions characterized by the exponent, λ = 1.0 and 0.5 are attributed to two and three-dimensional Gaussian fluctuations respectively.

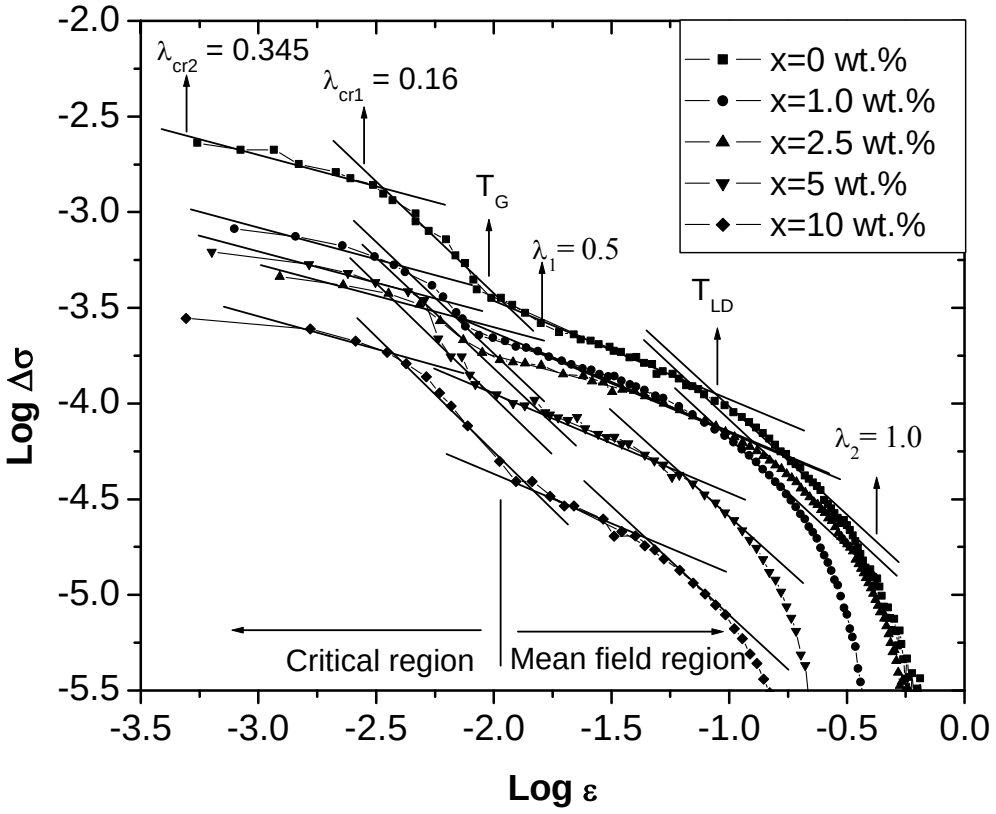

Fig. 6.13. Log-log plot of excess conductivity ($1/\rho - 1/\rho_R$) as a function of reduced temperature $\varepsilon = (T-T_c)/T_c$ for YBCO + *x*BZO composites (x = 0, 1, 2.5, 5 and 10 wt.%) in zero magnetic field.

The excess conductivity 'Δσ' versus 'ε' plots of equation (6.3) is shown in Fig. 6.13. These plots can be broadly divided into two regions: the mean field region and the critical region. In the mean field region for each of these samples 3D and 2D behavior of superconducting order

parameter fluctuation dominates. An upward shift of T_{LD} was found as a consequent dominance of the 3D region in 1 wt.% of BZO composite and in rest of the samples it occur a down ward shift. Farthest from T_c, λ_2 = 1.00 - 0.05 is identified which is an average value over several measurements. This value has a good agreement with estimations by others [38, 57] when the temperature approaches T_c from the above crossover to the observed regime. It is observed that the value of T_c is nearly constant at 92 K < T_c < 93 K and the T_c of YBCO + 1 wt.% BZO was found to be 92.66 K, which is greater than 92.55 K within the said small temperature range. Close to T_c - onset the values obtained for various cross over temperatures $T_{c0,}$ T_G and T_{LD} are shown in Table 6.2 where 'T_c' is mean field critical temperature and Ginzburg temperature 'T_G' is the temperature for finish of 3D regime. The Lawrence-Doniach temperature values for all the composite samples decreased successively from that of the values of x = 0 wt.% sample except for x = 1 wt.%, which has a T_{LD} value slightly greater than the pristine YBCO. In the sample of higher BZO contents (5 wt.% and 10 wt.%) a secondary phase peak arises in the temperature derivative of the resistivity curve. This is due to the extra deposition of BZO layers on the boundaries of YBCO grains. In x = 2.5 wt.%, though the secondary phase peak was not observed, T_c got significantly decreased from other samples. From the detailed analysis, x = 1 wt.%, was found to be a good superconducting sample as the T_{LD}, dρ /dT and T_c values exceed the YBCO pristine one.

Table 6.2
BZO content dependence of different transition temperatures (zero resistance, mean field, Ginzburg and Lawrence-Doniach).

BZO wt. %	T_{c0} (K)	T_c (K)	T_G(K)	T_{LD}(K)
0.0	90.11	92.52	93.31	99.78
1.0	90.12	92.66	93.46	100.72
2.5	87.21	92.15	93.77	99.40
5.0	89.00	92.32	93.92	96.37
10.0	85.85	92.02	94.40	95.82

In the temperature related to pseudo-gap regime where onset of fluctuations in the order parameter of superconductors sets in excess conductivity is clearly visible for the composites and is marked by fluctuations due to pair-formation and breaking through T_G and T_{LD}. Shifting of 3-D to 2D cross over temperature(T_{LD}) to higher temperature, particularly for 1 wt.% BZO composite in Table 6.2 signify reduction of magnetic vortex motion via improvement of pinning

capability within the sample and suggest the presence of strong pinning sources. It is also found that in dc magnetic fields a significant part of dissipation was sub-linear at 0 T, indicating some grain boundaries and/or weak links response, most probably due to non superconducting inclusions or to overall disorder effects. However, such analysis has been interesting on account of the enhancement of fluctuations in the layered quasi-2D structure of x = 1 wt.% composite in the present work. It has often been difficult to choose the temperature range for fitting T_G and T_{LD} due to various possible contributions to the variation of $\Delta\sigma$ with temperature T. Assuming that the fluctuation effects may add to the vortex motion contribution at high fields we analyzed the data for 8T.

6.5.5. Critical fluctuations in $YBa_2Cu_3O_{7-\delta}$ + $xBaZrO_3$ composites

In the critical region in Fig. 6.13, an additional power-law regime in $\Delta\sigma$ is identified when the temperature approaches close enough to T_c. Two power-law regimes, corresponding to two different exponents, labeled by the indices λ_{cr1} and λ_{cr2} are observed for measurements performed at zero or very low applied fields. In this region the critical thermodynamics of the superconducting transition is well described by the 3D-XY-universality class [58]. According to renormalization group calculations, $\nu = 0.67$ and $\mu = 0.03$ are expected and $z = 0.32$ being predicted by the theory of dynamical critical scaling [59]. Taking D = 3 and substituting these values in equation (6.7) the value obtained for $\lambda_{cr1} = 0.33$ which is called as the 3D XY-E because of the model-E dynamics [60]. For the static critical scaling the model 'A' predicts [61], $\nu = 0.67$, $z = 2$, $\mu = 0$ and D = 3, thus the value obtained for $\lambda_{cr2} = 0.67$.

Careful studies of the excess-conductivity in the neighborhood of the critical temperature yield information of the nature of the superconducting state as well as the influence of the granularity on the fluctuation regimes at microscopic and mesoscopic levels. The critical fluctuation and 3D fluctuation regions intersect at temperature T_G. Farthest from T_G, the critical exponent $\lambda_{cr2} = 0.345$ is found, which is consistent with expectations from the 3D - XY model. This scaling behavior, consistent with the 3D-XY model has recently been observed by Jurelo et al. [39] for the polycrystalline $Er_{1-x}Tb_xBa_2Cu_3O_{7-\delta}$ superconductors. They have analyzed the logarithmic temperature derivative of conductivity for polycrystalline system prepared by solid-state reaction technique. These findings had already been identified in polycrystalline and single-

crystal samples [40, 41] also. Still closer to T_G, a critical scaling regime beyond 3D - XY is observed, labeled by the exponent $\lambda_{cr1} = 0.16$. Above but close to T_c, some authors systematically found that the fluctuation conductivity in the critical regime is characterized by a power law with exponents $\lambda_{cr} \sim 3$, which they interpret as resulting from microscopic granularity [7, 62]. This exponent is known to characterize the critical resistive transition in classical granular arrays formed by metallic superconducting particles embedded in a poorly conducting matrix.

6.5.6. Fluctuation magnetoconductivity in $YBa_2Cu_3O_{7-\delta} + xBaZrO_3$ composites

The experimental data were analyzed by adopting the simplest approach where the magnetoconductivity fluctuation is supposed to diverge at the superconducting transition as a function of power law is denoted by:

$$\Delta\sigma(T, B) = A\ \varepsilon^{-\lambda} \tag{6.9}$$

Where A is a constant, λ is the critical exponent and $\varepsilon = (T - T_c(B))/T_c(B)$ is the field-dependent reduced temperature. The excess magnetoconductivity, $\Delta\sigma(T, B)$ is experimentally obtained similar to the conditions of equations (6.4 – 6.5). We determined numerically the logarithmic value of $\Delta\sigma(T, B)$ to correlate the values of λ to the 8T applied fields. Fits of the experimentally determined $\Delta\sigma$ allow us the simultaneous determination of λ and $T_c(B)$. Temperature derivative of the resistivity around the transition shows two-peak structures typical of two-phase sample. It is evident that the transition occurs in a two step process in the composites. This is particularly significant at high temperatures 10 K less than the T_c values. It reveals to new features suggesting the presence of two components i.e. superconductor + dielectric composite systems. For higher temperature we observed one sharp maximum in $d\rho/dT$, which is related with intra-granular fluctuations (fluctuations in the amplitude of the order parameter). These characteristic fluctuations define pairing transition. The temperature value of this maximum is about 20- 40 K less than the bulk critical temperature. For low temperature region a hump as a shoulder is discerned in the temperature derivative of resistivity.

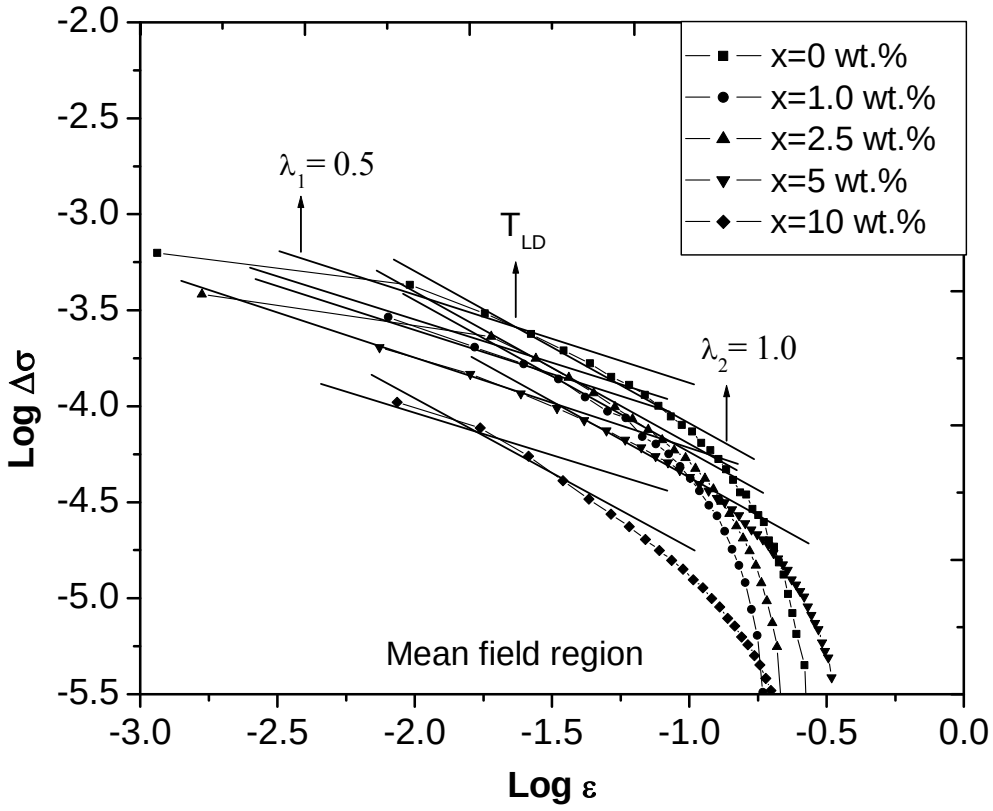

Fig. 6.14. Log-log plot of excess conductivity ($1/\rho - 1/\rho_R$) as a function of reduced temperature $\varepsilon = (T-T_c) / T_c$ for YBCO + *x*BZO composites (x = 0, 1, 2.5, 5 and 10 wt.%) in 8 T magnetic field.

Towards the approach to the zero resistance state below T_c, a characteristic scaling in curves has been observed for experimental data of 8 T magnetic fields. The values for different temperature labeled are tabulated in Table 6.3. It is clear from table that the T_c got reduced in presence of field. It is mostly affected for 2.5 wt.%, where T_c comes down to 88.6 K from a value of 92.15 K. For temperatures well above T_c, when the distance between grains is larger than the coherence length, a two-dimensional analog of the Aslamazov-Larkin law is realized. This analysis predicts a crossover between two to three-dimensional behaviors in the mean field region as has been observed by Sergeenkov et al. [63]. The same fittings are not observed in Fig. 6.14 due to smearing out of data points in the critical region for high magnetic field like 8 T. It has been described by A. R. Jurelo et al. [40] that 3D - XY scaling behavior is unaffected by the fields up to 50 mT. However in the present study we have applied a field beyond 50 mT. This

may be the reason that the sufficient data points are not available for fitting in the particular region. We now focus on the field dependence of various cross over temperatures at different wt.% of BZO. The T_{LD} values for 2.5 and 1 wt.% composites were less than pure YBCO and is more for 5 and 10 wt.% samples in 8T. It is a strikingly different feature than the zero fields. In fact for 1 wt.% BZO composite a good dependency of superconductivity and dielectricity is obtained. It helps to increase the superconducting property of YBCO grains by filling up the cracks and defects formed in YBCO grains during the sintering process and can be attained the greatest T_c in the sintered series of samples. In 2.5 BZO composite the optimum value of BZO addition is already achieved, hence it creates some sort of disturbance in the superconducting system. YBCO grains try to attain their superconducting behavior and BZO crystals try to attain their identity of dielectric behavior. So in 2.5 wt.% BZO composite T_c decreases creating a significant gap in T_c values of 1 wt.% and 2.5 wt.%. In case of higher BZO content samples both YBCO and BZO tried to show their identity properties and a secondary peak is observes in the dρ/ dT curve near the T_c peak. Thus the T_c values of 2.5wt.% have lower values than 5 wt.% composite both in presence and absence of field.

Table 6.3
Field dependence of various transition and cross over temperatures at different wt.% of BZO at 8 T.

BZO wt.%	T_{c0}(K)-8 T	T_c(K)-8 T	T_{LD}(8 T)
0.0	59.95	90.61	93.63
1.0	59.91	90.60	93.63
2.5	51.18	88.60	91.05
5.0	49.50	90.22	95.50
10.0	36.75	88.88	111.85

6.5.7. Discussion on $YBa_2Cu_3O_{7-\delta}$ + $xBaZrO_3$ composites

On studying the phases of X-ray diffraction pattern and micrographs for high values of BZO addition, it is probable that the critical temperature of the system does not increase with BZO addition for more than one optimum value. This investigation provides a possible explanation for the excess conductivity developed in the composite and gives an insight into the reasons for getting a better quality, 1 wt.% composite as compared to the pristine one. It can be concluded that the introduction of BZO inclusion of < 1000 nano-metric size in YBCO powder has improved the intra-grain vortex pinning at 1 wt.% of BZO.

Studying the temperature variation of resistivity and critical temperature in samples of varying granularity, it is observed that current conduction process through grains and grain boundaries of sintered YBCO composite pellets is significantly modified by path lengthening factors arising due to misalignment of highly anisotropic grains and structural defects like voids and cracks. The micro-cracks in the sample which adversely affect their superconducting and normal state properties are also arrested by composite formation of YBCO with the addition of BZO. The resistivity of polycrystalline samples contains two contributions, the intra-grain resistivity (single crystal) and the resistivity due to grain boundaries and the later usually dominates the total in the phase transition regions. Thus it appears that the grain boundary resistivity shows temperature dependence similar to that of a single crystal. In this context, it is believed that the same mechanisms were also operating in all the samples but is clearly distinguished in x = 1 wt.% sample. The observed decrement of T_{c0} is a consequence of the progressive decoupling of the superconducting grains with increasing BZO wt.%. T_{c0} shifting to lower temperature side with increase in BZO content for a particular field indicates that some of the inter-granular junctions are driven from non-dissipative to the dissipative state which drives them from the Josephson coupled state to the normal state. The combination of these effects makes the addition of BZO particles useful particularly in order to improve the high-frequency performances of YBCO.

It is worth noting to mention that, in polycrystalline composite (YBCO + x BZO) both intergrain and intragrain mechanisms determine the dissipation properties. While grain boundary-related dissipation dominates at low magnetic field intensity, the intragrain mechanisms constitute the ultimate limitation. It is well established that improving grain texture is beneficial for reducing the role of the grain boundary, while defects of order of vortex size are likely to be effective vortex pinning centers. Among the crystalline defects, sub-micron sized BZO are considered as the most significant pinning source having the same dimensionality of the magnetic vortex flux lines. It is thus suggested that the BZO, being a dielectric material probably acts as a weak link, which causes the global resistivity transition temperature to decrease in addition to extra BZO. The interplay between T_{c0} inhomogeneities and superconducting order-parameter fluctuations (SCOPF) leads to the conclusion that in the mean-field-like region (MFR) above the superconducting transition, the T_{c0} inhomogeneity contribution to the measured

resistivity is negligible. In contrast, the present analysis confirms that in the MFR, these effects may be interpreted quantitatively on the grounds of the Lawrence-Doniach theory for SCOPF.

6.6. Experimental details and interpretations of results (III)

6.6.1. Resistivity variations in $BaTiO_3$ composite systems of $YBa_2Cu_3O_{7-\delta}$

The temperature dependence of resistivity for composites YBCO + x $BaTiO_3$ is shown in Fig. 6.15. It is observed that the onset transition temperature T_c is decreasing with increase in $BaTiO_3$ content. The slope value increases as observed from resistivity slope vs. $\rho_{100\ K}$ resulting in an increase in the metallic property with increasing $BaTiO_3$ in the composite. From resistivity measurements ρ (T) we get the excess conductivity ($\Delta\sigma$) by subtracting the normal conductivity, σ_n(T) from the measured conductivity, σ(T) in a temperature interval close to T_c.

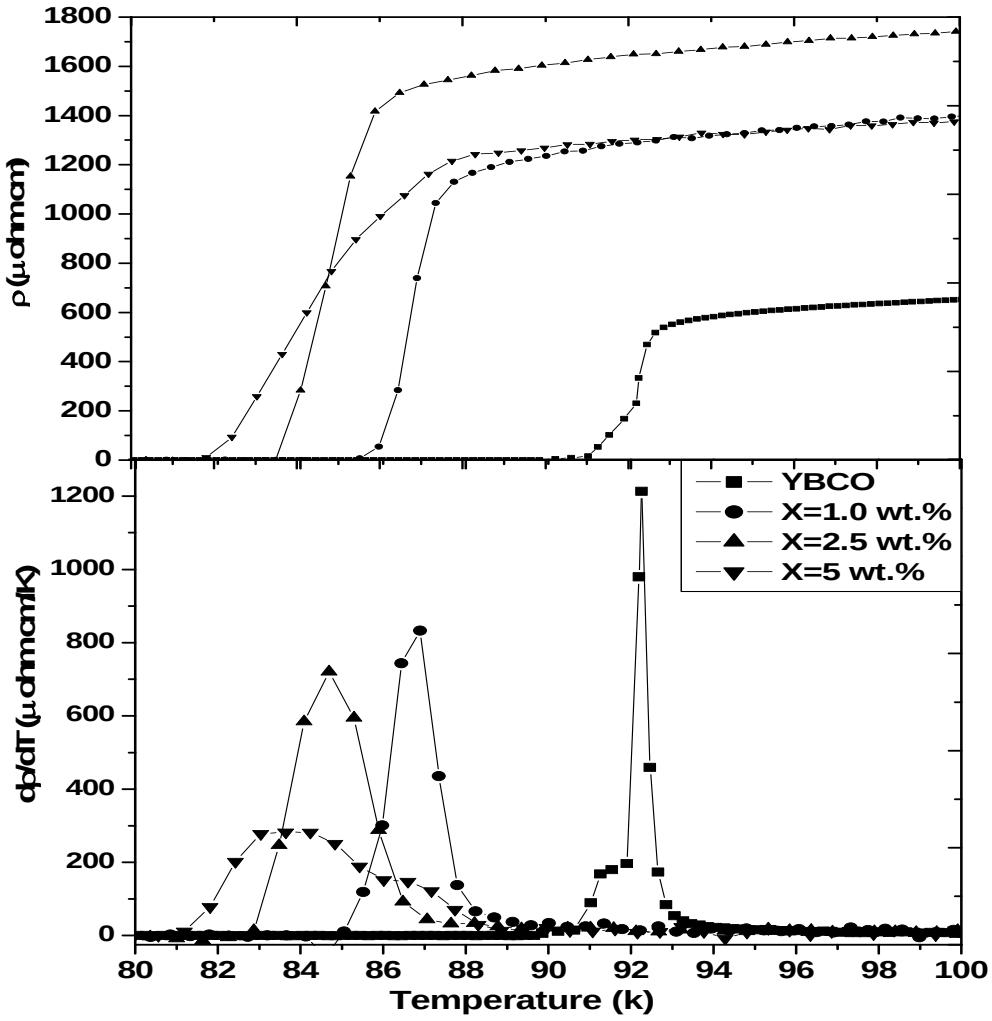

Fig. 6.15. Temperature dependent of resistivity and derivative of resistivity of YBCO + x $BaTiO_3$ composites (x = 0.0, 1.0, 2.5 and 5.0 wt.%).

The plot of dρ/dT is a simple procedure for magnifying details of the transition. In this plot it is seen clearly that the mean field transition temperature T_c (mean field) decreases monotonously as listed in Table 6.4 signifying intragranular changes due to incorporation of nano- $BaTiO_3$ particles. Also, our data curves reveal broadening of peaks (Fig. 6.16) as a mark for the modifications in intergranular properties. $BaTiO_3$ particles of micrometric order prepared through solid state reaction route, when made composites of YBCO, T_c did not get affected for lower concentrations (within 10 wt.%) rather the resistance of the system increased due to

insulating $BaTiO_3$ particles which effectively reduced the number of superconducting channels in the intergranular regime [24]. Therefore, in the current studies we have chosen $BaTiO_3$ up to 5 wt.% of some nanometric order to study the intragranular properties modified due to its incorporation with YBCO. It is observed that the different synthesizing processes used during the preparation $BaTiO_3$ produce larger alterations in the values of critical temperature, phase transitions and grain morphology which leads us to the detailed analytical studies in the superconducting order parameter fluctuation regime.

Table 6.4
Variation of Superconducting Order parameter with $BaTiO_3$ wt. %

$BaTiO_3$ wt. %	T_c(mean) (K)	T_{c0}(K)	T_{LD} (K)	dρ/dT	ρ_0 (μ Ohm-cm)
0.0	92.27	88.85	100.445	3.12	400.04
1.0	86.86	85.05	97.74	4.72	1038.10
2.5	84.71	82.87	88.74	5.51	1240.80
5.0	83.71	81.19	86.6	2.89	1117.27

6.6.2. Excess Conductivity in $YBa_2Cu_3O_{7-\delta}$ + $xBaTiO_3$

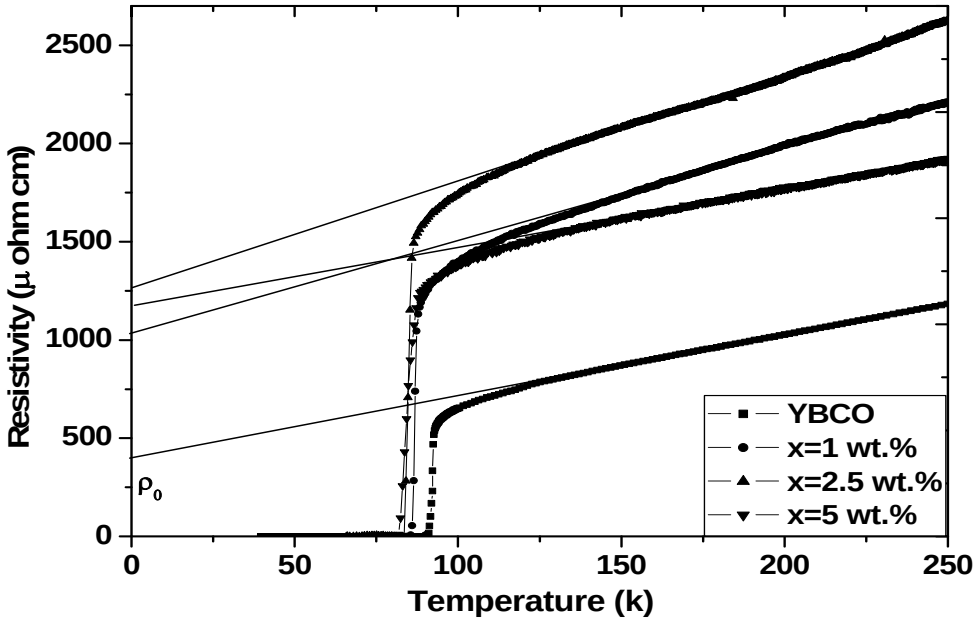

Fig. 6.16. Resistive transition and regular resistivity behavior extrapolated from the normal behavior. Linear fitting of resistivity in the temperature range 150 K to 250 K and extrapolated to 0 K gives resistivity slope (dρ /dT) and residual resistivity ρ_0 of YBCO + $x$$BaTiO_3$ composites (x = 0.0, 1.0, 2.5 and 5.0 wt.%).

The zero-resistance at the temperature T_{c0}, characterizes the onset of global superconductivity in the samples. In the temperature interval between T_c and T_{c0}, excess conductivity occurs and the resistivity is expected to exhibit a highly non-ohmic behavior due to intragranular modifications. Aslamazov and Larkin (AL) [44] phenomenological relation has been used for calculation and analysis of the fluctuation effects in this excess conducting region. We have fitted our data to AL theory for the fixed values of exponent $\lambda = -1.0$ and -0.5 and by varying the coefficients for 2D and 3D (equations 6.7 and 6.8) respectively. Various temperature parameters obtained are listed in Table 6.4. Fluctuation conductivity analysis shows that superconducting order parameter fluctuation (SCOPF) region is affected due to $BaTiO_3$ incorporation as observed from the T_{LD} values (Table 6.4). The variation of crossover temperature T_{LD} indicated that intragranular region has been modified as SCOPF is largely dependent on the intragranular contribution. The residual resistivity (ρ_0) is found by linear extrapolation of the resistivity curve in the range $2T_c$ up to room temperature. As an inherent property of conducting materials, ρ_0 is modified progressively with the added composites. This signifies that intergranular connectivity is also modified by these composites.

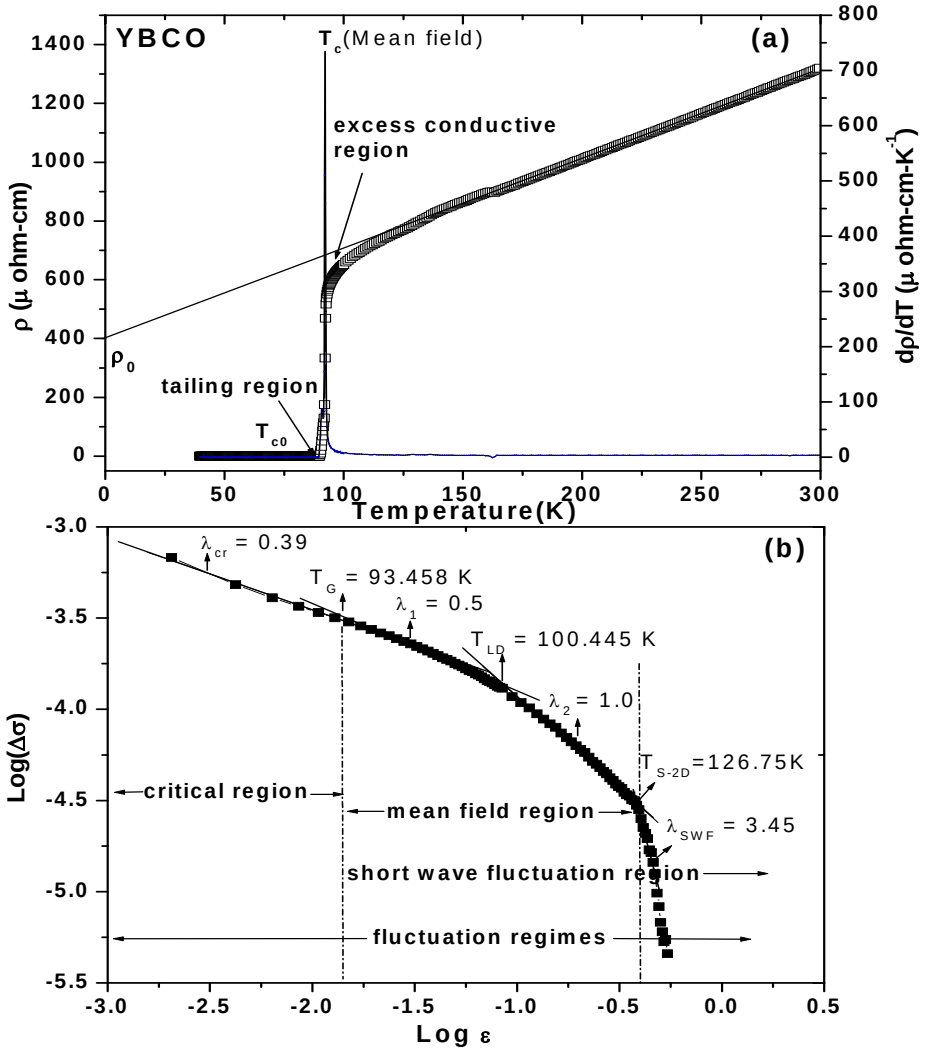

Fig. 6.17. Results of excess conductivity for YBCO. Panel (a) describes the resistivity curve showing the approximate location of each temperature region. Panel (b) shows the effect of different T_c values on excess conductivity.

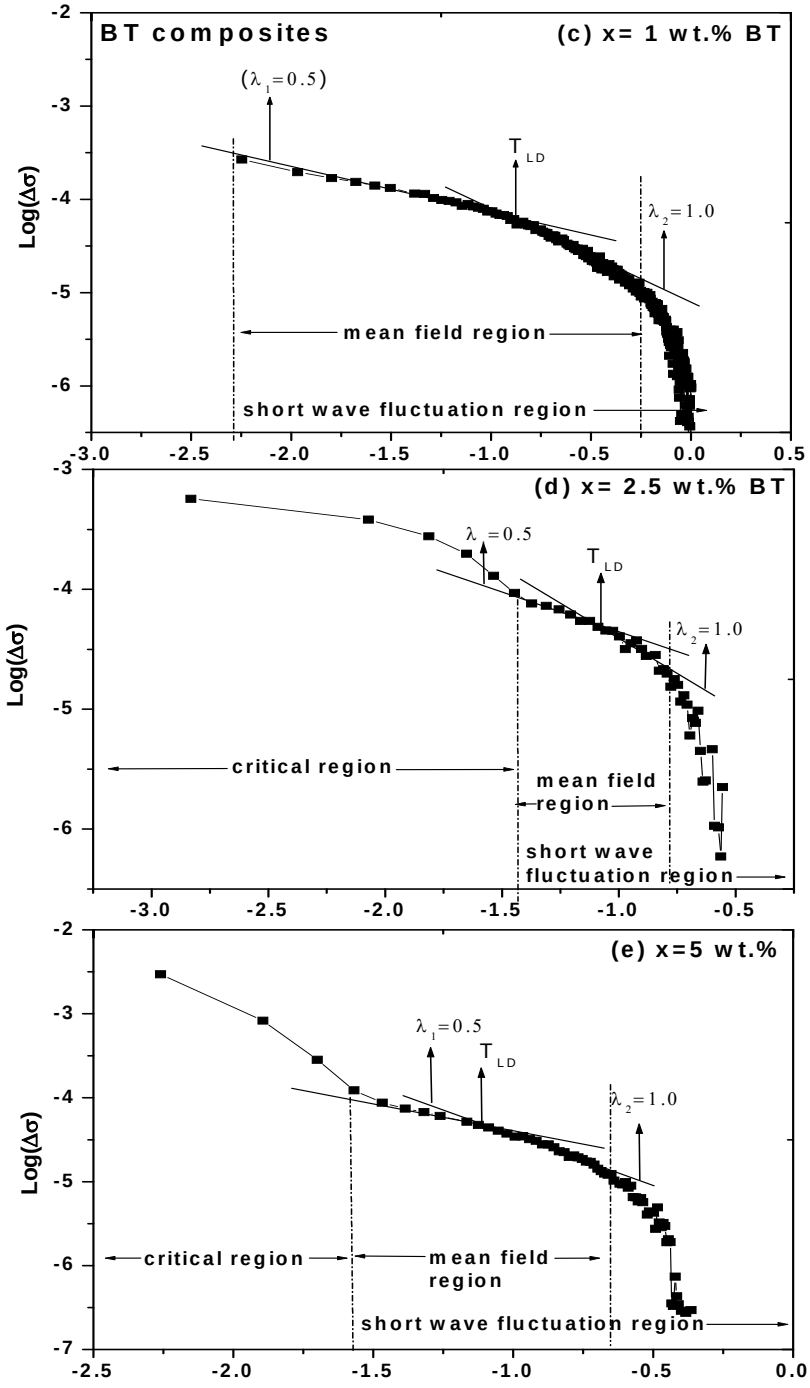

Fig. 6.18. Results of excess conductivity for YBCO+x$BaTiO_3$ (x = 1.0, 2.5 and 5.0) composites. Panels (c), (d) and (e) show the sensitivity to transition temperature, which is more pronounced in the critical region close to T_c in the $BaTiO_3$ composites. (c) x =1 wt.%, (d) x = 2.5 wt.% and (e) x = 5 wt.%.

The region between T_c and T_{LD} is called the pseudogap region. Several experimental and theoretical investigations support the idea that the pseudogap observed and thermodynamic properties of most HTSC's in an extended temperature region above T_c is due to some precursory superconductivity. In our excess conductivity studies T_{LD} observed for 1 wt.% composite sample is 97.74 K which is quite a higher value than the observed mean field critical temperature 86.86 K. It reveals that the thermodynamically activated Cooper pairs for 1 wt.% $BaTiO_3$ composites are generated within the grain at comparatively higher temperatures but due to the intragranular disturbances the mean field critical temperature comes down to lower value. A detailed study on the dimensionality can lead to the correlation of the superconducting order parameter fluctuations (SCOPF) related with this pseudo-gap phase between T_{LD} and T_c (mean Field) seen in these YBCO + $x$$BaTiO_3$ materials. In addition to their intrinsic interests the thermodynamically activated Cooper pairs well inside the normal state may directly concern in HTSC's the formation of the superconducting state itself and hence address the very mechanism of the superconductivity in HTSC's which is still elusive. At lower temperature, where the intergrain coupling energy exceeds the thermal energy, global phase ordering occurs and the sample enters the zero-dissipation state. T_{c0} is a temperature which is close to the so-called zero resistance temperature (Fig 6.17). T_{c0} decreases from 88.85 K to 81.19 K with increasing $BaTiO_3$ from 0 to 5 wt. %. This state is of particular relevance to cuprate superconductors where superconduction occurs mostly in two dimensions in ab- planes and the global superconductivity sets in by Josephson coupling of these planes.

6.6.3. Discussion on $YBa_2Cu_3O_{7-\delta}$ + x $BaTiO_3$

Fluctuation-induced excess conductivity studies in granular $YBa_2Cu_3O_{7-\delta}$ + x $BaTiO_3$ composites (with $BaTiO_3$ content from 0 to 5 wt. %) has been carried out. The Log $\Delta\sigma$ vs. log ε plots show that both 3D and 2D behavior characterized by their exponents λ in the mean field region of SCOPF are retained for composites with all $BaTiO_3$ contents. The excess conductivity being an intra-granular property it is not expected that grain boundaries would have any influence on it. However, the inhomogeneities introduced into the grains either in the form of lattice impurities, defects and strains produced by fine $BaTiO_3$ particles are expected to have a strong influence on the excess conductivity. It thus seems evident that the interplay between the inhomogeneities

(extrinsic effects) and SCOPF effects (intrinsic effects) is a topic of considerable interest, the resistivity above T_c being probably one of the best magnitudes to probe such an interplay and the relative contribution of both the intrinsic and non-intrinsic effects to the measured excess conductivity.

Thicker grain boundaries lead to increased resistivity, broadened transition width, reduced critical current etc. Small coherence length implies that inhomoheneities such as structural (twin boundaries, stacking faults, grain boundaries etc.) and chemical imperfections (oxygen deficiencies etc.) will influence both normal state and superconducting properties. The 3D region was seen to broaden due to upward shifting of the T_{LD} in 1 wt.% of $BaTiO_3$ composite (Fig. 6.17b) as compared to higher inclusions. The gap in the observed T_{LD} values for 1 wt.% and 2.5 wt.% of $BaTiO_3$ can be interpreted as introduction of a large number of inhomogeneities into the later in the composite system. This type of observation is similar to others observations [8, 13] for different system of composites in YBCO and clearly indicates that the LD - crossover temperature which demarcates the 2 to 3 – dimensional nature of fluctuation inside the grains, is influenced by $BaTiO_3$ (Fig. 6.18) content at the grain boundaries. The variation of T_{LD} shows an opposite behavior to that of T_{c0} with $BaTiO_3$ content. T_{c0} shows a progressive decrease with increasing $BaTiO_3$ concentration from 0 to 5 wt.%. In YBCO + $x$$BaTiO_3$ composites, it is believed that $BaTiO_3$ resides mostly at the grain boundaries in 2.5 and 5 wt.% composites. The observed decrease of T_{c0} with $BaTiO_3$ content can thus be explained as arising due to $BaTiO_3$ induced modification of grain boundary characteristics and progressively decoupling of the superconducting grains.

This explanation however cannot account for the large variation of T_{LD} for 1 wt.% $BaTiO_3$ content YBCO composite, characterizing the transition from 3- to 2-dimensional nature of thermodynamic fluctuation of superconducting order parameter, also a measure of intra-granular characteristics. If the $BaTiO_3$ wt.% content is relatively higher i.e. 2.5 and 5 wt.%, most of the $BaTiO_3$ adhere to the grain boundaries. But at lower wt.% content, like 1 wt.% a sizable fraction of the $BaTiO_3$ occupying lattice site in the grains. Therefore $BaTiO_3$ residing inside the grains affects T_{LD}. T_{LD} being a sensitive parameter to the electronic structure in the normal state is strongly influenced by $BaTiO_3$ content in the composites as observed. $BaTiO_3$ incorporation thus influences the charge fluctuation in the grains, thus modifying the overall electronic

structure of YBCO. It can be noted that the composite with larger $BaTiO_3$ (of the order of few microns) incorporated to YBCO does not show the two close genuine superconducting transitions while sample with nano-$BaTiO_3$ inclusion does. This clearly demonstrates that it was the penetration of Ti ions into the YBCO matrix that resulted in an increase in the value of the exponent. Such a change in the value of the exponent is probably related to the change of structure due to the presence of the Ti ion inside the grain or to the production of nano-scaled defects most likely due to $BaTiO_3$ on the grain boundaries. The grain size is reduced and morphology is improved with the nano-$BaTiO_3$ inclusion. The enlargement of grain size is linked to fluctuation-induced conductivity (FIC) in the light of Aslamazov–Larkin (AL) theory. The fluctuation induced conductivity measurements have shown that the improved grain morphology is the most likely source for shifting in the cross-over temperature, T_{LD} to higher values in 1 wt. % of $BaTiO_3$.

The analysis of fluctuation-induced conductivity has shown that nano- $BaTiO_3$ inclusions results in a decrease in the width of the three-dimensional region of fluctuations as seen by fitting of our data to AL theory. We have attributed this behaviour to the decrease in grain size because, with the decrease of grain size, the number of grain boundaries (which contribute to the weak links between the grains) is increased; the larger the number of grain boundaries the smaller the coherence between the carriers across these weak links will be. A higher numbers of grain boundaries of the polycrystalline sample imply a greater numbers of weak links and consequently minor dimensional effects in the transport properties [64-66]. Finally we conclude that dimensionality of fluctuations in YBCO + x $BaTiO_3$ superconductors depends both on the intrinsic properties (i.e. introduction of Ti ions into the YBCO matrix) and also on the extrinsic properties such as the grain morphology of the samples. It could also be seen that the width of the 2D region is decreasing after nano- $BaTiO_3$ inclusions at higher temperatures. This may possibly be due to the reduced grain size, increase in number of insulating parts in the grains along with some segregations in the grain boundaries, the homogeneity of the grains decreases leading to a larger ΔT_c [67] and 2D fluctuation induced conductivity over a short temperature range. Similar observations reported by previous investigators further support this possibility [6].

6.7. Conclusions

The occurrence of a two-stage transition from the normal to the long-range superconducting state depicts the characteristics of a granular superconductor. In the normal phase, both Gaussian and critical scaling regions are observed in a small temperature interval above T_c. $BaTiO_3$ and $BaZrO_3$ affect the temperature window between T_c and T_{c0} by introducing inhomogeneities of both mesoscopic and microscopic type. The inhomogeneities at long length scales do not directly affect the thermal fluctuations, but they deeply affect the measured behaviour of any observable around the transition together with the thermal fluctuations. The emphasis is centered on the role played by the presence of T_c inhomogeneities at the long length scales and uniformly or non-uniformly distributed in the samples, on the in-plane transport properties in composite systems of YBCO superconductors.

The zero resistance at the temperature T_{c0} characterizes the onset of global superconductivity in the samples where the long-range superconducting order is achieved. The approach to this state from T_c in the form of tailing indicates that Josephson tunneling across the grain boundary weak links progressively couples the superconducting grains to each other. This type of tailing feature in the resistive transition close to T_{c0} has been seen mostly in granular superconductors [11] where mesoscopic inhomogeneities like secondary phases, grain boundaries, twin boundaries, cracks, voids influence the occurrence of global superconductivity in the sample. The mesoscopic inhomogeneities being of length scale much larger than the superconducting coherence length are not expected to influence T_{LD}, which is a measure of intra-granular characteristics [12].

At the microscopic level, the interlayer coupling strength, J shows a strong dependence on the doping content in the sample like that of T_{LD} (since T_c is almost constant). This observation clearly indicates that, in addition to $BaTiO_3$ and $BaZrO_3$ occupying the inter-granular region, a fraction of Ti ion also goes into the grains as has been seen in a few experiments [24, 40]. The resulting microscopic inhomogeneities like local variation of oxygen stoichiometry and strain lead to T_c inhomogeneity in the grains. In $BaTiO_3$ and $BaZrO_3$ composites of $YBa_2Cu_3O_{7-\delta}$, it is believed that $BaTiO_3$ and $BaZrO_3$ resides at the grain boundaries and modifies the microstructure of the sample to a large extent [24, 34]. The observed decrease of T_{c0} is therefore a consequence

of the progressive decoupling of the superconducting grains with increasing $BaTiO_3$ and $BaZrO_3$ content in the films.

This Chapter presents the research findings involving the incorporation of sub-micron sized BZO particles and ferroelectric material like $BaTiO_3$ with fine particles has been taken for preparing composites of YBCO and demonstrates feasibility of using dielectrics and ferroelectrics to superconducting materials. The electrical conduction behavior is discussed on relevance to structural features for composites prepared through solid state reaction route. Conductivity fluctuation analysis performed around T_c, i.e. the excess conductivity region ($T \sim T_c$), the tail region ($T_{c0} < T < T_c$) and the superconducting region ($T < T_{c0}$), with their associated exponents provides evidence that dimensionality of fluctuations depends on the doping level in the mean field regimes. Studies on excess conductivity of granular samples of YBCO + *x*BZO superconductors reveal that an increase in the bulk transition takes place at x = 1.0 and occurrence of a coherence transition of BZO is observed for all concentrations. An upward shift of the 2D to 3D crossover temperature (T_{LD}) from the general trend in the mean field region confirms progressive broadening of 3D region for 1 wt.% $BaTiO_3$, which could be attributed to the enhanced sample quality of the interfacial regions in the composite and is in contrast to the studies done for incorporation of micron sized particles of $BaTiO_3$ to YBCO. It suggests that inclusion of sub-μ sized BZO particles and nano-$BaTiO_3$ to the YBCO matrix brings about structural as well as dimensional fluctuation changes in the electrical transport properties.

References

[1] L. T. Romano, O. F. Schilling and C. R. M. Grovenor, Physica C. 178 (1991) 41.

[2] O. F. Schilling, Applied Physics Letters. 52 (1988) 1817.

[3] I. S. Beloborodov, A. V. Lopatin, , V. M. Vinokur and K. B. Efetov, Reviews of Modern phys. 79 (2007).

[4] M. Tinkham, Phys. Rev. Lett. 61(1988) 1658.

[5] P. Pureur, R. Menegotto Costa, P. Rodrigues Jr, J. Schaf , J. V. Kunzler, Phys. Rev. B. 47 (1993) 11420.

[6] A. A. Khurram, N.A. Khan, M. Mumtaz, Physica C 469 (2009) 279.

[7] A. R. Jurelo, J. V. Kunzler, J. Schaf, P. Pureur, J. Rosenblatt, Phys. Rev. B. 56 (1997) 14815.

[8] U. K. Mohapatra, R. Biswal, D. Behera, N. C. Mishra, Supercond. Sci. Technol. 19 (2006) 1.

[9] A. Mohanta and D. Behera, Physica C 470 (2010) 295.

[10] T. Sato, H. Nakane, S. Yamazaki and N. Mori Physica C 1208 (2002) 372.

[11] D. Behera, N.C. Mishra, Supercond. Sci. Technol. 15 (2002) 72.

[12] J. Maza and F. Vidal, Phys. Rev. B 43 (1991) 10560.

[13] D. K. Aswal, A. Singh, S. Sen, M. Kaur, C. S. Viswandham, G. L. Goswami, S.K. Gupta, J. Phys. and Chem.of solids 63 (2002) 1797.

[14] G. Blatter, M. V. Fiegel'man, V. B. Geshkenbein, A. L. Larkin, V. M. Vinokur, Rev. Mod. Phys. 66 (1994) 1125.

[15] M. Tinkham, Phys. Rev. Lett. 61(1988) 1658.

[16] R. Ikeda, T. Ohmi, T. Tsuneto, Phys. Rev. Lett. 67 (1991) 3874.

[17] F. Tang, Q. Yuan, and Y. Yuan, J. Mater. Sci. 30 (1995) 347.

[18] J. Jung, M.A.K. Mahamed , S.C. Cheng and J.P. Frank, Physical Rev. B

[19] C. Zhang, A. Kulpa, A.C.d. Chaklader, Physica C 252 (1995) 67.

[20] J.P. Singh, H.J. Leu, R.B. Poeppel, E. Van Voorhees, G.T. Goudey, K. Winsley and D. Shi, J. Appl. Phys. 66 (1989) 3154.

[21] J. Lin and Teng-Ming Chen, Z. Phys. B-Condensed Matter 81 (1990) 13

[22] R. Pinto, P.R. Apte, M.S. R. Rao, Ramesh Chandra, C.P. D'Souza, S.P. Pai, L.C. Gupta and R. Vijayaraghavan, K.I. Gnanasekhar and M. Sharon, Appl. Phys. Lett. 68 (1996) 1006.

[23] M. Kahiberga, M. Livinsh, M. Kundzinsh, A. Sternberg, I. Shorubalko, L. Shebanovs, K. Bormanis, J. of low temperature Physics. 105 (1996) 1433.

[24] A. Mohanta, D. Behera, S. Panigrahi and N. C. Mishra Indian J. Phys. 83 (2009) 1.

[25] M. Safonchik, K. Traito, S. Tuominen, P. Paturi, H. Huhtinnen and R. Laiho, Supercond. Sci.Technol. 22 (2009) 065006.

[26] J. Gutierrez, A. Llordes, J. Gazques, M. Gilbert, N. Roma, S. Ricart, A. Pomar, F. Sandiumenge, N. Mestres, T. Puig, X. Obradors, Nature Materials**.** 6 (2007) 367.

[27] J. MacManus-Driscoll, S. R. Foltyn, Q. X. Jia, H. Wang, A. Serquis, L. Civale, B. Maiorov, M. E. Hawley, M. P. Maley, D. E. Peterson, Nature Materials. 3 (2004) 439.

[28] L. Ciontea, G. Celentano, A. Augieri, T. Ristoiu, R. Suciu, M. S. Gabor, A. Rufoloni, A. Vannozz, V. Galluzzi, T. Petrisor, Journal of Physics: Conference Series**.** 97 (2008) 012289 .

[29] N. Pompeo, V. Galluzzi, A. Augieri, F. Fabbri, G. lentano, T. Petrisor, R. Rogai, E. Silva, IEEE/CSC & ESAS European Superconductivity News Forum. 3 (2008).

[30] A. Augieri, V. Galluzzi, G. Celentano, F. Fabbri, A. Mancini, A. Rufoloni, A. Vannozzi, U. Gambardella, G. Padeletti, A. Cusmà, T. Petrisor, L. Ciontea, Journal of Physics: Conference Series. 97 (2008) 012209.

[31] H. Padma Kumar, C. Vijay Kumar, Journal of Alloys and Compounds. 458 (2008) 528.

[32] Anurag Gupta, A J Deshpande, V P SAwana, S Balamurugan, K N Sood, Ram Kishore, HariKishan, E Takayama-Muromachi, and A V Narlikar , Supercond. Sci. Technol. 20 (2007) 1084–1091.

[33] B. Dwir, M. Affronte and D. Pavuna, Appl. Phys. Lett. 55 (1989) 399.

[34] A. Mohanta and D. Behera , J Supercond Nov Magn 23 (2010) 275–283

[35] A. Mohanta, D. Behera, Physica B(2010), doi:10.1016/j.physb.2010.12.017

[36] J. Roa-Rojas, D. A. Landínez Téllez, Revista Colombiana De Física. 34 (2002) 1.

[37] Alcione Roberto Jurelo, Celmir Lupack de Ara´ujo, Ezequiel Costa Siqueira, Brazilian Journal of Physics. 35 (2005) 3A.

[38] U. K. Mohapatra, R. Biswal, D. Behera, N. C. Mishra, Supercond. Sci. Technol. 19 (2006) 1.

[39] A.R. Jurelo, P. Rodrigues Jr. and R.M. Costa, Mod. Phys. Lett. B. 23 (2009) 1367.

[40] A.R. Jurelo, P.R. Junior, A.E. Carrillo, T. Puig, X. Obradors, J. Barbosa, Physica C. 399 (2003) 87.

[41] A.R. Jurelo, C.L. de Araujo, E.C. Siqueira, Brazilian Journal of Physics, 35, (2005) 3A.

[42] K. Maki Prog. Theor. Phys. 39 (1968) 897.

[43] R. S. Thompson, Phys. Rev. B 1 (1970) 327.

[44] L.G. Aslamazov, A. I. Larkin, Sov. Phys.-Solid State. 10 (1968) 875.

[45] J. Lawrence, S. Doniach,In Proc. 12th Conf. Low-temp. Phys, Kyoto, 1970 ed. E. Kanda (Tokyo, Keigaku) pp.361

[46] V. L. Ginzberg, L. D. Landau, Zh. Eksperimi, Teor Fiz. 20 (1950) 1064.

[47] S. H. Han, Yu. Eltsev, O. Rapp, Phys. Rev. B. 61 (2000) 11776.

[48] F. Vidal, J. A. Veira, J. Maza, F Garcia-Alvarado, E. Moran and M. A. Alario,. J. Phys.: Condens. Matter 21 (1999) L599.

[49] S. H. Han and O. Rapp, Solid State Commun. 94 (1995) 661.

[50] A. K. Ghosh, S. K. Bandyopadhyay, and A. N. Basu, J. Appl. Phys. 86 (1999) 3247.

[51] P. K. Nayak, S. Ravi, Supercond. Sci. Technol. 19 (2006) 1209.

[52] C. Baraduc, V. Pagnon, A. Buzdin, J. Y. Henry and C. Ayache, Phys. Lett. A 166 (1992) 267

[53] Najmul Hassan and Nawazish A. Khan Jornal of Applied Physics 104 (2008) 103902.

[54] Y. Y. Luo, Y. C. Wu, X. M. Xiong, Q. Y. Li, W. Gawalek, Z. H. He. Journal of Superconductivity: Incorporating Novel Magnetism. 13 (2000) 4.

[55] A. K. Singh, Advanced X-Ray Techniques in Research and Industry, Capital Publishing Company, New Delhi, 2006.

[56] P. Konsin, B. Sorkin, M. Ausloos, Supercond. Sci. Technol. 11 (1998) 1.

[57] R. M. Costa, P. Pureur, M. Gusmao, Solid State Communications. 113 (2000) 23.

[58] C. J. Lobb Phys. Rev. B 36 (1987) 393.

[59] J. C. Le, J. Guillou Zinn-Justin, Phys. Rev. B. 21 **(**1980) 3976.

[60] C. Hohenberg, B.I. Halperin, Rev. Mod. Phys. 49 (1977) 435.

[61] D.S. Fisher, M.P.A. Fisher and D.A. Huse, Phys. Rev. B 43 (1991) 130.

[62] Udayan De, K. Manda, D. Sanya and C.K. Majumdar, Physica C 339 (2000) 113

[63] S.A. Sergeenkov, Z. Phys. B 82 (1991) 325.

[64] L.A.A. Pereira, P.R. Junior, A. R. Jurelo, Physica C 470 (2010) 159.

[65] Todor Mishonov, Anna Posazhennikova, and Joseph Indekeu, Physical Review B, 65 (2002) 064519

[66] A. A. Khurram, M. Mumtaz, Nawazish A. Khan, M. M. Ahadian and Azam Iraji-zad, Supercond. Sci. Technol. 20 (2007) 742.

[67] P. Maleki and M. Akhavan, Jpn. J. Appl.Phys. 44 (2005) 7934.

Chapter 7

Magneto-resistivity and Current Density in YBCO + BZO Composites

CHAPTER 7

7. MAGNETO-RESISTIVITY AND CURRENT DENSITY IN YBCO + BZO COMPOSITES

7.1. Introduction

Type-II superconductors have vortex state. To achieve high critical current density the pinning of vortices is essential. Dissipative loss occurs if Lorentz force dominates the pinning force. In the presence of external magnetic field the movement of flux lines across the sample should be resticted. This issue becomes more important for the high T_c superconductors, because of the strongly enhanced thermal fluctuations which make the Abrikosov flux lattice unstable. Therefore, well below the upper critical field $H_{c2}(T)$ line, there exist a first order melting transition leading to a normal conducting flux liquid phase. The presence of such phases limits the critical current density and put restriction in high field application of these materials. The conduction perpendicular to the Cu-O planes has been intensely debated [1], in particular the origin of the resistivity peak and the negative magnetoconductivity. It has been disputed whether the magnetoconductivity at high temperatures (150 - 300 K) is due to a normal-state effect or to superconducting fluctuations, in particular whether the Maki-Thompson (MT) fluctuation contribution is present or not. This is of fundamental interest, as motivated in Chapter 6. Vortex dynamics in high temperature superconductors gives information for many important properties such as critical current density, quantized flux trapping, vortex flow and activation energy. When magnetic field is applied to type-II superconductors magnetic flux can penetrate in the form of Abrikosov vortices (also called flux lines, flux tubes of fluxions) each carrying a quantum of magnetic flux $\Phi_0 = h/2e$. As density of flux lines increases due to application of magnetic field these vortices form flux line lattice (FLL) due to interaction.

The cuprate superconductors show a two-stage resistive transition: the step part of the superconducting transition region, where there is an onset of transition remains unaffected by the applied fields and the tail part, which is affected by the applied field. With increasing magnetic filed the transition shifts to the lower temperature side. The broadening of resistive transition is analyzed through thermally assisted flux motion theory [2]. A strong magnetic field is required

to observe a considerable resistive broadening in oriented and single crystals but a similar broadening can be observed in polycrystalline bulk samples with a low field of ~ 10 G. This broadening was first quantitatively shown by Tinkham [3] in a magnetic field. Subsequently, this feature has been explained successfully by several authors [4, 5] based on the Ambegaokar–Halperin (AH) phase-slip theory. An increase in magnetic field results in the penetration of more magnetic flux lines into the material. This enhances the Lorentz force that causes more flux lines to move. It is difficult to pin vortex liquid consisting of strongly fluctuating flexible flux lines by point defects. Therefore in such conditions the extended defects (columnar defects) give strong pinning.

To make this chapter selfcontained attempts has been made to explain the pinning mechanism in composits (section 7.2), role of grain boundaries for the critical current density (section 7.3) and magnetoresistivity and critical current density studies in composites (section 7.4). Experimental details and interpretation of results are illustrated in section 7.5. This chapter ends with a brief conclusion (section 7.6).

7.2. Pinning mechanism in composites

Improvement in microstructure and better connectivity between the grains in flux-pinning mechanism has been proposed by some authors [6-10]. Again importance of flux pinning mechanism for the Jc enhancement in the composites has been emphasized by others [11, 12]. Therefore to have a detail understanding of the $BaZrO_3$-induced modification of the grain boundary characteristics is necessary.

The enhancement of flux pinning by defect engineering in the nano-scale to maintain high current densities at high magnetic fields has drawn a lot of attention from the scientific community. Barium zirconate (BZO) is the most attractive material to induce artificial pinning centers in YBCO bulk, melt textured and thin films in order to increase the critical current density [13]. BZO one of the artificial pinning centers serves as source of arresting vortex motion in HTSC. The main reasons for using BZO as artificial pinning centre in YBCO are: (i) BZO has a high melting temperature with respect to YBCO so that the growth kinetics should be slow leading to small particles, (ii) zirconium does not substitute in the YBCO structure and (iii) although BZO can grow epitaxially with YBCO, it has a large lattice mismatch (approximately 9 %), therefore strain between the phases could introduce defects for enhanced pinning. It was

shown by Driscoll et al. [12] that, inclusions of BZO particles of dimensions in the 10-100 nm range could result in a significant improvement of dc properties of YBCO. Very steep pinning potentials of BZO inclusions and an improvement of the critical current density, J_c have been registered by Ciontea et al. [14] and Pompeo et al. [15]. Generation of this sub-micron sized defect BZO has many favourable properties like toughness enhancement towards the composite formation with YBCO. These sub-μ-sized BZO particles at the grain boundaries form strong flux pinning centers enhances some of the superconducting properties of YBCO [16]. The effect of adding nanocrystalline BZO powders to YBCO target on the flux pinning properties of YBCO + x BZO films has been extensively investigated by Kumar et al. [17]. It has been known that when the ferroelectric materials are preferentially oriented in the (00*l*) direction, they do not exhibit polarization hysteresis integrated with YBCO superconductors. The perovskite ferroelectric (Ba, Sr) TiO_3 and perovskite YBCO superconductor possess similar lattice structure (2 – 3 % lattice mismatch in a-b planes) and crystal chemistry. These ferroelectrics embedded in HTSC have shown to generate a stress field and can therefore act as pinning centers [18,19].

7.3. Role of grain boundaries for critical current density

Grain boundaries in complex oxides pose particularly interesting and difficult problems whose solutions are vital to a number of practical and fundamental issues related to high Tc superconductors. In many cases, these issues are generic to other complex electronic oxides as well, such as ferroelectric and colossal magnetoresistive manganites as well as issues of grain boundaries in general. In cuprate superconductors, the relevance of the grain boundary issue becomes prominent because of their much shorter coherence length, high superconducting anisotropy and reduced dimensionality [20]. This is at variance with classical superconductors whose much higher coherence length is reduced by the presence of grain boundaries. Another consequence of practical significance is the suppression of the critical current density at grain boundaries. Even if two grains meet without intervening chemical barrier, but with a slight crystallographic misalignment, the symmetry of the order parameter leads to a reduced wave function overlap, further aggravated by the very short coherence length, to diminished critical current. Misalignment therefore creates a weak link.

Sintering at elevated temperatures does not eliminate the intra- and inter-grain boundaries completely. They remain in the samples to a sizable fraction and limit the applicability of these

ceramic superconductors. The grain boundaries make the sample brittle deteriorating their mechanical properties. In addition, these high resistive grain boundaries acting like tunnel junctions reduce critical transport current density (J_c) of the grains [21-23]. The cuprate structure being highly anisotropic with resistivity along c-axis, ρ_c orders of magnitude higher than that in the ab-plane, ρ_{ab} further imposes restriction on the flow of current depending on the alignment of the grains. The greater the angle of misorientation at a grain boundary, the worse is the critical current [24]. This is quite different from that in the case of conventional superconductors where one deliberately introduces grain boundaries to raise the critical current density.

7.4. Magnetoresistivity and critical current studies in composites

Transport and magnetic properties of the granular system such as $YBa_2Cu_3O_{7-\delta}$ (YBCO), has drawn attention for the intrinsic properties due to the grains and the extrinsic properties due to grain boundaries. The BZO particles seeded YBCO grains, give rise to multigrain growths. BZO fine particles exclude themselves as effective flux pinning centers in the textured YBCO [6]. The main reasons for using BZO as artificial pinning centres are: (i) it has a high melting temperature with respect to YBCO, so that the growth kinetics should be slow leading to small particles, (ii) zirconium does not substitute in the YBCO structure and show non-reactivity with YBCO (iii) it can grow epitaxially with YBCO and has a large lattice mismatch (~ 9 %), [10, 12, 25] therefore strain between the phases, could introduce defects for enhanced pinning. For this reason vortex engineering is done by controlling the influence of defects and their interaction with vortex in BZO doped YBCO [26].

This aspect of activation energy has been studied through various techniques such as dc resistivity, remnant magnetization and ac susceptibility [2]. The vortex hops between neighbouring positions in the vortex lattice. This generates resistance when the Lorentz force is more than the pinning force. This hopping occurs in bundles as the distance between the individual flux lines is smaller as compared to lattice distance and the vortex lattice is quite rigid. The bundles hop at a rate determined by the frequency of vibration of flux lines and activation energy. The dissipation is low at small hopping rate and goes down with temperature. For this reason superconductors are operated at lower temperature, for below T_c such as below□ λ point of He liquid for low T_c superconductors. Under the action of Lorentz force the thermally

activated flux flow (TAFF) occurs and the dependence of activation energy on temperature and field is determined by two major mechanisms (a) thermally activated excitation of dislocations and (b) thermally activated creep of preexisting quenched dislocations [27]. It is speculated that vortex regions work as strong repulsive pinning centers resulting from the kinetic energy of the order parameter under a significant proximity effect [28].

7. 5. Experimental results and interpretation

7.5.1 Sample preparation and characterization

The preapration procedure of superconducting composite samples of YBCO + x $BaZrO_3$ with varying wt.% (0, 1.0, 2.5, 5.0, 5.0) is described in chapter 3. Resistivity vs. Temeperature in presence of magnetic field and magnetic studies (M-H measurement) using vibrating sample magnetometer (VSM) is done at UGC-DAE-CSR, Indore.

7.5.2. Magneto resistive transitions in $YBa_2Cu_3O_{7-\delta}$ + $xBaZrO_3$ composites

Fig. 7.1 shows ρ(T) for four different YBCO + BZO composite samples measured at different values of constant magnetic fields. The superconducting transitions become extremely broad in presence of applied fields. It is very amazing to note that the addition of BZO in the samples makes the two-step superconducting transition from normal to the long-range superconducting state, depicting the characteristics of a granular superconductor similar to the results obtained by Anurag et al. [29]. In the normal phase, both Gaussian and critical scaling regions are observed in a small temperature interval above T_c. BZO can affect these regions as well as the region in the temperature window between T_c and T_{c0} by introducing inhomogeneities of both mesoscopic and microscopic type. Besides, the fact that the second step occurring at lower temperatures (the characteristic value defined as Tc_{on2}) is not as sharp as the first step $Tc_{on1.}$ The obvious difference between them is that Tc_{on2} is observed due to the inter-granular parameters and Tc_{on1} due to intra-granular parameters. In composites, the value of Tc_{on1}(92 K) is nearly independent of fields where as Tc_{on2} gets broader and shifts to lower temperature with consequence of the progressive decoupling of the superconducting grains with increasing BZO content in the samples.

On increasing magnetic field, the mean field transition temperature T_c is not affected much rather T_{c0} (R=0) moves to a broad range of lower temperature side. The Tc_{on1} represents the onset

of superconductivity in the grains of composites. Values for Tc_{on1} in 1wt.% and 2.5 wt.% BZO show different behavior to the increasing field indicates that inclusion of submicron sized BZO particles affects the intra granular region to some extent which can be clearly distinguished in presence of external magnetic fields (Fig. 7.2). In 1 wt.% BZO composite a good dependency of superconductivity and dielectricity is obtained. It helps to increase superconducting property of YBCO grains by filling up cracks and defects formed in YBCO grains during the sintering process and attain the greatest T_c in sintered series of samples. But in 2.5 wt.% BZO composite the optimum value of BZO addition is attained, creating some sort of disturbance in the superconducting system and Tc_{on1} declines to lowest values for all fields for the entire series of samples. On increasing the wt % content to 5 and 10 it is believed that the Zr-ions concentrate more near the grain boundaries which substantially reduces grain mobility and leading to reduced superconducting properties in the paracoherent state. Hence, $T_{c0}(R=0)$ decreases with magnetic field suggesting that, grain boundaries (Josephson junctions) are affected more than the grains (Abrikosov junctions). This leads to the decrease in T_{c0} from 85.4 K to 36 K for 10 wt % composite sample at fields of 0T and 8T respectively, where as the corresponding values are 90 K and 63.3 K for pristine sample.

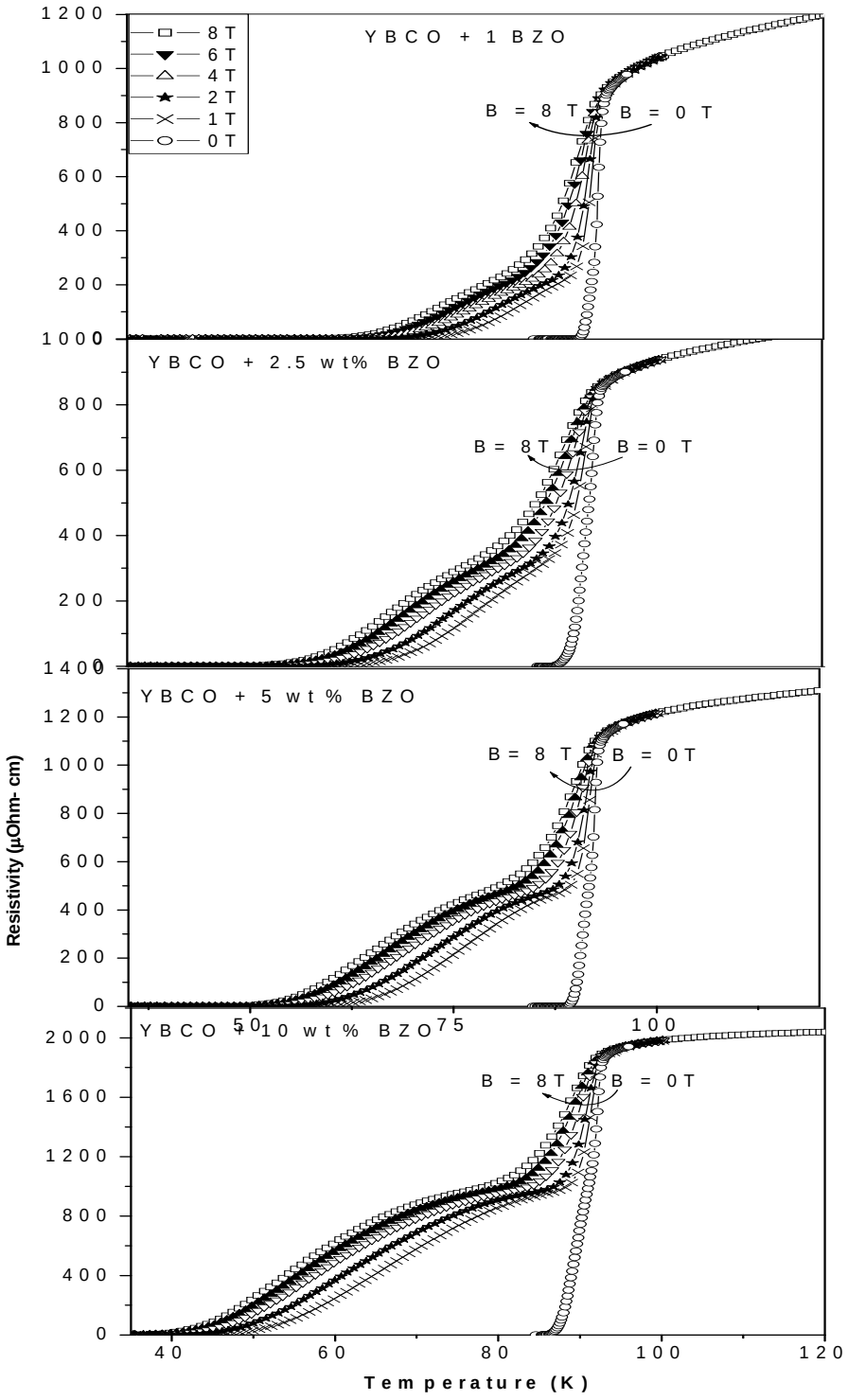

Fig. 7.1. Resistivity versus temperature plots of various YBCO + x BZO composite samples in presence of B = 0, 1, 2, 4, 6 and 8 T.

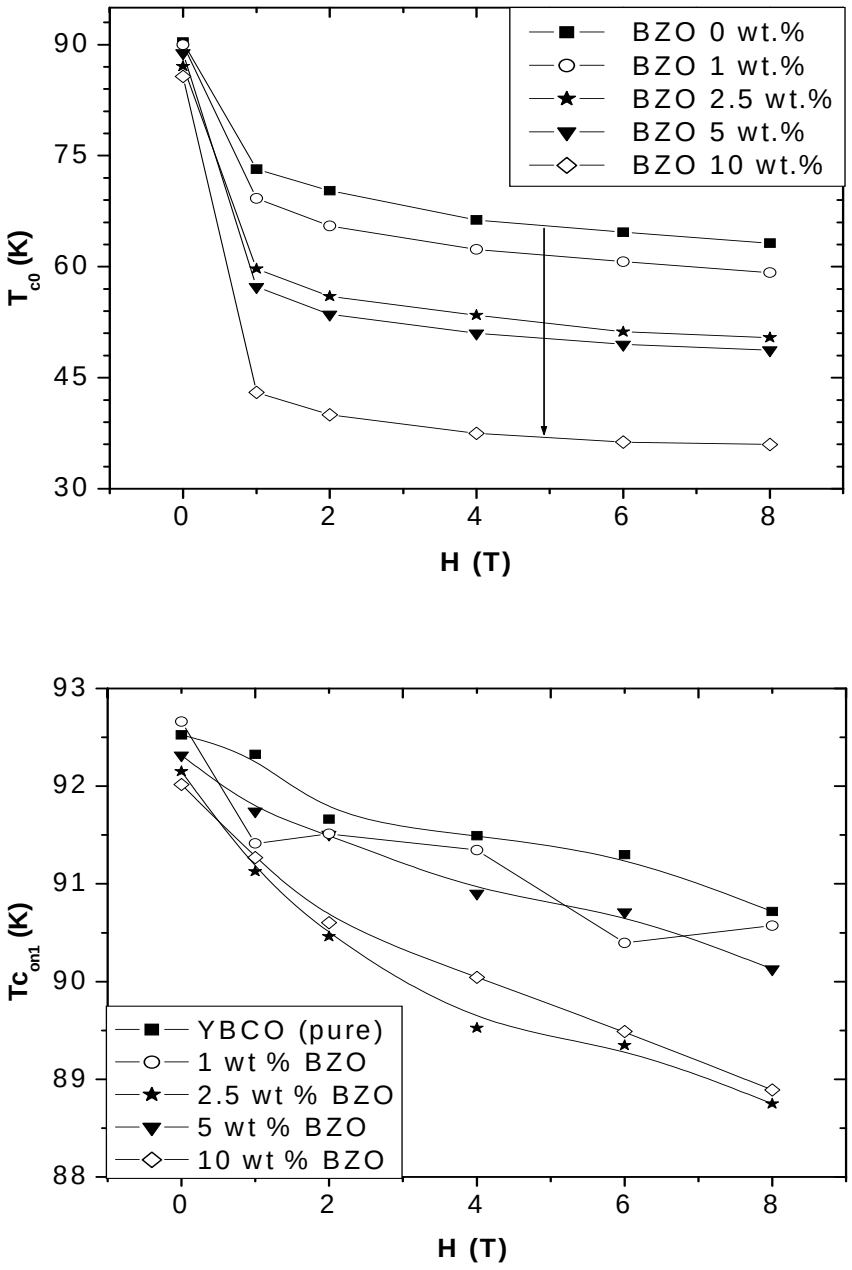

Fig. 7.2. The effect of magnetic fields on Tc_0 and Tc_{on1} on YBCO + x BZO composites with BZO (x = 0, 1, 2.5, 5 and 10 wt %) in zero magnetic field.

In Fig. 7.3 close to T_{c0}, this heterogeneous medium consists of two components. For the first component the superconducting grains and the grain boundary weak links has been considered where superconductivity is established through Josephson tunneling. The second component

consists of weak links which are not superconducting, either due to the link being too weak or due to the measuring current exceeding the J_c of the corresponding link or the temperature being higher than the T_c of that link. For $T<T_{c0}$, the first component provides the channel for the transport of supercurrent. For $T_{c0} < T < T_c$, the volume of the first component is not adequate enough to provide a percolative path for supercurrent and the ρ-T transition shows a tail with $\rho \neq 0$. Only when $T \leq T_{c0}$, a percolative path through the first component is established and a global superconductivity is obtained in the sample.

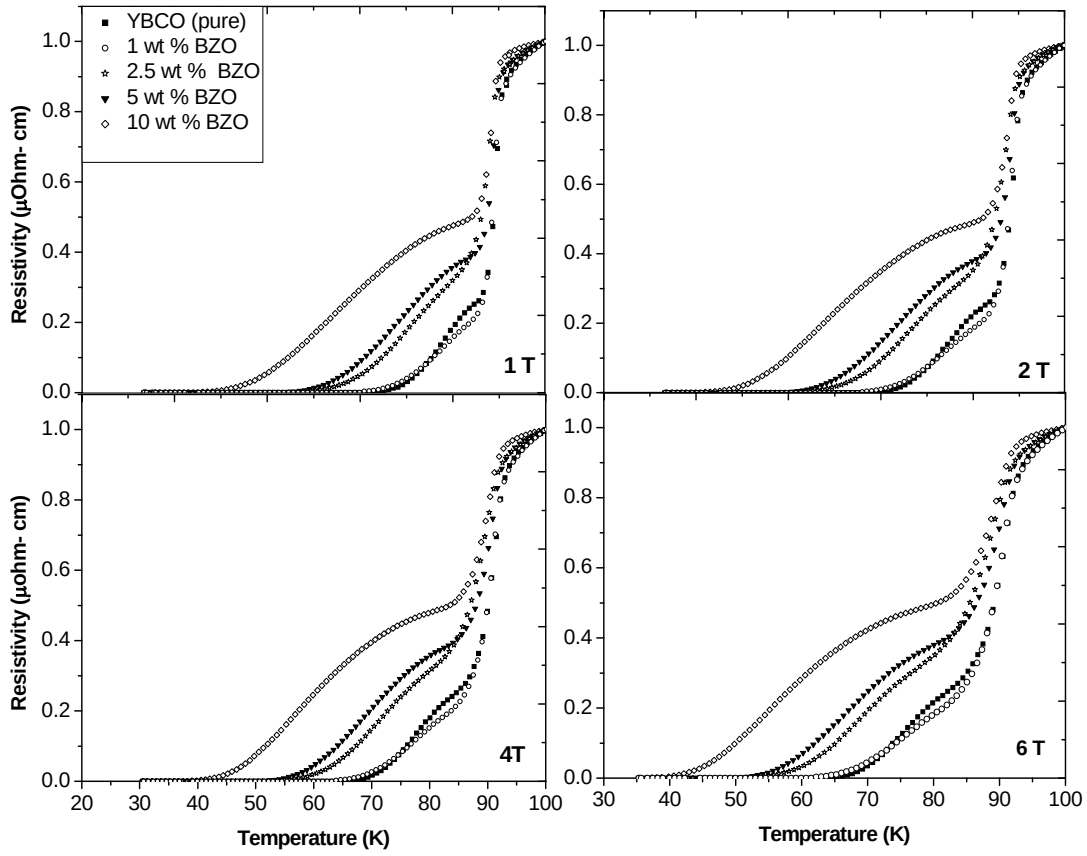

Fig. 7.3. Normalized resistivity versus temperature of YBCO+ x BZO composites with (x = 0, 1, 2.5, 5 and 10 wt %) measured for different Magnetic fields (B = 1, 2, 4 and 6T).

This provides simple explanation of the anomalous secondary peaks observed for present composites and attributed to the explanation of some cases not well settled intrinsic mechanisms around T_c region. In a two-stage transition, at the first stage grains become superconducting, giving rise to a sharp resistivity drop, while in the second part of the transition intergrain weak

links have a Josephson-like behaviour and lock-in phase to each other as temperature decreases, giving rise to larger superconductive islands. The non-linearity structure at the tailing region is attributed to sample inhomogeneity, contact effects, or quantum tunneling. It is assumed that the global zero resistance state at T_{c0} region of high temperature superconductors (HTSC) are governed by the excitations in the weak link net work [6].

7.5.3. Thermally activated flux pinning in $YBa_2Cu_3O_{7-\delta}$ + $xBaZrO_3$ composites

This broadening of the resistive transition and magnetoresistance is explained through AH model for phase slip in Josephson junction. The pinning potential in the intergrain region as found from AH model is similar to that of J_c of an array of Josephson junction [30]. The necessary fitting of the experimental data to the AH model's expression has been made through the equation 7.1 & 7.2 [31-32];

$$\rho = \rho_n \{I_0(\frac{\gamma_0}{2})\}^{-2} \tag{7.1}$$

$$\gamma_0 = \frac{U_0}{K_B T} = A(1-t)^q \tag{7.2}$$

Where ρ_n is the average normal state resistivity of the junction, I_0 is the modified Bassel function, and γ_0 is the normalized barrier height for thermally activated phase-slip (TAPS). U_0 is the activation energy, A is constant depend on H (magnetic field) and t is the reduced temperature (T/T_c). The transition behaviour below T_c is fitted to AH model in Fig. 7.4 and Fig. 7.5 for YBCO and YBCO + 10 wt.% BZO respectively. The exponent q varies from 1.0 to 1.5 for YBCO and from 3.0 to 3.1 for the 10 wt.% composite sample respective in presence of magnetic field varying from 1 to 8 T. It is believed that the broadening behaviour in the low-resistance region near T_c ($\rho = 0$) could be explained by a thermally activated flux creep model.

The cuprate superconductors show a two-stage resistive transition: the step part of the superconducting transition region, where there is an onset of transition remains unaffected by the applied fields and the tail part, which is affected by the applied field. With increasing magnetic filed the transition shifts to the lower temperature side. For low current ($I \leq 200$ mA) the authors[15] have shown the branching point as R_f which separates ohmic (upper part) and non-

ohmic region (lower part) of the transition in YBCO/Ag composites. In case of low magnetic field ($H \leq 180$ Oe) the authors[16] have observed the branching of $R(T_{cj})$) in YBCO+CuO composites. The region above the branching and below the mean field temperature is well described by AH model (phase slip process) and in the broadening region is well explained by flux creep model [33, 34]. In the region of the superconducting transition the samples showed two distinct sections, a steep part associated with the onset of superconductivity in the individual grains and a transition tail due to the weak links coupling the grains [35]. It has been reported that for different composites the steep section remained unchanged with applied field while the tails moved considerably to lower temperatures with this dissipation region being very sensitive to both transport current and applied field as the percolation limit was approached by some authors [31, 32]. They have measured the magneto-resistance of high T_c cuprate superconductors and fitted their experimental data in the superconducting transition broadenimg region by AH phase slip model. It has been observed that the activation energy depends not only on the temperature and magnetic field but also on the doping concentration.

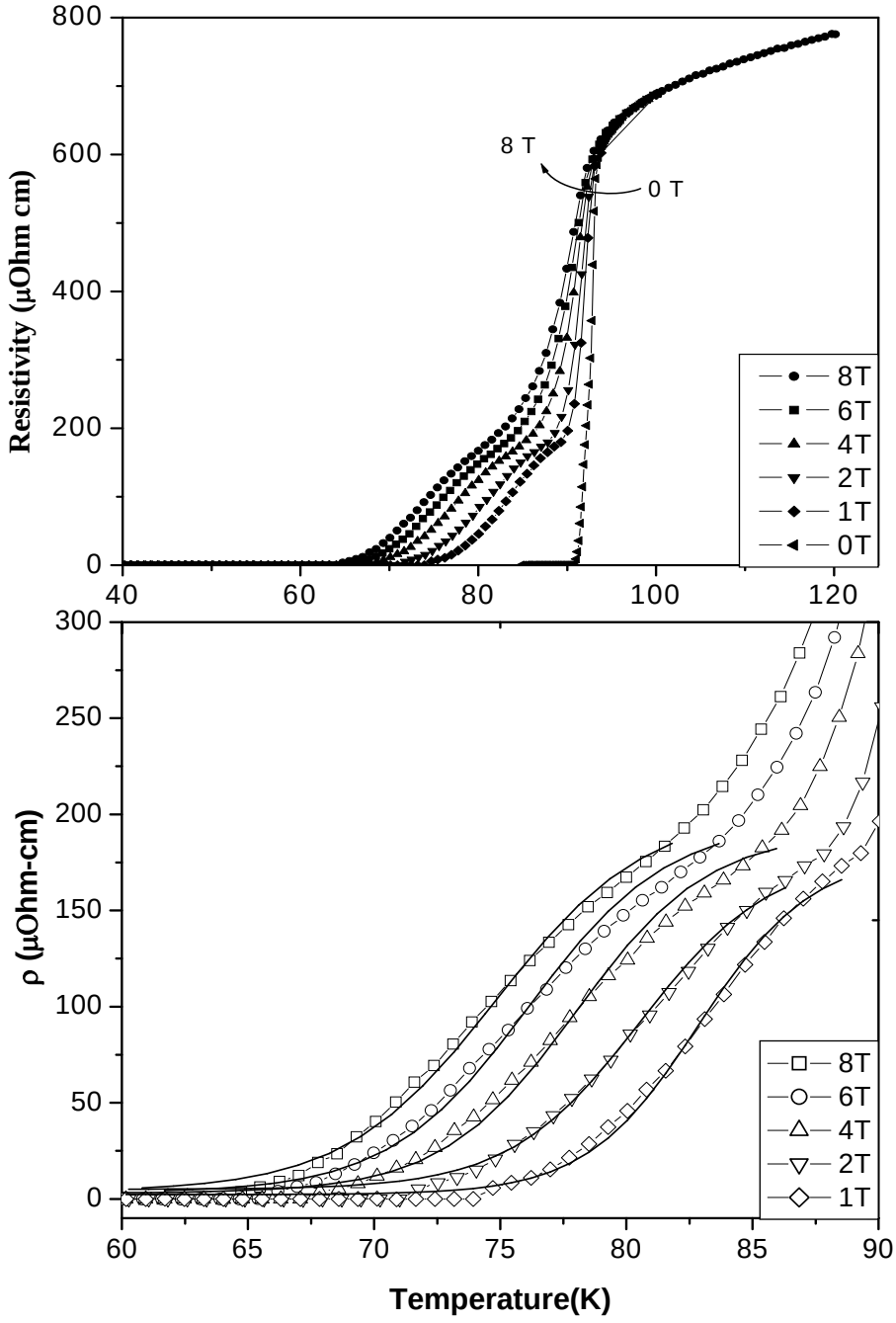

Fig. 7.4. Temperature dependence of resistivity of YBCO in presence of magnetic field varying from 1-8 T . The points represent the data and the solid lines represent the fitting to equation (7.1).

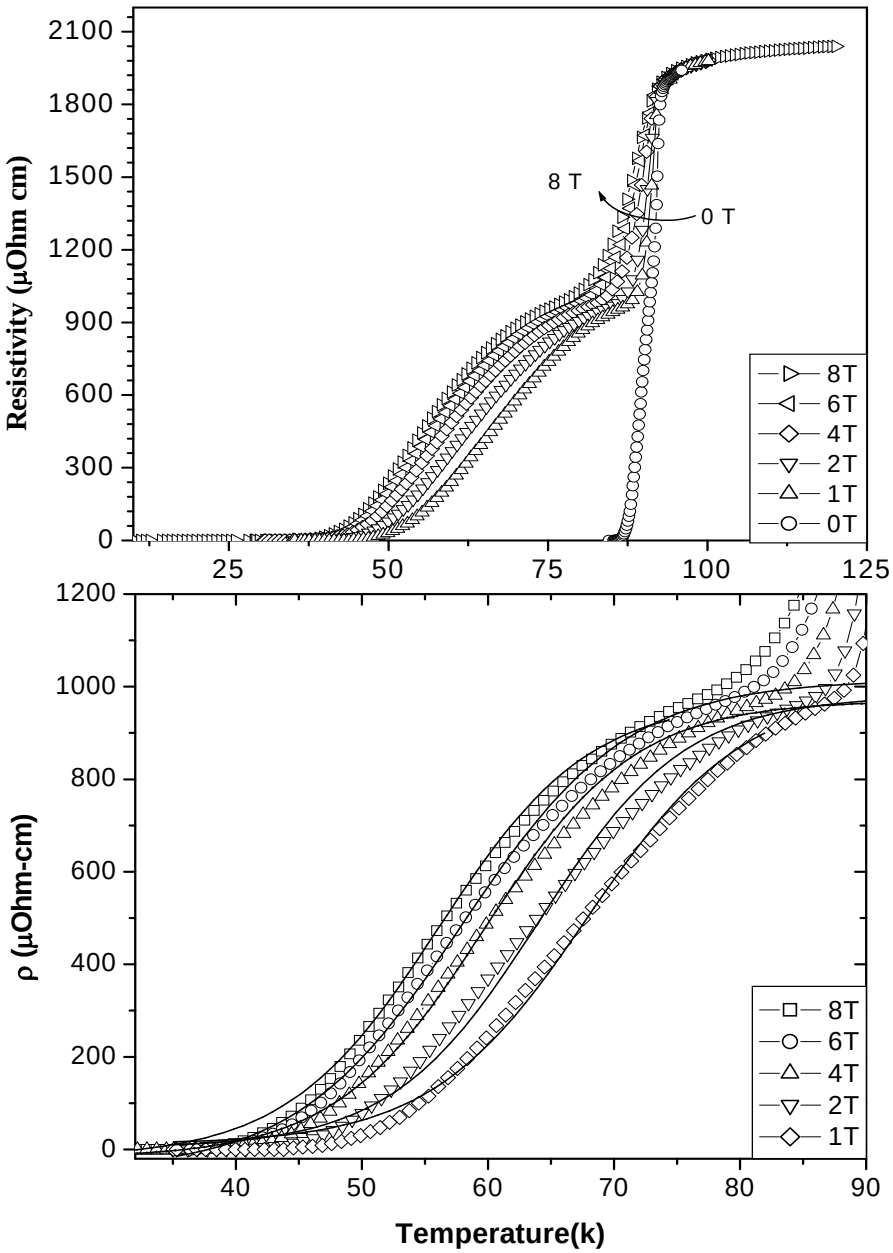

Fig. 7.5. Temperature dependence of resistivity of YBCO + 10 wt. % BZO in presence of magnetic field varying from 1-8 T. The points represent the data and the solid lines represent the fitting to equation (7.1).

The broadening of resistive transition is analyzed through thermally assisted flux motion theory as [2];

$$\rho (T, H) = \rho_n \exp[-U(T, H)/T] \quad (7.3)$$

where ρ_n is the normal state resistivity and U is the activation energy.

The activation energy has the form $U(T, H) = f(T) (H/H_0)^{-\beta}$, where H_0 is a characteristic field. They have obtained the activation energy with $U(T, H) \alpha (1-t) H^{-\square 2/3}$ where $t = T/T_c$, the reduced temperature for YBCO thin film [35]. This relation has been modified to $U(T, H) \alpha (1-t)^m H^{-\square\beta}$ where m and β are magnetic field dependent [2]. The Arrhenius law as in equation (7.3) with universal field dependent of the activation energy has been reported in MgB_2 system [36] as $U (T,H) = U_0(T)(1- B/B_{c2})^2$ above the irreversibility field $B_i(T)$. Considering the dimensionality of the vortex system Blatter et al.[37, 38] using the thermodynamic critical field H_c and coherence length ξ as $H_c \alpha (1-t)$ and $\xi \alpha (1-t)^{-1/2}$ has calculated the activation energy $U \alpha (1-t)^m$ where m = 2 - n/2 (n = 0 - 3 , the dimension).

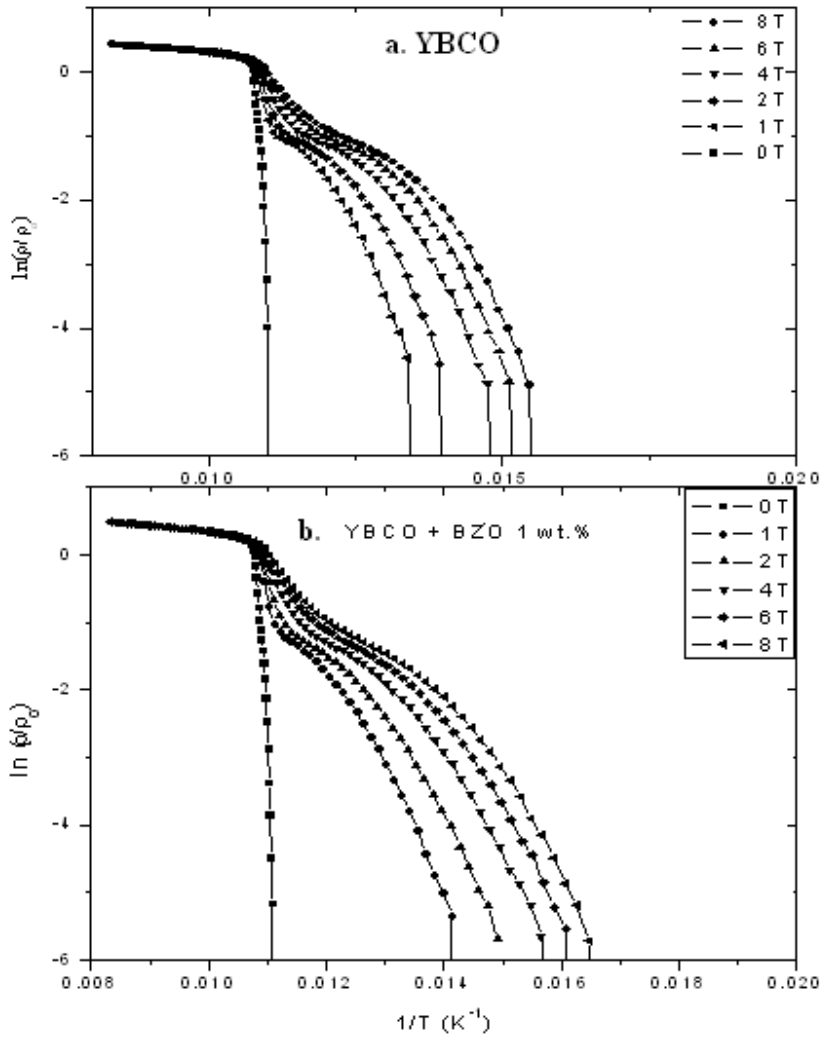

Fig. 7.6. (a-b). Arrhenius plot of the electrical resistance of YBCO + x $BaZrO_3$ (where x = 0, 1.0, wt.%) for magnetic field 0-8 T perpendicular to the ab- plane. The activation energy is determined from the slope in the linear region $\ln(\rho/\rho_0)$ vs 1/T.

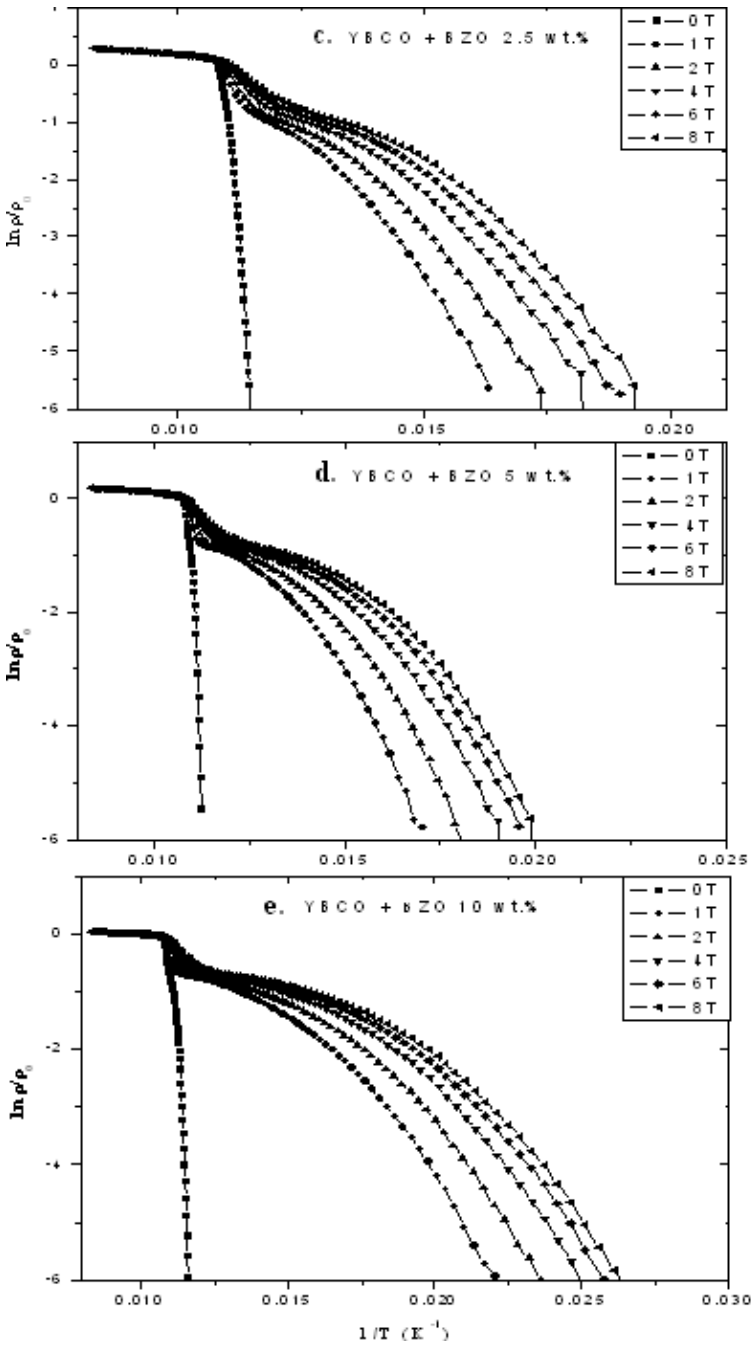

Fig. 7.6. (c, d and e). Arrhenius plot of the electrical resistance of YBCO + x BZO (where x = 2.5, 5, 10 wt.%) for magnetic field 0-8 T perpendicular to the ab- plane. The activation energy is determined from the slope in the linear region $\ln(\rho/\rho_0)$ vs 1/T.

In the same perspective, the activation energy is evaluated through resistive broadening with varying measurement magnetic field from 0 to 8 T (Fig. 7.6, 7.6a) for varying content of BZO in YBCO. Data were obtained under the self-field condition. The self-field is generally neglected

when working at a high magnetic field however; this effect is considerable in the absence of the magnetic field. Particularly, dealing with the experiment on polycrystalline samples where J_c depends on the weak links at the grain boundary, self-fields strongly affect Josephson current. When working at a low magnetic field the role of both self-field and flux-creep in resistive transition is important. With increasing magnetic field the resistive transition shifts to the lower temperature side like current variations [39]. The tail of the resistivity curve becomes longer indicating the predominance of weak links between superconducting grains [40]. This slope of the straight line in the curve $\ln(\rho/\rho_0)$ vs 1/T (Fig. 7.6a- 7.6e) gives the activation energy $U_0(T,H)$ for the flux lines at different magnetic fields. The activation energy decreases with increasing magnetic field.

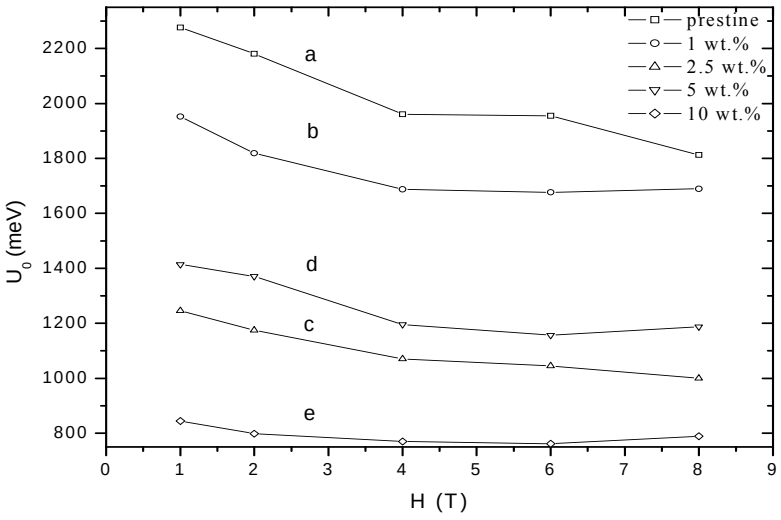

Fig. 7.7. Magnetic field dependence of $U_0(H)$ for the different wt.% of BZO doped with YBCO sintered samples.

The dependence of $U_0(H)$ was predicted to obey the power law of the form $U_0(H) \sim H^{-\alpha}$ by which the exponent was calculated for different composites. The exponent varies within 0.94 ± 0.05 (Fig. 7.7). This nonlinear variation predicts the exponent value in the range of 0.14 to 1.5. The authors [41, 42] have obtained a similar observation where the activation energy decreases with increasing Pr doping in YBCO. The variation of activation energy with magnetic field is sample dependent – it decreases as thickness increases [43]. Efficient pinning centers are observed when the particles are of the order of coherence length[22], however authors have

reported that effective pinning can be created in particles size ~ penetration depth rather than coherence length [44]. We observe the decrease of activation energy in our BZO inclusions to YBCO. This may be due to the particle size which is more than the penetration depth in the bulk system. The activation energy decreases with increasing magnetic field has been reported [31, 32]. The activation energy is decreased with increasing BZO concentration in contrast to as has been observed by Safonchik et al [45]. The corresponding grain size of BZO they have considered are about 40 nm and particle sizes ranging in 5-10 nm. The discrepancy in activation energy behaviour lies in their method of preparation of the samples where PLD thin film was prepared from superconducting $YBa_2Cu_3O_{7-\delta}$ nanopowder by the citrate-gel modification of the sol–gel. They have chosen an optimal conc. 3.9 wt. % of BZO in YBCO for PLD. It has been reported that the critical current density is dependent on particle size i.e. nanocrystalline has higher J_c as compared as microcrystalline size.

7.5.4. Magnetization studies in $YBa_2Cu_3O_{7-\delta}$ + $xBaZrO_3$ composites

There are numerous advantages of superconducting properties over composite formation in magnetic fields based on YBCO + xBZO sub-micron scaled particles. Doping with BZO improves the irreversibility and de-pinning lines and increases the value of critical current density (J_c) [7]. Recently, it has been shown [10, 12] that inclusions of BZO particles of dimension range 10–100 nm could determine a significant improvement in dc properties of (YBCO). The high efficiency of such defects is in that strong pinning centers, such as columnar defects like BZO sub-micron particles, when suitably distributed during the composite formation with YBCO, significantly extend the range of linear response by acting as pinning centers for fluxons nucleated by the RF field.

The temperature dependence of DC magnetization for one sample (BZO 5 wt %) has been shown in Fig. 7.8 both in field cooled (FC) and zero field cooled (ZFC) in the presence of magnetic field of 500 Oe. Below about 92 K the ZFC and FC curves start to open, indicating an irreversibility effect induced by the flux pinning. This measurement confirms the transition temperature (T_c) 92 K as has been measured from resistivity vs. temperature plot. The onset of irreversibility where the two curves merge is connected with the onset of the upper transition at 92 K. Higher magnetization is observed in FC as compared to ZFC because BZO acts as pinning centers in the matrix of YBCO. If a cycle of cooling with field (FCC) and warming with field

(FCW) is made for magnetization measurement at a particular magnetic field, a hysteresis is observed showing the effect of temperature on pinning (Fig. 7.9).

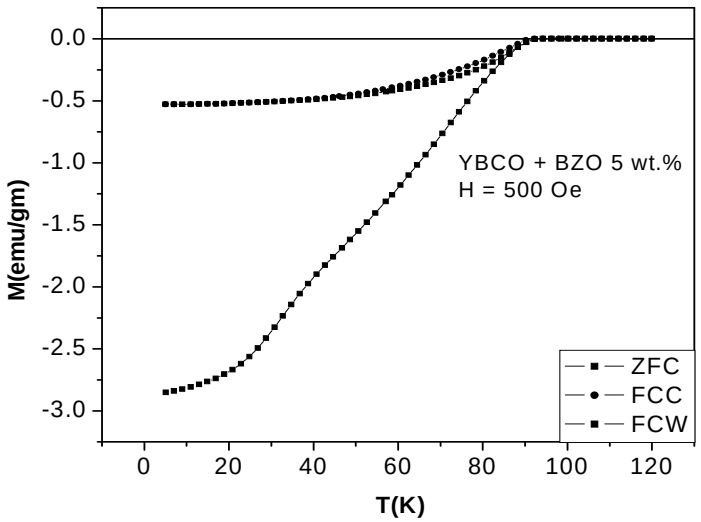

Fig. 7.8. Magnetization (M) vs. Temperature (T) at a constant low field showing the opening of ZFC and FC curves.

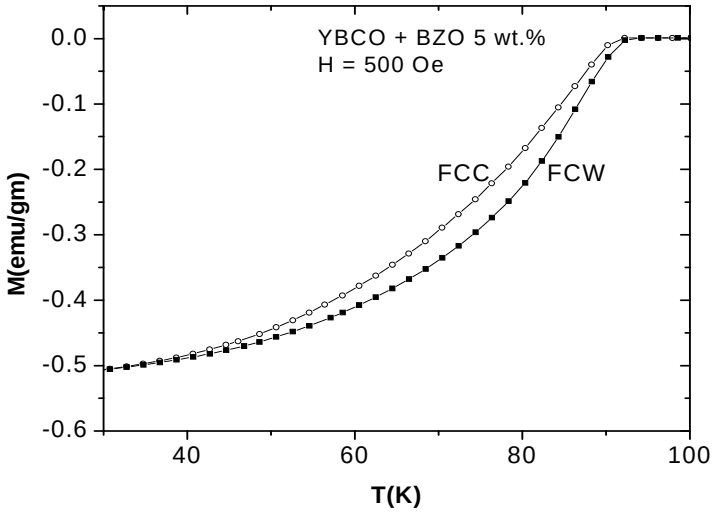

Fig. 7.9. Magnetization (M) vs. Temperature (T) at a constant low field showing hysteretic behaviour for FCC and FCW in YBCO + BZO (5 wt %) sample.

Recently quasi-continuous nanoscale network of defects can be generated for creating effective vortex-pinning centers. BZO nano-dots distributed randomly within YBCO matrix serves as defects for pinning centers. Chemically prepared nano-composite is distinguished from samples prepared from vacuum deposited methods. The random crystalline orientation of the nanodots prepared by chemical process is effective in preventing the vortex motion at high field and at high temperature [29].

7.5.5. Critical current density (Jc) measurements in $YBa_2Cu_3O_{7-\delta}$ + $xBaZrO_3$ composites

MacManus-Driscoll et al. [12] have reported enhancement of J_c in YBCO coated conductor with $BaZrO_3$. Films carry one to two orders of magnitude higher current densities than other form of materials. For the measurement of critical current density at different temperatures below T_c the measuring current was passed through the two outer probes by current pulse technique and voltage developed was measured through the two inner probes. Pulsing of current was necessary to avoid sample heating and damage to the contacts. The setup for resistivity measurement was used for J_c measurement. Our observation for critical current density (J_c) shows an increase from 8 x 10^4 A cm^{-2} to 2 x 10^5 A cm^{-2} for pristine YBCO and 5 wt.%BZO composite sample respectively in 1 - 16 (Tesla) field at temperature (T) of 40 K. J_c is calculated considering the Bean's critical state model and results are plotted in Fig. 7.10. The formula used here as [46, 47].

$$J_c = \frac{20\Delta M}{a(1-\frac{a}{3b})} \tag{7.4}$$

Where, a < b and $\Delta M = |M_+| - |M_-|$ which is extracted from M (H) loop and a is the thickness and b is the width of the bar shaped sample. The pinning effect of BZO enhancing critical current density has been reported [7, 45]. In our case the J_c is observed to be low as compared to the reported system [25, 35]. This may be due to reduction of particle size (nano dimension) in their samples.

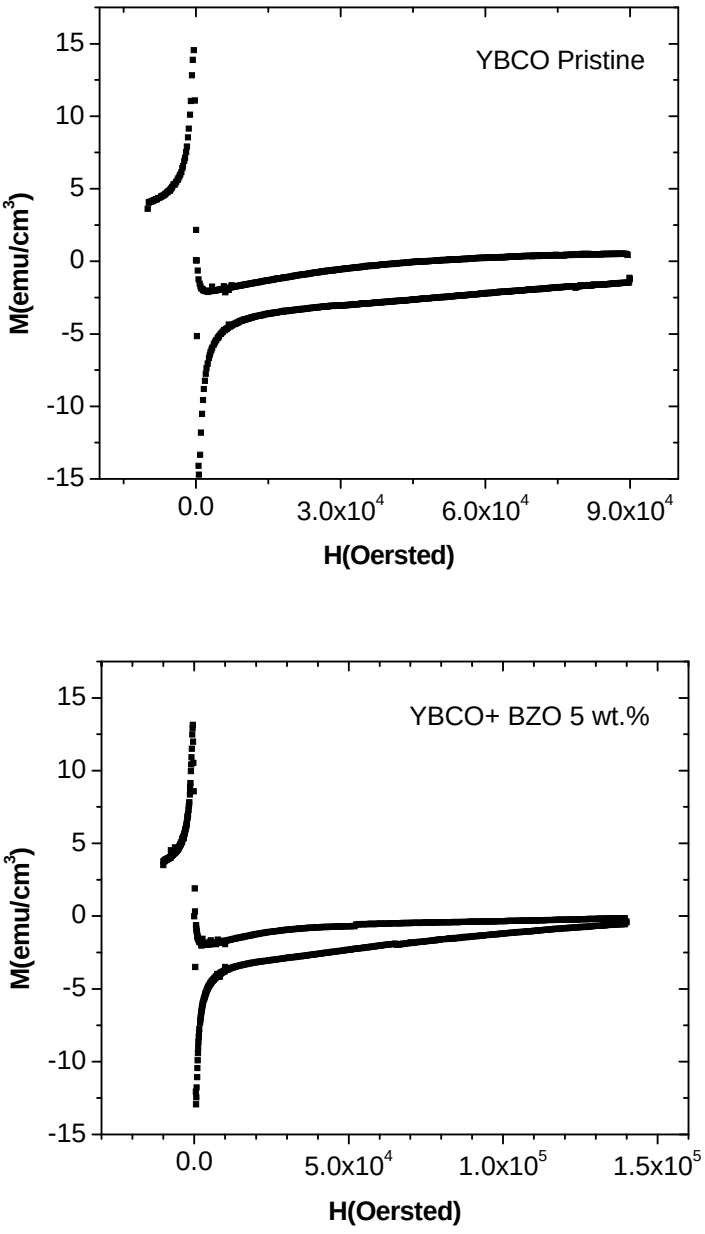

Fig. 7.10. M-H plot for pristine YBCO and YBCO + 5 wt % BZO sample for J_c measurement

7.6. Conclusions

The composite sample of YBCO+ $BaZrO_3$ was prepared through solid state route employing nitrate precursors of BZO. Due to flux pinning effect of submicron particles of BZO in presence of magnetic field critical current density is enhanced in the composites. The activation energy

due to thermally activated flux creep process has been determined using the relation $U_0(H) \sim H^{-\alpha}$ with $\alpha \sim 0.94 \pm 0.05$ for our different samples. The lower part of the resistive transition (intergranular) is affected by the magnetic filed rather than the transition due to grains. As the resistive broadening varies with magnetic fields the composite materials can be used as active elements in magnetic field sensor devices for low magnetic field. It has been observed that activation energy is dependent not only on particle size but also on the penetration depth. Due to flux pinning effect of submicron BZO particles, in presence of magnetic field, critical current density (J_c) is also seen to have improved marginally in the composites. On implementation of Beans critical state model in the present work, it is noticed that the value of J_c increases from 8 x 104 A-cm^{-2} to 2 x 105 A-cm^{-2} from pristine YBCO to YBCO + 5 wt % BZO composite samples in 1 - 16 T at a temperature of 40 K. The resistive broadening in the tail part is suggested to be associated with the link between the grains and to be extremely sensitive to magnetic field. The magnetic field enhances the phase slip in the Josephson junction and broadens the resistive transition. The exponent q and T_c in the AH model are related to each other. These parameters are dependent on magnetic filed and BZO composition.

References

[1] J. Axnas, W. Holm, Yu. Eltsev and O. Rapp, Phys. Rev. Lett. 77, (1996) 2280.

[2] S. L. Liu, J. Supercond. Nov. Magn. 21 (2008) 199.

[3] M. Tinkham: Phys. Rev. Lett. 61 (1988) 1658.

[4] I. L. Landau and H. R. Ott, Physica C 331 (2000) 1.

[5] H. Shakeripour and M. Akhavan, Supercond. Sci. Technol. 14 (2001)234.

[6] Y. Y. Luo, Y. C. Wu, X. M. Xiong, Q. Y. Li,1 W. Gawalek, and Z. H. He, J. Supercond.Nov.Magn. 13 (2000) 575.

[7] M. Peurla, H. Huhtinen, M.A. Shakhov, K. Traito, Y.P. Stepanov, M. Safonchik, P. Paturi, Y.Y. Tse, R. Palai and R. Laiho, Phys. Rev. B 75 (2007) 184524.

[8] M Peurla, P Paturi, Yu P Stepanov, H Huhtinen, Y Y Tse, A C Bodi, J Raittila and R Laiho, Supercond. Sci. Technol. **19** (2006) 767–771

[9] S. Sathyamurthy, K. J. Leonard, M. S. Bhuiyan, T. Aytug, S. Kang, R. D. Hunt, P. M. Martin, and M. Paranthaman, IEEE Transactions On Applied Superconductivity,17(2) 2007.

[10] S. Kang, K. J. Leonard, P M Martin, J. Li and A. Goyal, Supercond. Sci. Technol. **20** (2007) 11–15.

[11] A. Augieri, V. Galluzzi, G. Celentano, F. Fabbri, A. Mancini, A. Rufoloni, A. Vannozzi, U. Gambardella, G. Padeletti, A. Cusmà, T. Petrisor, L. Ciontea, Journal of Physics: Conference Series 97 (2008) 012209.

[12] J. L. Macmanus-Driscoll, S. R. Foltyn, Q. X. Jia et al., Nat. Mater. 3 (2004) 439.

[13] L. T. Romano, O. F. Schilling and C. R. M. Grovenor, Physica C. 178 (1991) 41.

[14] L. Ciontea, G. Celentano, A. Augieri, T. Ristoiu, R. Suciu, M. S. Gabor, A. Rufoloni, A. Vannozz, V. Galluzzi, T. Petrisor, Journal of Physics: Conference Series**.** 97 (2008) 012289.

[15] N. Pompeo, V. Galluzzi, A. Augieri, F. Fabbri, G. lentano, T. Petrisor, R. Rogai, E. Silva, IEEE/CSC & ESAS European Superconductivity News Forum. 3 (2008).

[16] A. Augieri, V. Galluzzi, G. Celentano, F. Fabbri, A. Mancini, A. Rufoloni, A. Vannozzi, U. Gambardella, G. Padeletti, A. Cusmà, T. Petrisor, L. Ciontea, Journal of Physics: Conference Series. 97 (2008) 012209.

[17] H. Padma Kumar, C. Vijay Kumar, Journal of Alloys and Compounds. 458 (2008) 528.

[18] W. Gawalek, T. Habisreuther, K. Fischer, G. Bruchlos, P. Görnert Cryogenics. 33(1993) 65.

[19] Morsy Abou Sekkina, Abdul Raouf Tawfik, Osama Hemeda, Mohamad Ahmad Taher Dawoud, Samy Elattar, Turk J Phys, 29 (2005) 329.

[20] M. Prester, Supercond. Sci. Technol. 11 (1998) 333.

[21] A.V. Narlikar, C.V. Narasimha Rao and S.K. Agarwal (Nova Science Publications, New York, (1989) 341.

[22] B. W. Veal, H. You, A.P. Paulikas, H. Shi and J.W. Downey, Phys. Rev. B 42 (1990) 4770.

[23] B. W. Veal and A. P. Paulikas, Physica C 184 (1991) 321.

[24] D. Dimos, P. Chaudhuri, I. Mannhart, F. Legoues, Phys. Rev. Lett. 61 (1988) 219, Phys. Rev. B 41 (1990) 4038.

[25] A.Goyal, S. Kang, K.J. Leonard, P.M. Martin, A.A. Gapud, M. Varela, M. Paranthaman, A. O. Ijaduola, E.D. Specht, J.R. Thompson, D.K. Christen, F.A. List, Supercond. Sci. Technol. 18 (2005) 1533.

[26] B. Maiorov, S.A. Baily, H. Zhou. O. Ugurlu, J.A. Kennison, P.C. Dowden, T.G. Holesinger, S.R. Foltyn and L. Civale, Nature Materials 8 (2009) 398.

[27] S. Patnaik , A. Gurevich, S. D. Bu, S. D. Kaushik, J. Choi, C. B. Eom, and D. C. Larbalestier, Phys. Rev. B 70 (2004) 064503.

[28] T. Matsushita, Supercond. Sci. Technol. 13 (2000) 730.

[29] Anurag Gupta, A. J. Deshpande, V. P. Awana, et al.: Supercond. Sci. Technol. 20 (2007)1084.

[30] D. A. Balaev, A. A. Dubrovskiy, S .I. popkov, K. A. Shaykhutdinov and M. I. Petrov, J. Supercond. Nov. Magn. 21 (2008) 1557.

[31] H. Shakeripour and M. Akhavan: Supercond. Sci. Technol. 14 234 (2001).

[32] H. S. Gamchi, G. J. Russell, and K. N. R. Taylor, Phys. Rev. B 50 (1994) 12950.

[33] R.J. Soulen Jr., T.L. Francavilla, W.W. Fuller-Mora, M.M. Miller, Phys. Rev. B 50 (1994) 478.

[34] D.A. Balaev, S.I. Popkov, K.A. Shaihutdinnov, M.I. Petrov, Physica C 435 (2006) 12.

[35] D. Behera, R. Biswal, U.K. Mohapatra and N.C. Mishra, Indian J. Phys. 82 (2008) 317.

[36] S. Patnaik, A. Gurevich, S.D. Bu, S.D. Kaushik, J. Choi, C.B. Eom, and D.C. Larbalestier. Phys. Rev. B 70 (2004) 064503.

[37] G. Blatter, M.V. Feigelman, V.B.Geshkenbein, A.I. Larkin, ans V.M. Vinokur, Rev. Mod. Phys. 66 (1994) 1125.

[38] J.A. Xia, N.J. Long, N.M. Strickland, P. Hoefakker and E.F. Talantsev, Current Applied Physics, 262 (2008).

[39] I. L. Landau and H. R. Ott, Physica C 331 (2000) 1.

[40] S. Hadi, A. Ali, B. Brojeny and S. Medhi, Supercond. Sci. Technol. 14 (2001) 816.

[41] P. Maleki and M. Akhavan, Jpn. J. Appl. Phys. 44 (2005) 7934.

[42] C. Kwon, M. Damaske, Qi Li, L. Senapati, P. A. Warburton, and T. Venkatesan, IEEE transactions on applied superconductivity, 5, (1995) 1355.

[43] Teruo Matsushita et al Supercond. Sci. Technol. 20 (2007) 89.

[44] N. Moutalibi and A. M'chirgui, Physica C 469 (2009) 95.

[45] M. Safonchik, K. Traito, S. Tuominen, P. Paturi, H. Huhtinen and R. Laiho, Supercond. Sci. Technol. 22 (2009) 065006.

[46] V.P.S. Awana, Arpita Vajpaye, Monika Mudgel, H. Kishan, V. Ganesan, A.M. Awasthi, G. L. Bhalla, J. Euro. Phys. B 62 (2008) 281.

[47] S. Meslin, K. Iida, N. Hari Babu, D.A. Cardwell and J.G. Noudem, Supercond. Sci. Technol. 19 (2006) 711.

Chapter 8

Conclusions

CHAPTER 8

8. CONCLUSIONS

The present work addresses the Superconducting Order Parameter Fluctuation (SCOPF) in (i) Doped and (ii) Composite Cuprate Superconductors. We have examined the charge transport process in Ca, Zn doped system and Ga, Zn doped systems of YBCO with composites of $BaZrO_3$ (paraelectric material) and $BaTiO_3$ (ferroelectric material) to YBCO. The broadening of resistive transition is analyzed through thermally assisted flux creep theory. The activation energy is calculated from a varying magnetic field induced quantized flux in the composites of YBCO with BZO. The flux pinning effect of BZO composites show the enhancement of critical current density measured through M-H loop. The current chapter discusses the problem addressed and important findings from these studies.

8.1. Problem addressed

The defects that make the very existence of superconductivity possible in cuprates, also drive these systems away from equilibrium by way of lattice mismatch and coordination incompatibility at the various cation sites. Considering the importance of the various types of chemical and structural disorder in influencing the superconductivity in the cuprates, a large number of authors have studied the evolution of superconductivity with defects and disorder introduced artificially into the cuprate structure. The fluctuations due to finite cooper pair formation probability induce excess conductivity or paraconductivity in the normal phase close to T_c.

8.2. Important findings

Studies on the temperature dependence of resistivity in polycrystalline sintered samples of $Y_{1-x}Ca_xBa_2(Cu_{1-y}Zn_y)_3O_{7-\delta}$ were significantly modified with various dopants in YBCO superconductor. The results obtained from the analysis for all the samples fit well with the 3D AL equation and a crossover from 2D to 3D has been found at a temperature T_{LD}. It has been observed that with the increase of Zn substitution to the Y0.9Ca0.1 -123 systems the fluctuating

region of superconductivity shrinks considerably and becomes centered at lower temperature values. It has been again witnessed that the temperature range for dimensionality of fluctuations in YBCO superconductors depends on the on-site cationic substitutions. Particularly the simultaneous substitution of Ca as hole dopant and Zn as an in plane disorder contribute significant changes in the characteristic behaviour of pseudogap temperature.

- The presence of small stoichiometric and structural inhomogeneities seemed to deeply affect the ρ(T) behavior around T_c. Zinc doping to YBCO superconductors gives rise to a redistribution of charges in the superconducting system which breaks the cooper pairs therefore, resulting in a T_c decrease. With increase in Zn concentration both T_c and T_{c0} values decrease for $YBa_2(Cu_{0.95}Zn_{0.05-x}Ga_x)_3O_{7-\delta}$. T_c is not affected much by Ga^{3+} as much as it is affected by doping Zn^{2+}. The exponent values for fluctuation conductivity in the T_{c0} region decrease with increase of substitution concentration. The dual exponent character shows that the intergranular weak links develop more resistance with increasing impurities.
- Studies on excess conductivity of granular samples of YBCO + *x*BZO superconductors reveal that an increase in the bulk transition takes place at x = 1.0 and occurrence of a coherence transition of BZO is observed for all concentrations. An upward shift of the 2D to 3D crossover temperature (T_{LD}) from the general trend in the mean field region confirms progressive broadening of 3D region for 1 wt.% $BaTiO_3$, which could be attributed to the enhanced sample quality of the interfacial regions in the composite and is in contrast to the studies done for incorporation of micron sized particles of $BaTiO_3$ to YBCO. It suggests that inclusion of sub-μ sized BZO particles and nano-$BaTiO_3$ to the YBCO matrix brings about structural as well as dimensional fluctuation changes in the electrical transport properties.
- Due to flux pinning effect of submicron particles of BZO in presence of magnetic field in YBCO+ $BaZrO_3$, critical current density is enhanced in the composites. It has been observed that activation energy is dependent not only on particle size but also on the penetration depth. On implementation of Beans critical state model in the present work, it is noticed that the value of J_c increases from 8 x 10^4 A-cm^{-2} to 2 x 10^5 A-cm^{-2} from pristine YBCO to YBCO + 5 wt % BZO composite samples in 1 - 16 T at a temperature of 40 K. The resistive broadening in the tail part is suggested to be associated with the

link between the grains and to be extremely sensitive to magnetic field. The magnetic field enhances the phase slip in the Josephson junction and broadens the resistive transition. The exponent q and T_c in the AH model are related to each other. These parameters are dependent on magnetic field and BZO composition.

8.3. Future work

Composite superconductors like YBCO + x $BZrO_3$ are attractive candidates for wires and tapes which are potential candidates for the manufacture of superconducting power devices like superconducting fault current limiters, transformers and cables due to its high critical current density. In this work superconducting order parameter fluctuation studies have been studied and analyzed on the basis of a brief review on some theoretical models. In future these theories may be used for other HTSC materials to study the physics and mechanism of superconductivity varying the doping concentrations. The scope for future work of the thesis may be strengthening by considering few aspects:

- By providing in-depth analysis of the transport properties of doped and composite systems of YBCO. Some more advanced characterizing techniques such as Rietveld analysis of the XRD data, high resolution transmission electron microscopy (HRTEM), X-ray photoelectron spectroscopy (XPS) for compositional analysis, Raman spectroscopy for the oxygen content of the samples may be carried out to extract further information for understanding the basic superconducting properties.
- It will be more informative to characterize all the chosen systems for magnetic studies. All the samples may be characterized for critical density measurement for application point of view. The extent of pinning due to the composite formation may be estimated through the calculation of pinning forces for all the considered composite systems.
- Thin films of nanocomposite YBCO can be prepared to get information for microstructural modifications and to observe finite size effect.
- Close to T_c interpretations for the 3D *XY* universality class with model-*E* dynamics is confirmed but still closer to T_c the new scaling is to be interpreted and confirmed.